LAWRENCE
LIVERMORE
NATIONAL
LABORATORY

LLNL-TR-676944

Real-Time Characterization of Special Nuclear Materials

S. Walston, J. Candy, D. Chambers, H. Chandrasekaran, N. Snyderman

September 4, 2015

Disclaimer

This work performed under the auspices of the U.S. Department of Energy by Lawrence Livermore National Laboratory under Contract DE-AC52-07NA27344.

Real-Time Characterization of Special Nuclear Material

Sean Walston,[a] Jim Candy, Dave Chambers, Hema Chandrasekaran, and Neal Snyderman
Lawrence Livermore National Laboratory, Livermore, California[b]

(Dated: 31 August 2015)

We discuss what has been accomplished over the past three years for the online statistical analysis of neutron time intervals (OSANTI) algorithm project.

I. EXECUTIVE SUMMARY

A. Objective

When confronting an item that may contain nuclear material, it is urgently necessary to determine its characteristics. Our goal is to provide accurate information with high-confidence as rapidly as possible.

B. Existing Methods

Assay of nuclear materials using neutron multiplicity methods has, to date, been based on the combinatorial moments of the neutron counting distributions from, usually, randomly-triggered time gates[1–12] as detailed in Eqs. 79-96.

To assay a low-count-rate neutron source such as highly-enriched uranium (HEU), current neutron multiplicity analysis methods require a significant amount of data especially when using low-efficiency neutron multiplicity counters. Current methods also require the user to provide an estimate of the detection efficiency a priori because, in the analysis, detection efficiency can be exchanged for mass and multiplication. Only if the third moment $Y_3(T)$, and thus R_3, are well-constrained are the existing algorithms somewhat self-calibrating. For low-count-rate sources, this often requires many hours of data.

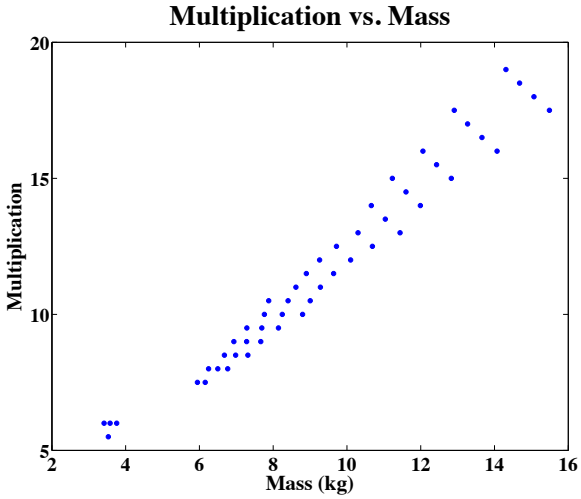

FIG. 1. The first 50 "BigFit" solutions for multiplication M vs. ^{238}U mass m_S for the first test object discussed below in §I E. The user is left with the conundrum of trying to estimate the detection efficiency to narrow down the actual multiplication M and ^{238}U mass m_S.

This degeneracy has long been a serious problem because the neutron-absorbing properties of materials may not by known and additional nearby reflectors greatly complicate the determination of the efficiency. This single issue has caused numerous erroneous assays and much effort has been devoted to finding a work-around.

Currently, the most sophisticated neutron multiplicity analysis is "BigFit" which compares measured count distributions $b_n(T)$, Eq. 50, for $T = 1, 2, 3, \cdots, 512$ μs to a grid of theoretical distributions precomputed from first principles. "BigFit" uses precomputed distributions for e_m, Eq. 62, and folds in the diffusion time λ^{-1} according to Eq. 77. An analysis of the first test object discussed in §I E below provides an array of answers as shown in Fig. 1. The user is then left with the conundrum of trying to estimate the detection efficiency to narrow down the actual multiplication M and ^{238}U mass m_S.

When creating a neutron counting distribution using randomly-triggered time gates, one incurs a substantial loss of information. The first test object discussed below in §I E had a count rate of 12.9 neutrons per second. In

[a] Electronic mail: walston2@llnl.gov

This work performed under the auspices of the U.S. Department of Energy by Lawrence Livermore National Laboratory under Contract DE-AC52-07NA27344.

This work was supported by the U.S. Defense Threat Reduction Agency (DTRA), under DTRA10027-10273.

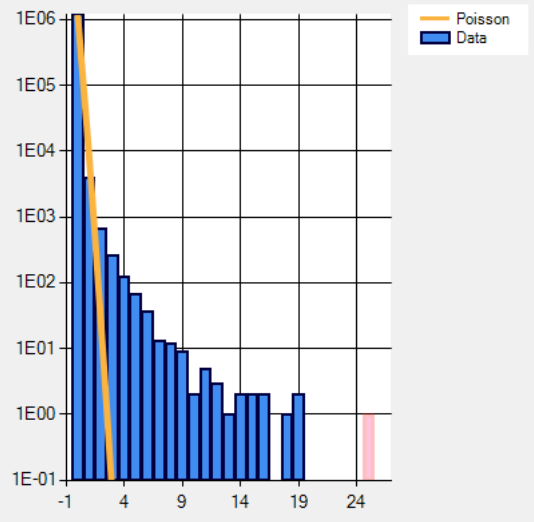

FIG. 2. Feynman histogram for the number of neutrons counted during a randomly-triggered time gate of duration $T = 499$ μs for a 10 minute measurement of the first test object discussed below in §I E. A total of 7,741 neutrons were counted.

10 minutes, a total of 7,741 neutrons were counted. The time-tagged, list-mode data consisting of the arrival time of each neutron therefore starts with 7,741 pieces of information for a continuous variable (limited only by the time resolution of the detector's electronics). The neutron counting distribution has only 20 pieces of information—the non-zero multiplets—for a discrete variable as shown in Fig. 2. An apt analogy would be to consider the degradation in image quality that would result if one went from an image with 7,741 pixels to only 20.

Lastly, methods based on neutron counting distributions must consider count distributions for time gates of varying durations T. Because the method is so inefficient, the same neutrons are invariably used in the count distributions for every value of T (an example of a commonly-used time-binning structure is shown in Fig. 21). The problem is, the covariance between count distributions for different values of T is unknown making it impossible to rigorously compute even basic statistical uncertainties.

C. Improvements Over Existing Methods

We have developed a new method that considers the waiting time from one neutron to the next on a neutron-by-neutron basis. This method, by comparison, incurs no loss of information relative to the original time-tagged, list-mode data. Our method has demonstrated several significant benefits compared with existing methods:

- We converge to an answer within ≤ 500 neutrons—about one minute. Existing methods typically require $\gtrsim 1$ hour of data to be able to develop an answer.
- We are able to assay the neutron source without an a priori estimate of the detection efficiency. The algorithm is self-calibrating. Existing algorithms require the user to provide an estimate of the detection efficiency to constrain the analysis to a reasonable range of mass m_{S} of ^{238}U and k_{eff}.
- Because our algorithm computes the probability distribution function (PDF) for an answer (e.g. k_{eff}), it automatically provides confidence intervals and quantifies the uncertainties. Existing methods do not provide an estimate of any confidence intervals or uncertainties.

D. Our New Method

This new algorithm, in broad strokes, required us to develop several new approaches:

1. Rapid computation of the probability distribution e_n for the number n of neutrons detected from a fission chain (discussed in §II). We were able to make the computation of this distribution approximately 50,000 times faster.
2. Extension of the theory for the waiting times between the correlated neutrons from a fission chain to include background neutrons (which may themselves be correlated) (discussed in §III). For the low-count rate sources this algorithm is intended to assay, background neutrons can account for $\approx 50\%$ of the neutrons.
3. A sequential Bayesian "particle filter" to compute the PDF for a physical parameter of interest where the answer is taken as the most probable value—the maximum a posteriori probability (MAP) estimate (discussed in §IV).

E. Results

Two highly enriched uranium (HEU) sources were assayed:

1. The first source had a count rate of 12.9 neutrons per second, included a mass $m_{\mathrm{S}} \approx 6$ kg of ^{238}U, and the configuration had $k_{\mathrm{eff}} \approx 0.87$. No hydrogenous material was present making the neutron diffusion time $\lambda^{-1} \approx 40$ μs which is the diffusion time in the high-density polyethylene (HDPE) in the MC-15 Joint Multiplicity Counter used to make the measurements.
2. The second source had a count rate of 2.7 neutrons per second, included ≈ 1.6 kg of ^{238}U, and the configuration had $k_{\mathrm{eff}} \approx 0.5$. A 4 inch thick layer of moderating material loosely surrounded the HEU making the neutron diffusion time $\lambda^{-1} \approx 75$ μs. This includes the

Source	Count Rate	Count Rate, No Bkgd	Time to Count 500 n	Time to Analyze 500 n
Bkgd; 2 MC-15s	1.06 s^{-1}	—	—	—
First; 2 MC-15s $m_S \approx 6$ kg ^{238}U $k_{eff} \approx 0.87$	12.9 s^{-1}	≈ 11.8 s^{-1}	≈ 38 s	≈ 120 s
Second; 2 MC-15s $m_S \approx 1.6$ kg ^{238}U $k_{eff} \approx 0.5$	2.7 s^{-1}	≈ 1.6 s^{-1}	≈ 190 s	≈ 120 s

TABLE I. Comparison of the count rates and typical times to count and analyze 500 neutrons for the two sources.

non-negligible time-of-flight and the diffusion time in the MC-15's HDPE.

Count rates, count times, and typical analysis times are summarized in Table I.

An overnight measurement of background neutrons was made using two MC-15 detectors connected together to function as a single, larger detector. In total, the measurement counted 53,330 neutrons. The distribution of waiting times between successive neutrons is shown in Fig. 3. The background count rate was 1.06 neutrons per second. Given that there were only $\lesssim 30$ plausibly-correlated neutrons in the overnight measurement, the random approximation was deemed perfectly adequate. It also has the advantage that it can be parameterized with only a single quantity—the count rate. The likelihood function that was used for the analyses presented here was the much simpler Eq. 126.

Results of measurements made at the NTS DAF with the new MC-15 Joint Multiplicity Counter are shown below. For the first test object, the result of measurements by two MC-15s connected together to function as a single larger detector are shown in Fig. 5. The data set was then evaluated considering 500 neutrons at a time and the result of an ensemble of 100 runs are shown in Fig. 6. A comparison of the theory constructed using the estimated parameters, Eq. 125 or 126, to the measured time interval distribution is shown in Fig. 7.

The results of a measurement of the first test object by a single MC-15 are shown in Fig. 8. For this evaluation, the background count rate was taken as 0.53 neutrons per second. The data set was again evaluated considering 500 neutrons at a time and the result of an ensemble of 100 runs are shown in Fig. 9. Note that the detection efficiency is roughly half what was found using two MC-15s, as expected.

For the second test object, the results of a measurement by two MC-15s connected together to function as a single larger detector are shown in Fig. 10. The data set was again evaluated considering 500 neutrons at a time and the result of an ensemble of 100 runs are shown in Fig. 11.

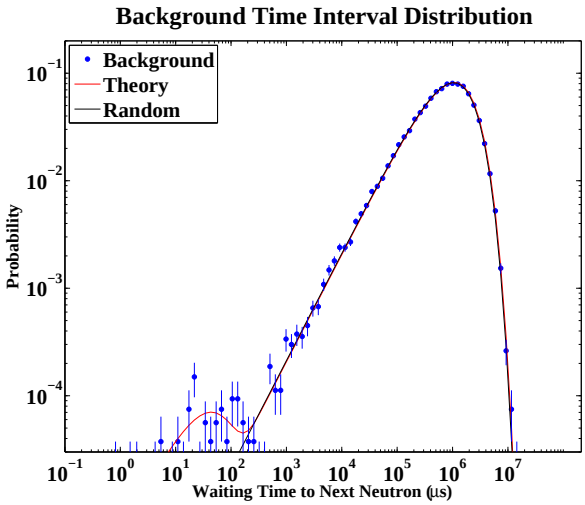

FIG. 3. Time interval distribution for an overnight measurement of 53,330 background neutrons at the DAF as measured by two MC-15 Joint Multiplicity Counters connected together. The solid red line is the theoretical distribution, Eq. 120. The solid blue line is the random (exponential) distribution. Given that there were only $\lesssim 30$ plausibly-correlated neutrons out of the 53,330 neutrons in the overnight measurement, the random approximation was deemed perfectly adequate. It also has the advantage that it can be parameterized with only a single quantity—the count rate R_1^{Bkg}.

F. Sensitivity

One take-away from these tests is that the assessed mass of ^{238}U is not well-constrained, particularly in the low-mass and low-k_{eff} case. As an additional test, the Monte Carlo N-Particle Transport Code (MCNP) was used to calculate the detection efficiency for the second test source in the configuration it was measured in including the detector and its position relative to the test object, and the size, composition, and measurement location within the room. The result of an ensemble of 100 runs are shown in Fig. 12. The interesting conclusion is that the assessed value of the mass does not improve.

MCNP was used to simulate a scenario, shown in Figs. 4 or 39, which was as follows:

1. HEU (93% enriched): $r = 7.5$ cm, $m = 33$ kg, $\rho = 18.67$ g/cm^3, mass of ^{238}U $m_S = 1.837$ kg
2. 72:18:10 (Fe:Cr:Ni) Steel: $r = 10.0$ cm, thickness $= 2.5$ cm, $m = 19.13$ kg, $\rho = 7.9$ g/cm^3
3. Inside air-filled, 1 mm thick 72:18:10 (Fe:Cr:Ni) Steel drum: $r = 30.0$ cm, $l = 88.0$ cm, $m = 17.57$ kg, $\rho = 7.9$ g/cm^3
4. One MC-15 joint multiplicity counter, front and back panels separated on either side of the drum 31 cm from the center of the source (shown in red in Fig. 4 or 39).

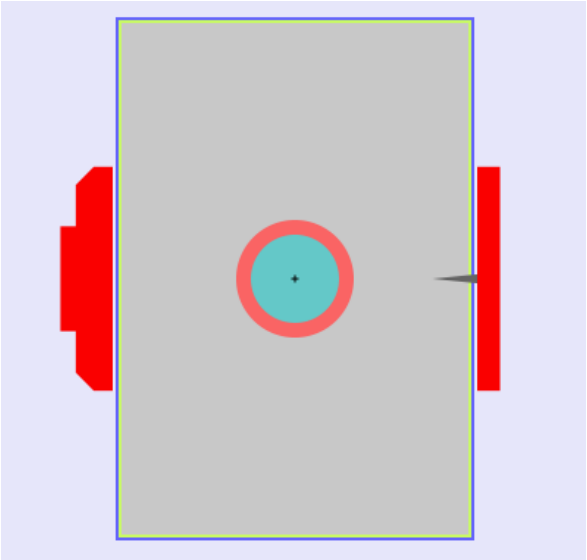

FIG. 4. Schematic of the setup of the HEU in steel configuration used in the MCNP simulation. The HEU is the turquoise ball at the center while the steel is the red layer surrounding it. This was in an air-filled 55-gallon steel drum painted with polyurethane paint. An MC-15 joint multiplicity counter was placed in close proximity to the steel drum with the front panel on the right side of the drum and the main portion of the detector on the left side.

5. Source and detector center 1 m above a 30 cm thick concrete floor. Source center 2.7 m from 30 cm thick concrete walls and ceiling.

The configuration had a high multiplication with $k_{\text{eff}} = 0.951 \equiv M = 20.5$. Because the system has no hydrogenous material to moderate the neutrons, the diffusion time $\lambda^{-1} \approx 40$ μs which coincides with the diffusion time in the MC-15 joint multiplicity counter. The true detection efficiency was $\epsilon = 1.511 \pm 0.007\%$.

As discussed in §IV E, the Kullback-Liebler distance D_{KL} was computed for the various possible values of ^{238}U mass, k_{eff}, detection efficiency ϵ, and the inverse of the neutron diffusion time λ. The Kullback-Liebler distance is a non-symmetric measure of the difference between two probability distributions and is always non-negative, $D_{\text{KL}}(P\|Q) \geq 0$, a result known as Gibbs' inequality. $D_{\text{KL}}(P\|Q) = 0$ if and only if the measured probability distribution P of waiting a certain about of time between successive neutrons equals the equivalent distribution Q calculated from, in this case, Eq. 118.

A Kullback-Liebler distance, $D_{\text{KL}}(P\|Q)$, closer to zero indicates a better estimate for the parameter in question. The ten surfaces shown (that appear stacked on top of one another) correspond to different values of detection efficiency ϵ. Note the relatively sharp canyon indicating $k_{\text{eff}} \approx 0.95$. This canyon, however, is relatively flat along ^{238}U mass showing that our algorithm is much less sensitive to mass compared to k_{eff}.

G. Moderation

The parameter λ is the fundamental-mode decay constant of the moderator-detector assembly.[11] In other words, λ^{-1} is the neutron lifetime against detection. It is the average time between when a neutron is created, diffuses through the moderator, the time-of-flight to the detector, diffusion in the detector, to finally being counted by the detector. All moderator effects are accounted for in this variable. For a ^{3}He-based detector, bare-metal sources have ≈ 0 diffusion time because of the lack of moderator as well as a time-of-flight of ≈ 0 leaving only the time for the neutrons to diffuse in the detector—typically $\lambda^{-1} \sim 40$ μs. For moderated sources, the diffusion time in the moderator and the time of flight can easily push $\lambda^{-1} \geq 100$ μs.

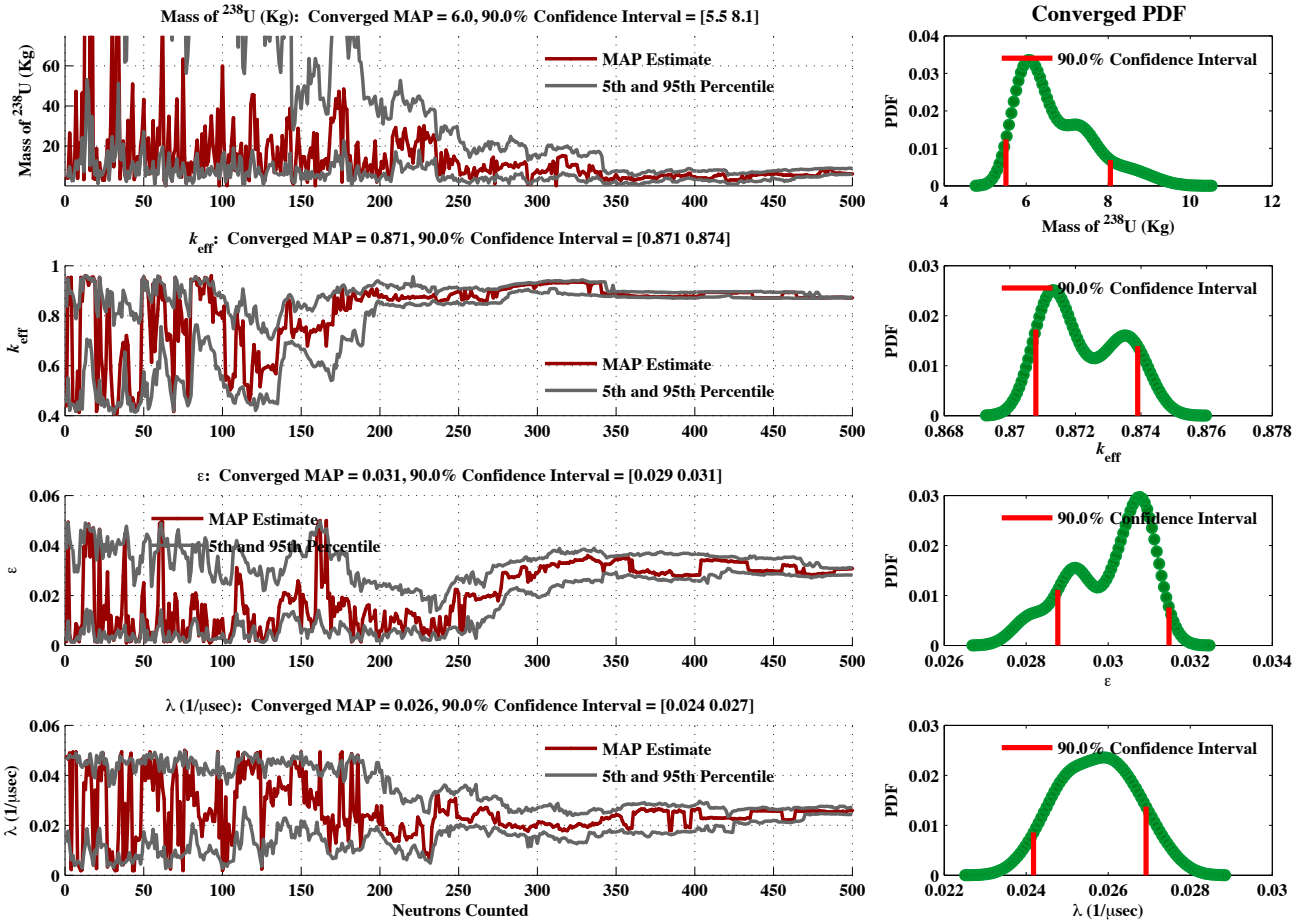

FIG. 5. Parameter estimates for 500 neutrons for the first HEU source using two MC-15 detectors connected together to function as a single, larger detector: (a) Mass of ^{238}U; (b) k_{eff}; (c) Detection efficiency ϵ; (d) Inverse diffusion time λ. The plots in the left column show the evolution of the estimate of the parameter as neutrons are counted; the x-axis is the number of neutrons counted. In the plots in the left column, the gray bands indicate the 90% confidence intervals. The plots in the right column are the PDFs for each parameter and the red lines highlight the 90% confidence intervals. The confidence intervals here use the highest-density interval (HDI) method.

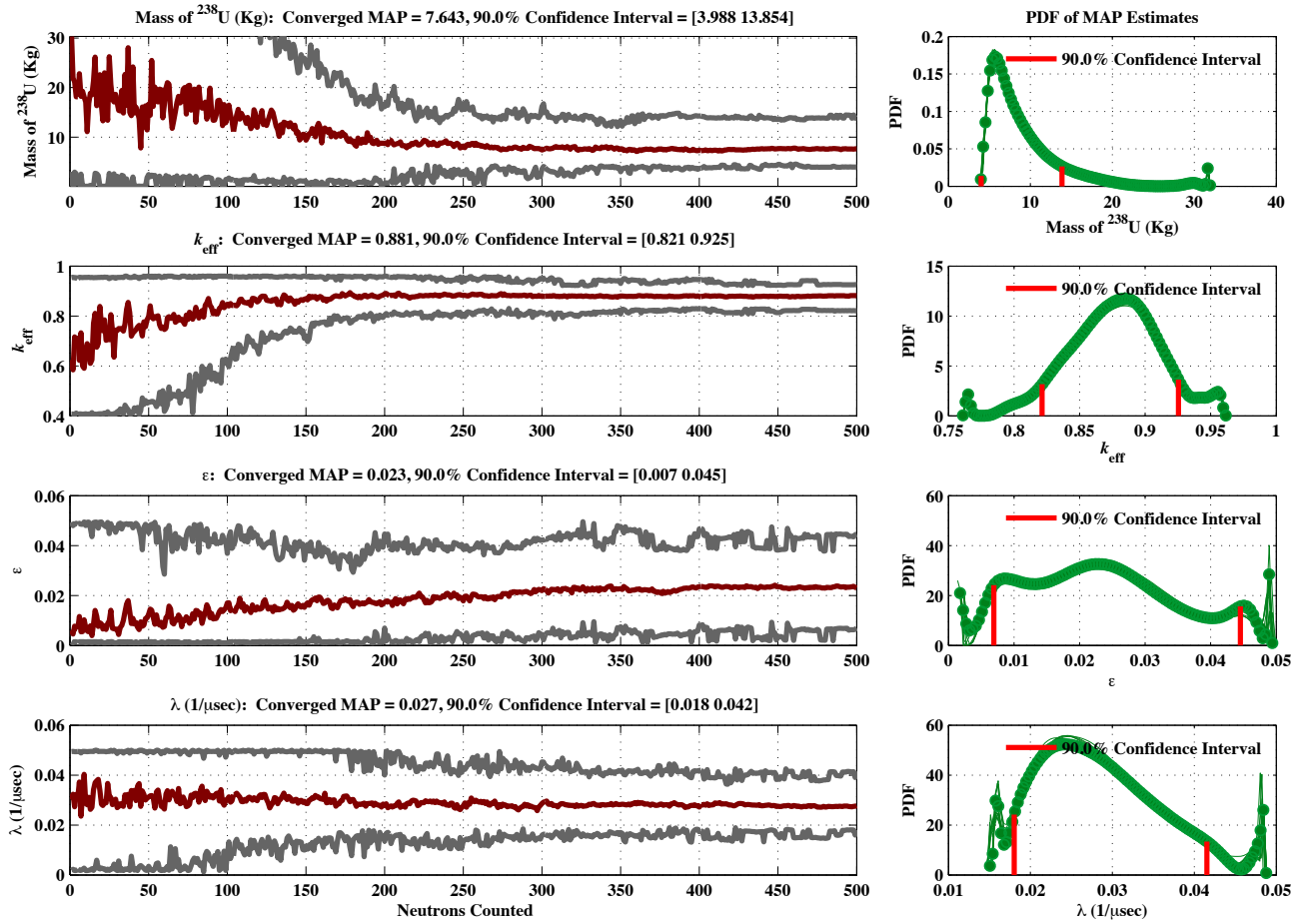

FIG. 6. Parameter estimates for an ensemble of 100 runs (500 neutrons each) for the first HEU source using two MC-15 detectors connected together to function as a single, larger detector: (a) Mass of ^{238}U; (b) k_{eff}; (c) Detection efficiency ϵ; (d) Inverse diffusion time λ. The plots in the left column show the evolution of the estimate of the parameter as neutrons are counted; the x-axis is the number of neutrons counted. In the plots in the left column, the gray bands indicate the 90% confidence intervals. The plots in the right column are the PDFs for each parameter and the red lines highlight the 90% confidence intervals. The confidence intervals here use the highest-density interval (HDI) method.

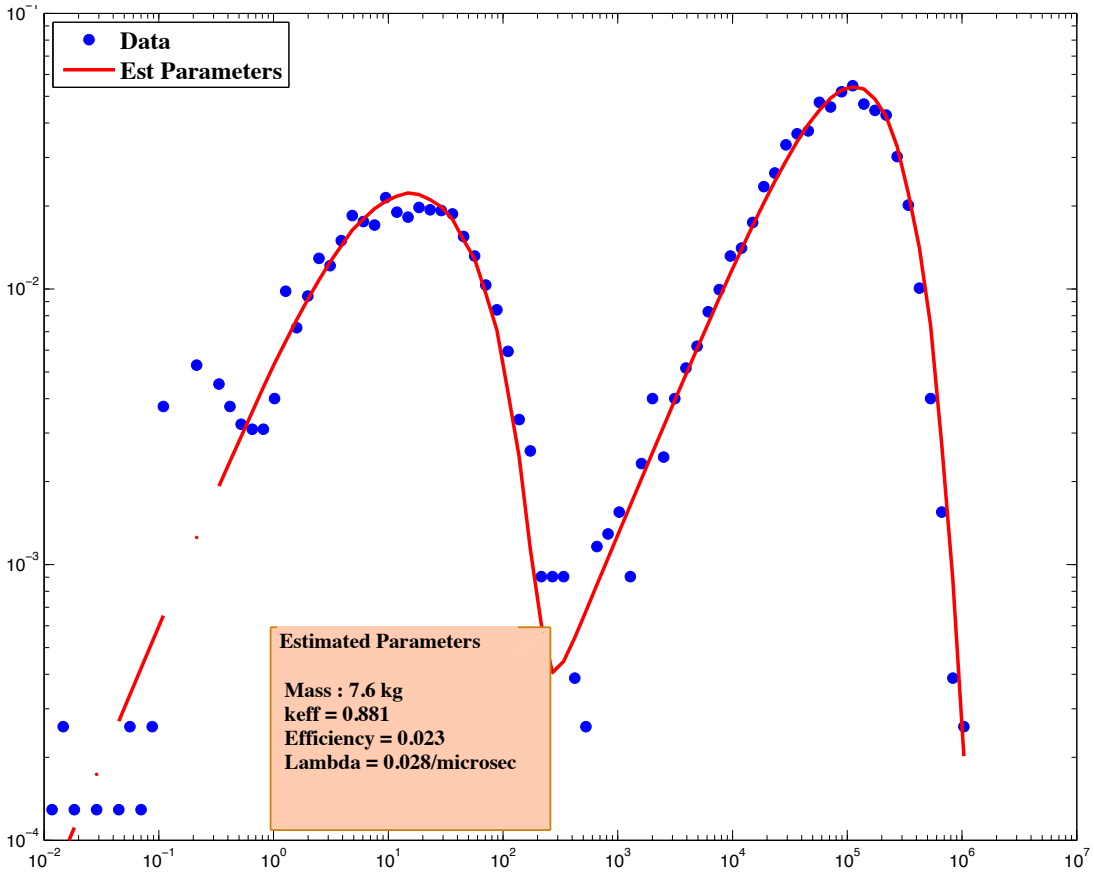

FIG. 7. Time interval distribution for the first source as measured by two MC-15 Joint Multiplicity Counters connected together. The solid red line is the theoretical distribution, Eq. 125 or 126, constructed using the estimated parameters. The blue points are the measured time interval distribution. The estimated parameters from the ensemble of 100 runs are shown in the box.

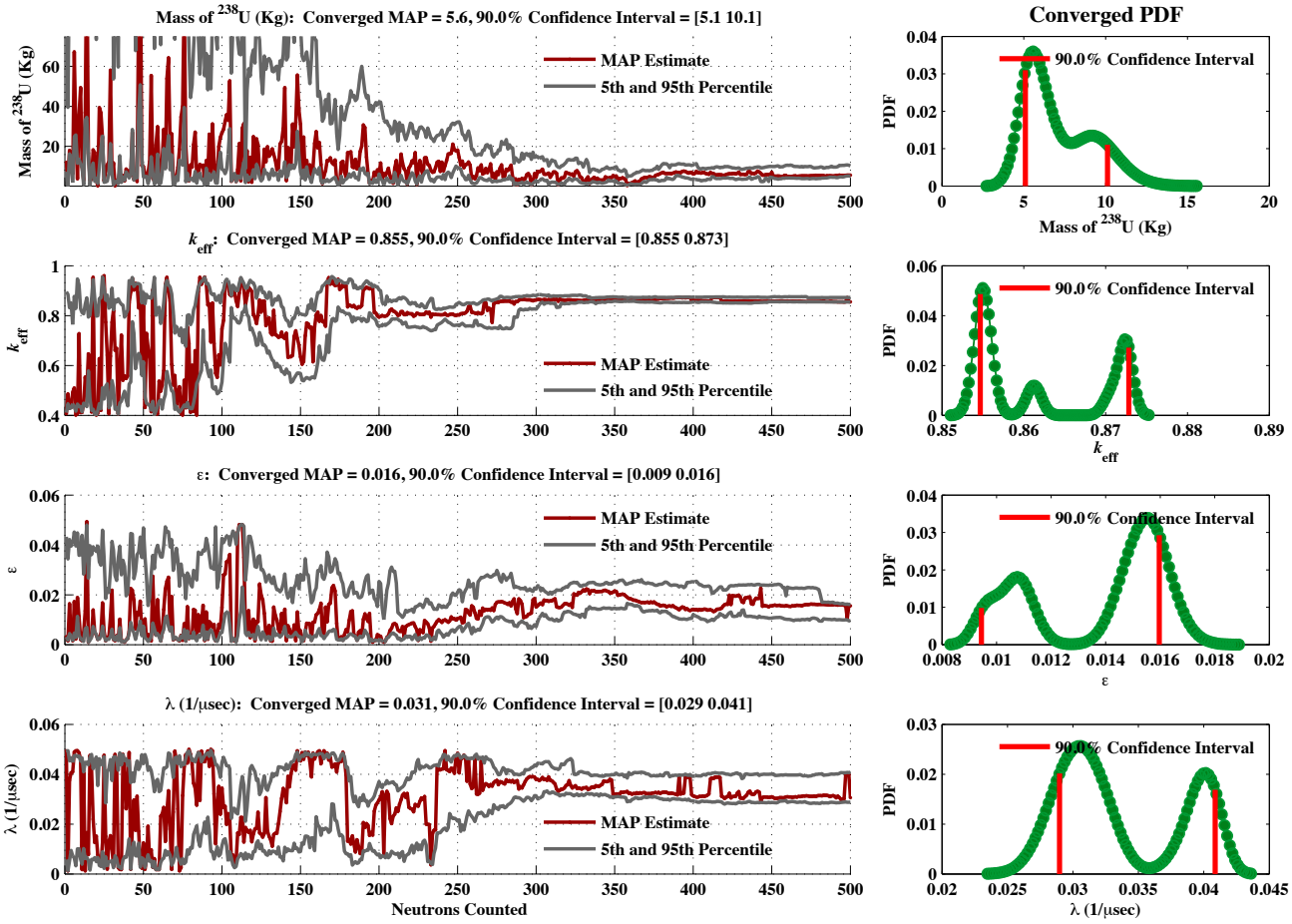

FIG. 8. Parameter estimates for 500 neutrons for the first HEU source using a single MC-15 detector: (a) Mass of ^{238}U; (b) k_{eff}; (c) Detection efficiency ϵ; (d) Inverse diffusion time λ. The plots in the left column show the evolution of the estimate of the parameter as neutrons are counted; the x-axis is the number of neutrons counted. In the plots in the left column, the gray bands indicate the 90% confidence intervals. The plots in the right column are the PDFs for each parameter and the red lines highlight the 90% confidence intervals. The confidence intervals here use the highest-density interval (HDI) method.

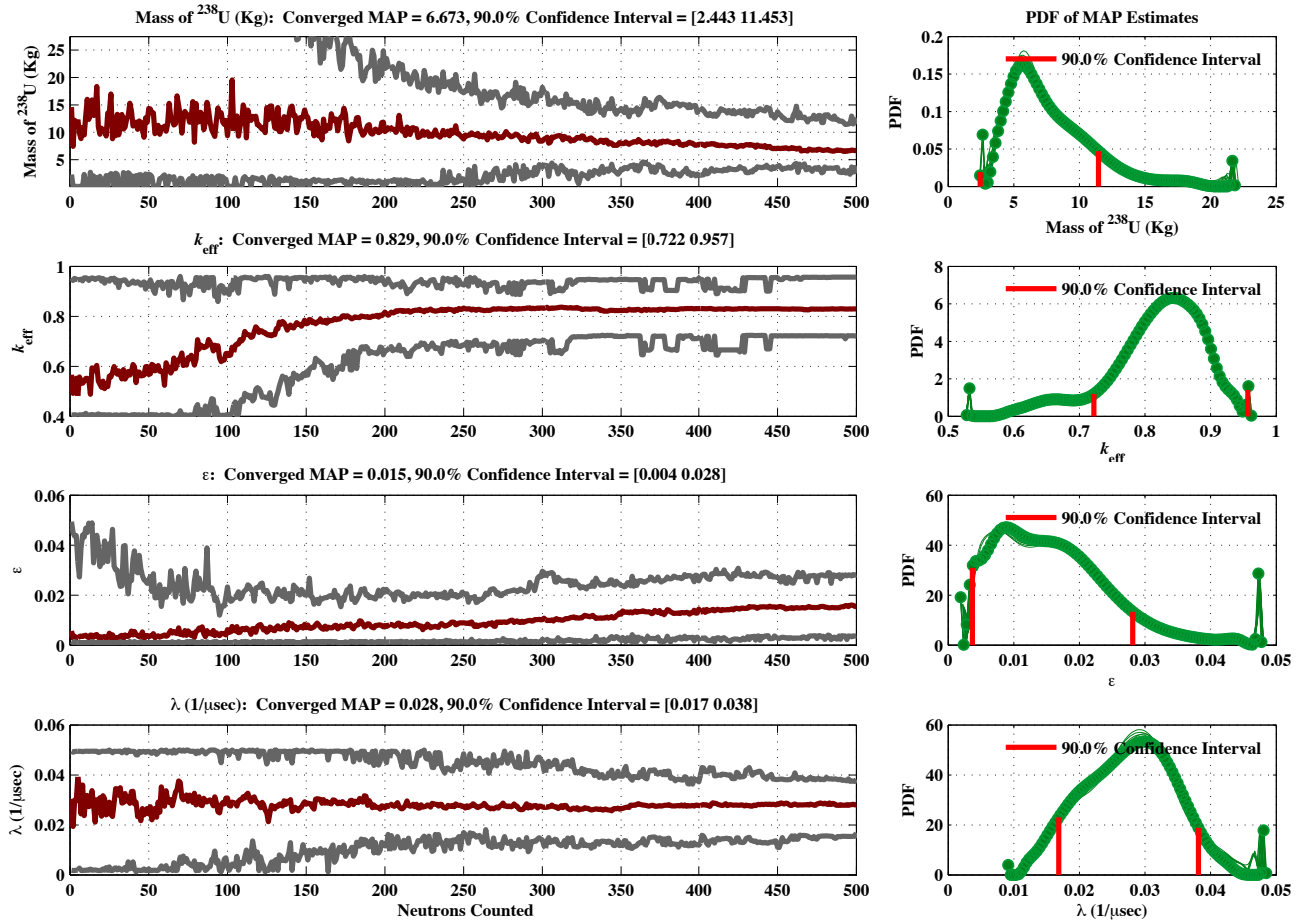

FIG. 9. Parameter estimates for an ensemble of 100 runs (500 neutrons each) for the first HEU source using a single MC-15 detector: (a) Mass of ^{238}U; (b) k_{eff}; (c) Detection efficiency ϵ; (d) Inverse diffusion time λ. The plots in the left column show the evolution of the estimate of the parameter as neutrons are counted; the x-axis is the number of neutrons counted. In the plots in the left column, the gray bands indicate the 90% confidence intervals. The plots in the right column are the PDFs for each parameter and the red lines highlight the 90% confidence intervals. The confidence intervals here use the highest-density interval (HDI) method.

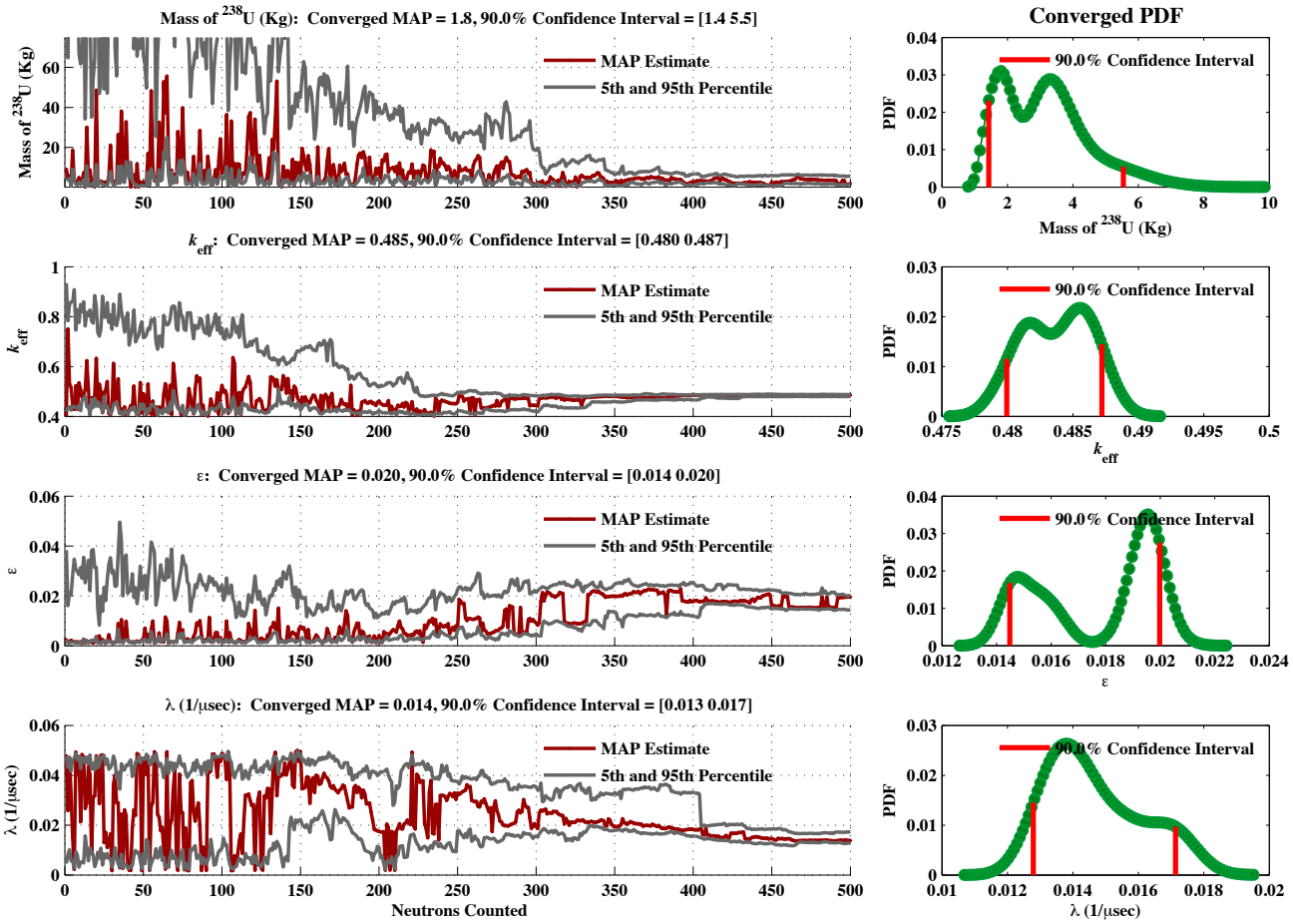

FIG. 10. Parameter estimates for 500 neutrons for the second HEU source using two MC-15 detectors connected together to function as a single, larger detector: (a) Mass of ^{238}U; (b) k_{eff}; (c) Detection efficiency ϵ; (d) Inverse diffusion time λ. The plots in the left column show the evolution of the estimate of the parameter as neutrons are counted; the x-axis is the number of neutrons counted. In the plots in the left column, the gray bands indicate the 90% confidence intervals. The plots in the right column are the PDFs for each parameter and the red lines highlight the 90% confidence intervals. The confidence intervals here use the highest-density interval (HDI) method.

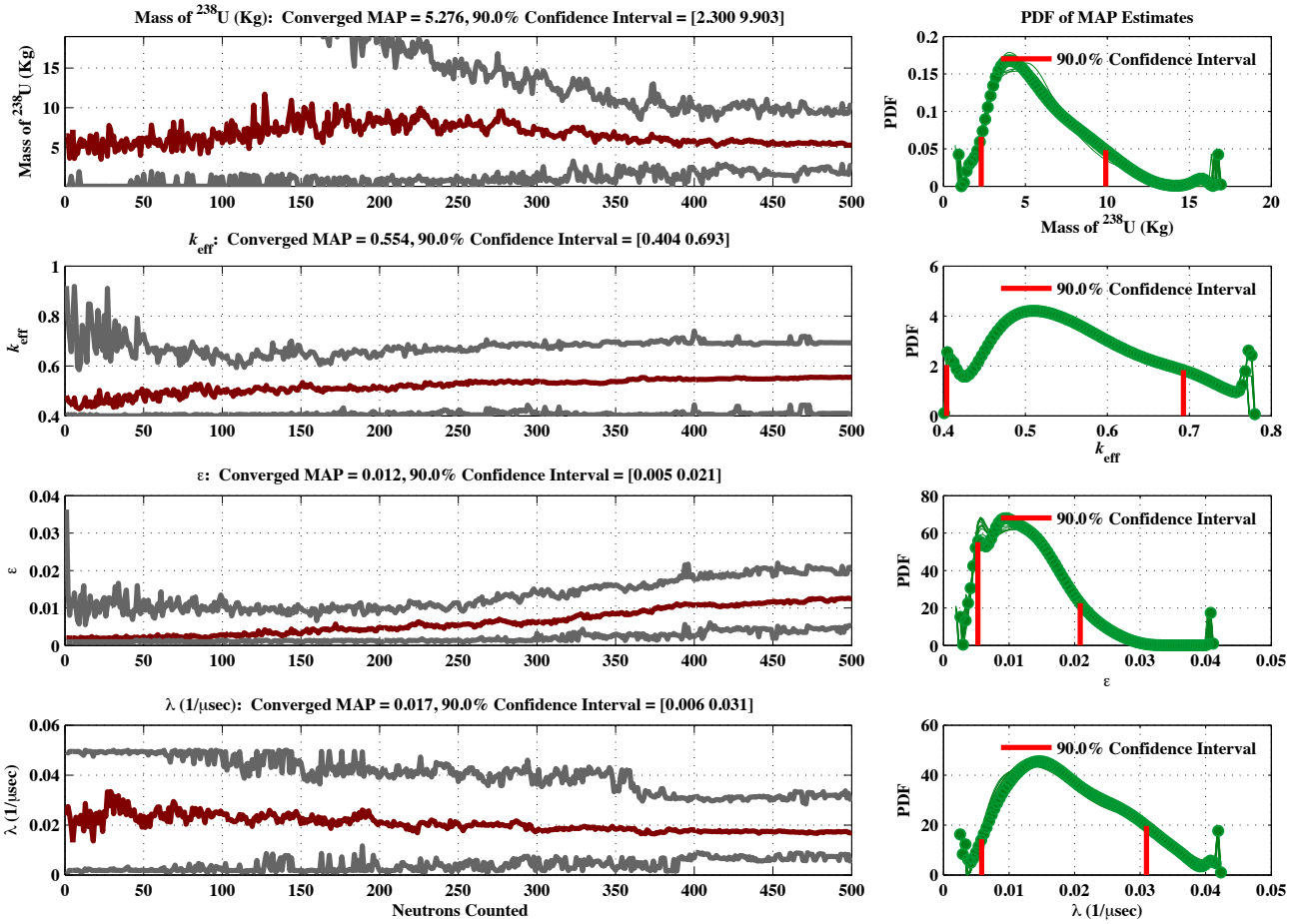

FIG. 11. Parameter estimates for an ensemble of 100 runs (500 neutrons each) for the second HEU source using two MC-15 detectors connected together to function as a single, larger detector: (a) Mass of ^{238}U; (b) k_{eff}; (c) Detection efficiency ϵ; (d) Inverse diffusion time λ. The plots in the left column show the evolution of the estimate of the parameter as neutrons are counted; the x-axis is the number of neutrons counted. In the plots in the left column, the gray bands indicate the 90% confidence intervals. The plots in the right column are the PDFs for each parameter and the red lines highlight the 90% confidence intervals. The confidence intervals here use the highest-density interval (HDI) method.

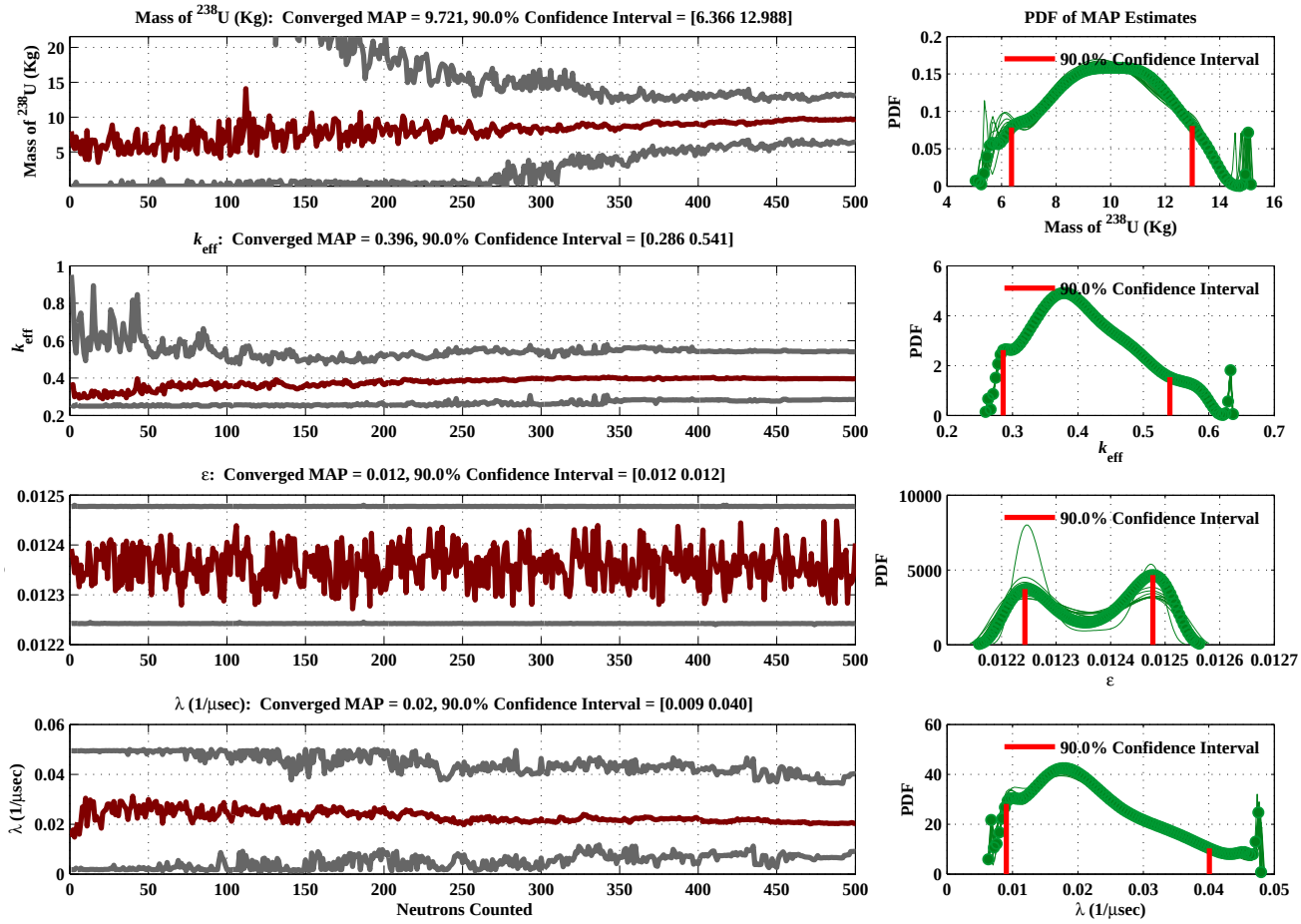

FIG. 12. Parameter estimates for an ensemble of 100 runs (500 neutrons each) for the second HEU source using two MC-15 detectors connected together to function as a single, larger detector: (a) Mass of ^{238}U; (b) k_{eff}; (c) Detection efficiency ϵ; (d) Inverse diffusion time λ. Detection efficiency was calculated independently by Monte Carlo using MCNP and the results were used to constrain that parameter in the analysis. The plots in the left column show the evolution of the estimate of the parameter as neutrons are counted; the x-axis is the number of neutrons counted. In the plots in the left column, the gray bands indicate the 90% confidence intervals. The plots in the right column are the PDFs for each parameter and the red lines highlight the 90% confidence intervals. The confidence intervals here use the highest-density interval (HDI) method.

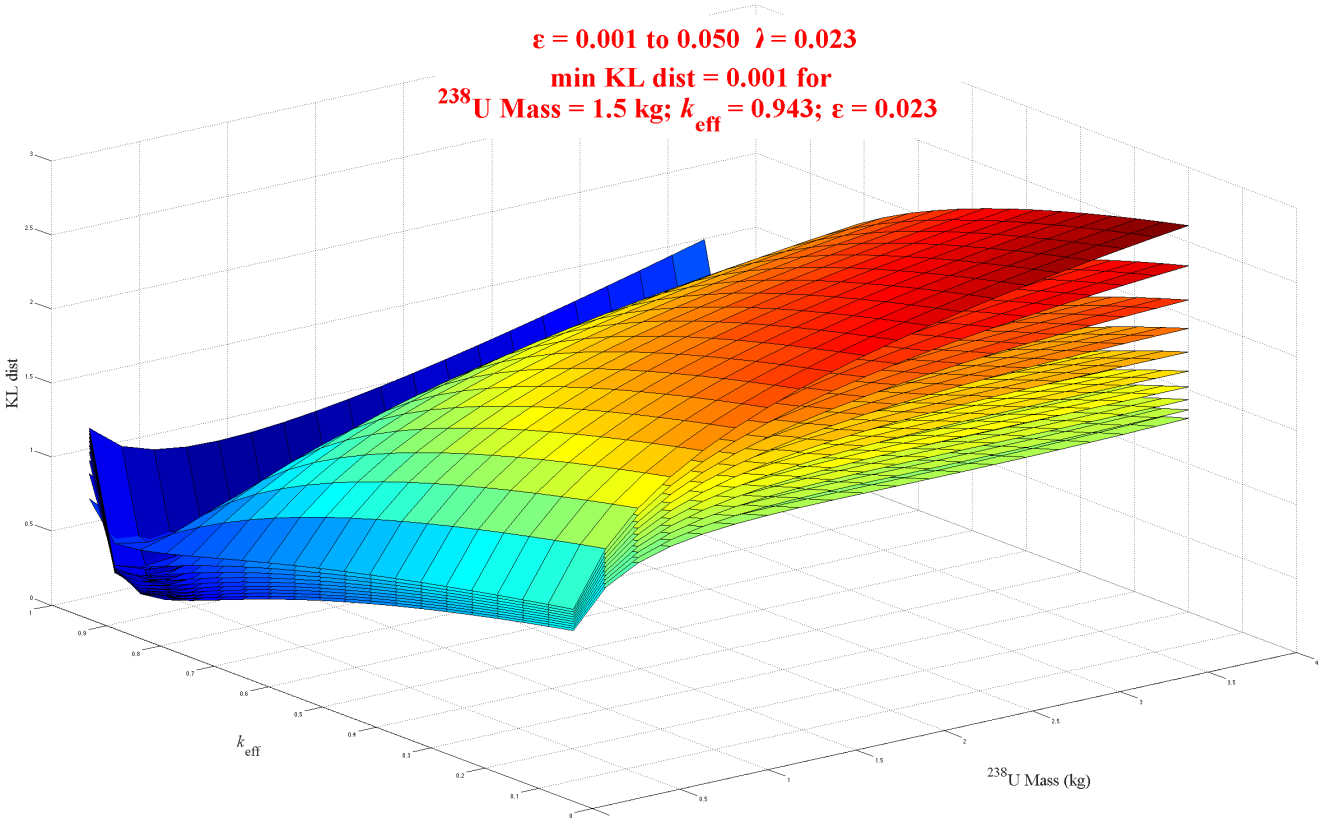

FIG. 13. Kullback-Liebler distance for the Monte Carlo simulation discussed in §IV E for the scenario shown in Figs. 4 or 39. A Kullback-Liebler distance closer to zero indicates a better estimate for the parameter in question. The ten surfaces shown (that appear stacked on top of one another) correspond to different values of detection efficiency ϵ. Note the relatively sharp canyon indicating $k_{\rm eff} \approx 0.95$. This canyon, however, is relatively flat along ^{238}U mass showing that our algorithm is much less sensitive to mass $m_{\rm S}$ compared to $k_{\rm eff}$.

II. RAPID COMPUTATION OF DISTRIBUTIONS

A. Statistical Theory of fission chains

Consider a multiplying medium at time $t = 0$ containing a *single* neutron where no neutrons have yet left. As a fission chain evolves in time, the neutrons produced by it may

1. do nothing,
2. leave the multiplying medium either through non-fission absorption or leakage, or
3. go on to induce a subsequent fission thus perpetuating the fission chain.

At time $t + \Delta t$, the probability $\mathcal{P}_{m,n}$ for m neutrons to remain in the system and n to have left can be developed by considering all the possible configurations the system can be in at time t: There could be m neutrons in the system with n having already left, and nothing happens during the time Δt; at time t, there could be $m+1$ neutrons in the system with $n-1$ having left, and one neutron could — with probability $1-p$ — get absorbed or leak out during Δt; there could be $m+1-\nu$ neutrons in the system at time t, and during Δt, one neutron could — with probability p — induce a fission with probability C_ν to produce ν neutrons; there could be $m+2$ neutrons in the system with $n-2$ having already left at time t, and two could get absorbed or leak out during Δt; and so on. The probability $\mathcal{P}_{m,n}(t+\Delta t)$ would then just be the sum of each of these probabilities,

$$\begin{aligned}\mathcal{P}_{m,n}(t+\Delta t) = {} & \mathcal{P}_{m,n}(t)\left(1-\frac{\Delta t}{\tau}\right)^m \\ & + (1-p)\mathcal{P}_{m+1,n-1}(t)\,(m+1)\,\frac{\Delta t}{\tau} \\ & + p\sum_\nu \mathcal{P}_{m+1-\nu,n}(t)C_\nu\,(m+1-\nu)\,\frac{\Delta t}{\tau} \\ & + (1-p)^2\mathcal{P}_{m+2,n-2}(t)\binom{m+2}{2}\left(\frac{\Delta t}{\tau}\right)^2 \\ & + \cdots \end{aligned} \tag{1}$$

where τ is the mean neutron lifetime against leakage and non-fission absorption. The probability p is related to the quantities k_{eff} and multiplication M as

$$k_{\text{eff}} = p\overline{\nu} \tag{2}$$

$$M = \frac{1}{1-k_{\text{eff}}} \tag{3}$$

where $\overline{\nu}$ is the average number of neutrons created by a fission.

There is no simple formula for the probabilities $\mathcal{P}_{m,n}$, but it is possible instead to give a formula for the sum of a power series whose coefficients are the probabilities $\mathcal{P}_{m,n}$ that we're interested in.[13] A generating function can be constructed by simply multiplying the probabilities $\mathcal{P}_{m,n}$ by $x^m y^n$ and summing over m and n,

$$\not{\mathcal{P}}(t,x,y) = \sum_{m=0}^{\infty}\sum_{n=0}^{\infty}\mathcal{P}_{m,n}(t)x^m y^n \tag{4}$$

where, throughout, the Feynman-slash notation denotes the generating function corresponding to a probability distribution. From Eqs. 1 and 4, the generating function $\not{\mathcal{P}}(t,x,y)$ is found to satisfy the equation[12]

$$\tau\frac{\partial\not{\mathcal{P}}}{\partial t} = \left[-x+(1-p)y+p\not{C}(x)\right]\frac{\partial\not{\mathcal{P}}}{\partial x} \tag{5}$$

where

$$\not{C}(x) = \sum_{\nu=0}^{\nu_{\max}} C_\nu x^\nu\,. \tag{6}$$

is the generating function corresponding to the probability distribution C_ν for an induced fission to produce ν neutrons.

In the limit $t\to\infty$, all neutrons are assumed to have left the system. As a result, $\not{\mathcal{P}}(t,x,y)$ becomes a function only of the neutrons that escape the system,

$$\lim_{t\to\infty}\not{\mathcal{P}}(t,x,y) \to \not{\mathcal{P}}_{\text{I}}(y) = \sum_{n=0}^{\infty}\mathcal{P}_{\text{I}n}y^n\,. \tag{7}$$

The probability distribution $\mathcal{P}_{\text{I}n}$ is the probability that a fission chain, initiated by a single neutron inducing a fission, creates n neutrons. In this limit, the corresponding generating function $\not{\mathcal{P}}_{\text{I}}(y)$ satisfies the Böhnel equation,[9]

$$\tilde{B}(\not{\mathcal{P}}_{\text{I}},y) = (1-p)y - \not{\mathcal{P}}_{\text{I}}(y) + p\not{C}\left[\not{\mathcal{P}}_{\text{I}}(y)\right] = 0\,. \tag{8}$$

A series solution to the Böhnel equation, Eq. 8, using Lagrange's series formula[12] is

$$\not{\mathcal{P}}_{\text{I}}(y) = (1-p)y + y^n\sum_{k=1}^{\infty}\frac{P_p(k|n+k)}{k+n}\sum_{\nu_0,\nu_1,\nu_2,\cdots}\frac{k!}{\nu_0!\nu_1!\nu_2!\cdots}\left(C_0^{\nu_0}C_1^{\nu_1}C_2^{\nu_2}\cdots\right) \tag{9}$$

where

$$P_p(k|n+k) = \frac{(k+n)!}{k!n!}p^k(1-p)^n \tag{10}$$

is the binomial distribution[14] for k "sucesses" out of $k+n$ trials if the probability of a "success" is p, and where ν_0 is the number of fissions which produce zero neutrons, ν_1 is the number of fissions which produce one neutron,

ν_2 the number of fissions which produce two neutrons, and so on. The quantity k here has the interpretation of the total number of fissions in the chain. The probability distribution $\mathcal{P}_{\mathrm{I}n}$ that we want are the coefficients on y^n (Eq. 7).

B. Fourier method for computing the multiplicity distribution for induced fission-initiated chains

The Böhnel equation[9] $\tilde{B}(\mathcal{P}_{\mathrm{I}}, y)$ is a polynomial of order $\nu_{\max}$ in $\mathcal{P}_{\mathrm{I}}$ with coefficients as follows:

$$\underbrace{pC_{\nu_{\max}}}_{\nu_{\max}^{\mathrm{th}}}\left[\mathcal{P}_{\mathrm{I}}(y)\right]^{\nu_{\max}} + \cdots + \underbrace{pC_2}_{2^{\mathrm{nd}}}\left[\mathcal{P}_{\mathrm{I}}(y)\right]^2 + \underbrace{(pC_1 - 1)}_{1^{\mathrm{st}}}\mathcal{P}_{\mathrm{I}}(y) + \underbrace{pC_0 + (1-p)y}_{0^{\mathrm{th}}} = 0 \tag{11}$$

The generating function $\mathcal{P}_{\mathrm{I}}(y)$ is obtained by solving for the root of $\tilde{B}(\mathcal{P}_{\mathrm{I}}, y)$ at each value of y starting from $\mathcal{P}_{\mathrm{I}}(1) = 1$. Again, the quantity p is the probability that a neutron induces a fission and is related to the parameter k_{eff} by $k_{\mathrm{eff}} = \overline{\nu}p$, where $\overline{\nu}$ is the average number of neutrons produced by an induced fission. Though an exact solution, numerical evaluation of the series requires calculating multinomial coefficients (Eqs. 8 and 9) which can be problematic for large n. However, since the basic problem is calculating the roots of a low order polynomial (typically less than tenth order) as a function of a parameter (y for the generating function), we can consider approaches based on numerical root extraction.

If we set $y = e^{i\theta}$ in the generating function $\mathcal{P}_{\mathrm{I}}(y)$, we obtain the characteristic function for the induced neutron multiplicities:

$$g(\theta) = \mathcal{P}_{\mathrm{I}}\left(e^{i\theta}\right) \tag{12}$$

$$= \sum_{n=0}^{\infty} \mathcal{P}_{\mathrm{I}n} e^{in\theta} \,. \tag{13}$$

The characteristic function is periodic on the interval $-\pi \geq \theta < \pi$ (or any other θ interval of length 2π). The induced multiplicities can be calculated from $g(\theta)$ using the Fourier transform:

$$\mathcal{P}_{\mathrm{I}n} = \frac{1}{2\pi}\int_{-\pi}^{\pi} g(\theta) e^{-in\theta}\, d\theta \,. \tag{14}$$

Furthermore, the characteristic function can be obtained by calculating the roots of the complex Böhnel equation,

$$\tilde{B}(g, \theta) = (1-p)e^{i\theta} - g(\theta) + p\mathcal{C}\left[g(\theta)\right] = 0 \,. \tag{15}$$

The particular roots of physical interest lie within the unit circle in the complex g plane ($|g(\theta)| \leq 1$) and include the point $g(0) = 1$.

Figure 14 shows all roots of the Böhnel equation for both the generating function $\mathcal{P}_{\mathrm{I}}(y)$ (Eq. 8) and the characteristic function $g(\theta)$ (Eq. 15 for ^{235}U with $k_{\mathrm{eff}} = 0.8$ corresponding to a multiplication $M = 5$). These are generated by solving for the roots for each value of y or θ, as appropriate, for a set range of y and θ values. The number of roots is determined by the order of the polynomial $\mathcal{C}(x)$, *e.g.* seven for ^{235}U. As the parameters y or θ are varied, the roots change continuously and form a root locus diagram in the complex $\mathcal{P}_{\mathrm{I}}$ or g plane. The physical root for $\mathcal{P}_{\mathrm{I}}(y)$ that defines the multiplicity generating function is the root that lies along the real axis in

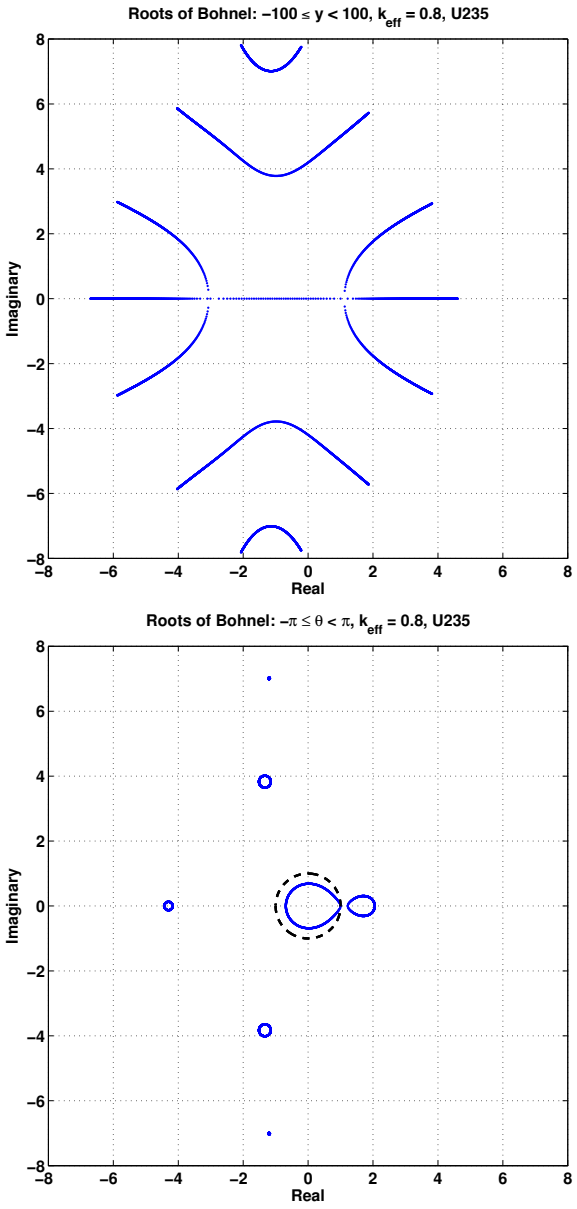

FIG. 14. Roots $\mathcal{P}_{\mathrm{I}}(y)$ of the Böhnel equation $\tilde{B}(h, y) = 0$ (top) and $g(\theta)$ of $B(g, \theta) = 0$ (bottom) for ^{235}U with $k_{\mathrm{eff}} = 0.8$. The physical root $\tilde{B}(h, y) = 0$ lies on the real axis of the h plane. The physical root for $B(g, \theta) = 0$ lies within the unit circle (dashed) on the complex g plane except for the point $g(0) = 1$.

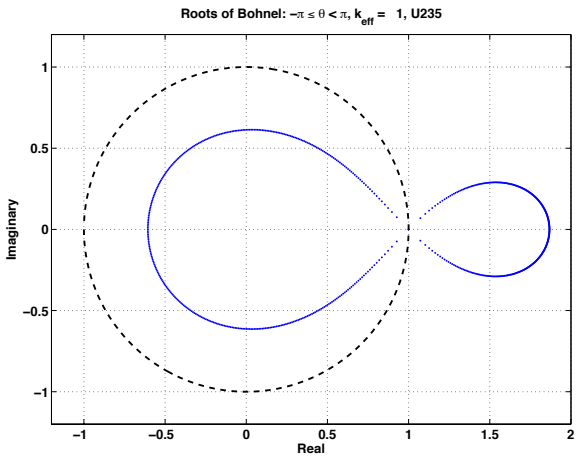

FIG. 15. Roots $g(\theta)$ of the Böhnel equation $B(g,\theta) = 0$ for ^{235}U with $k_{\rm eff} = 1.0$. The physical root lies within the unit circle (dashed) on the complex g plane but intersects a non-physical root, forming a double root at $g = 1$ when $\theta = 0$.

the complex $\mathcal{P}_{\rm I}$ plane. There are two points (particular values of y) where the real root is double, near $\mathcal{P}_{\rm I} = -3$ and $\mathcal{P}_{\rm I} = 1$. The length of the curves defined by the roots depends on the range of y ($-100 \le y \le 100$ in Fig. 14). The curves would extend to infinity as $|y| \to \infty$. This pattern of root loci does not change with different $k_{\rm eff}$.

The roots of $\tilde{B}(g,\theta) = 0$ are periodic functions of θ since the parameter appears as $e^{i\theta}$ in Eq. 15. The root locus diagram (second plot in Fig. 14) consists of seven (for the case of ^{235}U) closed loops, one for each root. The root corresponding to the characteristic function $g(\theta)$ is the loop enclosed by the unit circle. It also satisfies the condition $g(0) = 1$. A second, non-physical, root lies just outside the unit circle. As $k_{\rm eff}$ approaches unity, the physical root and this second root approach one another on the real axis until they intersect, forming a double root at $g = 1$ when $k_{\rm eff} = 1$ (see Fig. 15). The conditions for a double root are $\tilde{B}(g,\theta) = 0$ and simultaneously $\partial\tilde{B}/\partial g = 0$. Evaluating the second condition at $g = 1$ and $\theta = 0$ gives

$$\left.\frac{\partial \tilde{B}}{\partial g}\right|_{\substack{g=1,\\ \theta=0}} = p \left.\frac{d\mathcal{C}(g)}{dg}\right|_{g=1} - 1 \qquad (16)$$

$$= p\overline{\nu} - 1 \qquad (17)$$

$$= k_{\rm eff} - 1\,. \qquad (18)$$

This is zero when $k_{\rm eff} = 1$, proving that the point $g = 1$ is a double root in this limit.

After calculating the physical root $g(\theta)$ of the Böhnel equation (Eq. 15) as a function of the parameter θ over the range $-\pi \le \theta < \pi$, we can obtain the induced multiplicity distribution ($\mathcal{P}_{{\rm I}n}$, $n = 0, 1, ...$) by applying the Fourier transform, Eq. 14. Figure 16 shows the real and imaginary parts of $g(\theta)$ for three values of $k_{\rm eff} = 0.8$, 0.9, and 1.0. Multiplicity distributions for $k_{\rm eff} = 0.8$, 0.9, 0.95, and 0.975 are shown in Fig. 17. The Fourier transform relationship between $g(\theta)$ and $\mathcal{P}_{{\rm I}n}$ means the low order multiplicities (n small) depend on the overall shape (large scales) of $g(\theta)$, while the higher order $\mathcal{P}_{{\rm I}n}$ are governed by the behavior at small scales, in particular the region near $\theta = 0$ where the curvature is highest. The separation of scales is especially important as $k_{\rm eff} \to 1$ (high multiplications) and allows us to determine the asymptotic behavior of $\mathcal{P}_{{\rm I}n}$ for large n.

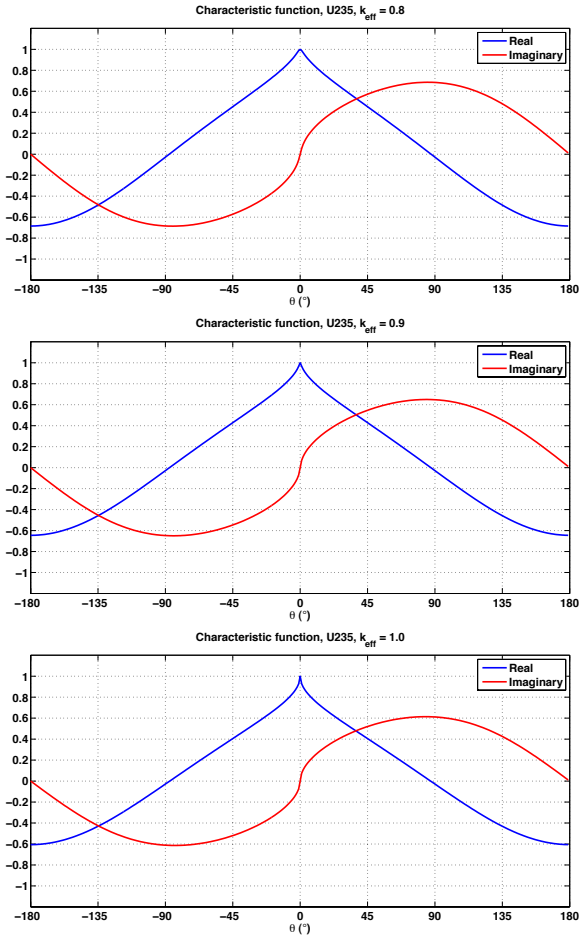

FIG. 16. Real and imaginary parts of $g(\theta)$ for $k_{\rm eff} = 0.8$ (top), $k_{\rm eff} = 0.9$ (middle), and $k_{\rm eff} = 1.0$ (bottom). In all cases the region with the most rapid variation is near $\theta = 0$. As $k_{\rm eff}$ approaches unity, the real part approaches a cusp at $\theta = 0$ and the imaginary part becomes a vertical slope.

The curvature of $g(\theta)$ at $\theta = 0$ can be calculated from the second derivative of Eq. 15 with respect to θ:

$$\left.\frac{\partial^2 g}{\partial\theta^2}\right|_{\theta=0} = -\frac{1-p}{1-k_{\rm eff}}\left[1 + \frac{p(1-p)\overline{\nu^2}}{(1-k_{\rm eff})^2}\right]\,. \qquad (19)$$

As $k_{\rm eff}$ approaches unity the second derivative (and curvature) becomes infinite. In Fig. 16, the real part $g(\theta)$ appears to form a cusp at $\theta = 0$, while the imaginary part appears to have a vertical slope. In fact, by assuming that $g(\theta)$ near $\theta = 0$ has the behavior $g(\theta) \sim 1 - g_1\theta^\beta$ (g_1 and β constants) when $k_{\rm eff} = 1$, we can derive the fol-

lowing expression for the local behavior of $g(\theta)$ around the origin:

$$g(\theta) \sim 1 - [1 - i\,\mathrm{sgn}(\theta)]\sqrt{\frac{\overline{\nu} - 1}{\overline{\nu^2}}|\theta|}\,, \tag{20}$$

$$\overline{\nu^2} = \left.\frac{d\not{C}^2(x)}{dx^2}\right|_{x=1}, \tag{21}$$

where $\mathrm{sgn}(\theta)$ is the sign of θ. This expression has the expected property that the second derivative at $\theta = 0$ is infinite. Furthermore, it confirms the numerical results that the real part of $g(\theta)$ has a cusp and the imaginary part has infinite slope. Since the cusp is described by $\theta^{1/2}$, the Fourier coefficients $\mathcal{P}_{\mathrm{I}n}$ for large order ($n \gg 1$) should decay as $n^{-3/2}$. [15]

For $k_{\mathrm{eff}} < 1$, $g(\theta)$ near $\theta = 0$ can be represented by the first two terms of the Taylor series:

$$g(\theta) \approx 1 + \frac{1}{2}\left.\frac{\partial^2 g}{\partial\theta^2}\right|_{\theta=0}. \tag{22}$$

Setting the right side to zero, we can derive a "length" scale θ_c:

$$\theta_c = \sqrt{-2\left(\left.\frac{\partial^2 g}{\partial\theta^2}\right|_{\theta=0}\right)^{-1}}. \tag{23}$$

For $\theta \ll \theta_c$, $g(\theta)$ is smooth and continuous. For scales greater than θ_c, $g(\theta)$ would appear to have the cusp discontinuity at $\theta = 0$. Thus $\mathcal{P}_{\mathrm{I}n}$ for $1 \ll n \ll \pi/\theta_c$ should decrease approximately as $n^{-3/2}$, then drop off faster for $n \gg \pi/\theta_c$. The distinction between these two regions of asymptotic behavior would become more prominent as $k_{\mathrm{eff}} \to 1$ and $\theta_c \to \infty$. From this, we can deduce how the first moment of $\mathcal{P}_{\mathrm{I}n}$ diverges as the multiplication $M = (1 - k_{\mathrm{eff}})^{-1}$ becomes infinite. Since the $\mathcal{P}_{\mathrm{I}n}$ decays rapidly for $n \gg \pi/\theta_c$, we can approximate the first moment as

$$\sum_{n=1}^{\infty} n\mathcal{P}_{\mathrm{I}n} \sim \alpha \sum_{n=1}^{\pi/\theta_c} n^{-1/2}\,, \tag{24}$$

where α is some constant and the upper limit of the second sum is understood to be the nearest integer to π/θ_c. As $k_{\mathrm{eff}} \to 1$, the upper limit π/θ_c becomes infinite and the sum diverges while maintaining the condition that the sum of $\mathcal{P}_{\mathrm{I}n}$ is unity.

C. Number of roots of the Böhnel polynomial $\tilde{B}(g,\theta)$ inside the unit circle

There is only one root of $B(z,\theta) = 0$ on or within the unit circle, $z = e^{i\phi}$, of the complex z plane. To show this, we will apply Rouche's theorem:[16]

Theorem (Rouche). *Let U be a bounded region in the complex plane with continuous boundary C, and let $f(z)$ and $h(z)$ be two functions analytic on U (and boundary C). Then $f(z)$ and $f(z)+h(z)$ have the same number of roots in U if the strict inequality*

$$|h(z)| < |f(z)| \tag{25}$$

holds on C.

We will first show there is only one root inside the unit circle for the case $\theta \neq 0$. Choose

$$f(z,\theta) = (1-p)e^{i\theta} - z \tag{26}$$

$$h(z) = p\not{C}(z) \tag{27}$$

where $B(z,\theta) = f(z,\theta) + h(z)$. The magnitude of $f(z)$ on the unit circle is

$$|f(e^{i\phi},\theta)| = \sqrt{(1-p)^2 + 1 - 2(1-p)\cos(\phi-\theta)}\,. \tag{28}$$

This has a tight lower bound of p, which is attained when $\phi = \theta$. A tight upper bound for $h(z)$ on the unit circle is

$$|h(e^{i\phi})| = p|\not{C}(e^{i\phi})| \le p\not{C}(|e^{i\phi}|) = p\,. \tag{29}$$

The upper bound is attained when $\phi = 0$. As long as $\theta \neq 0$ the upper bound for $|h|$ will not coincide with the lower bound of $|f|$, maintaining a strict inequality $|h(z)| < |f(z)|$ on the unit circle. The one root for $f(z)$ ($z_0 = (1-p)e^{i\theta}$) lies inside the unit circle. Thus $B(z,\theta)$ has only one root within the unit circle when $\theta \neq 0$.

For the case $\theta = 0$, the upper bound for $h(z)$ and the lower bound for $f(z)$ will coincide when $z = 1$ ($\phi = 0$), violating the strict inequality required for Rouche's theorem. Furthermore, we know $B(z,0) = 0$ when $z = 1$, which is on the unit circle. We can show that there are no other roots of $B(z,0)$ in the unit circle by factoring

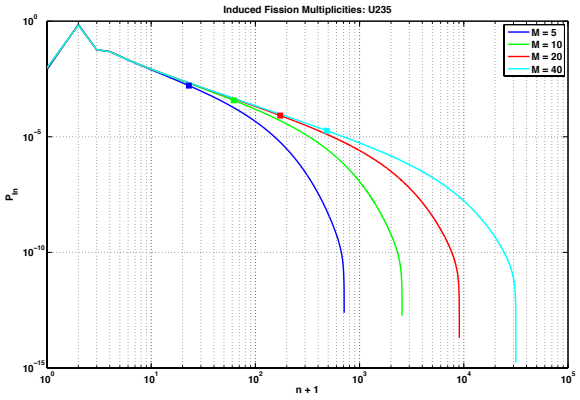

FIG. 17. Multiplicity distributions for induced fission of ^{235}U ($\mathcal{P}_{\mathrm{I}n}$). Shown are distributions for $k_{\mathrm{eff}} = 0.8$ ($M = 5$), 0.9 ($M = 10$), 0.95 ($M = 20$, and 0.975 ($M = 40$). Squares mark the estimated transition point (π/θ_c) between power law behavior $n^{-3/2}$ and a more rapid decrease as predicted by Eq. 23.

out the known zero, *i.e.* let $B(z,0) = (1-z)B_0(z)$, then

$$\begin{aligned} B_0(z) &= 1 - p\frac{1-\mathcal{C}(z)}{1-z} \\ &= 1 - p\frac{\mathcal{C}(1)-\mathcal{C}(z)}{1-z} \\ &= 1 - \frac{p}{1-z}\sum_{n=0}^{N} C_n(1-z^n) \\ &= 1 - p\sum_{n=1}^{N} C_n \sum_{m=1}^{n-1} z^m \\ &= 1 - p\sum_{m=0}^{N-1} z^m \sum_{n=m+1}^{N} C_n \,. \end{aligned} \tag{30}$$

Define

$$\begin{aligned} f_0(z) &= 1\,, \\ h_0(z) &= -p\sum_{m=0}^{N-1} z^m \sum_{n=m+1}^{N} C_n\,, \end{aligned} \tag{31}$$

and calculate an upper bound for $h_0(e^{i\phi})$:

$$\begin{aligned} |h_0(e^{i\phi})| &= p\left|\sum_{m=0}^{N-1} e^{im\phi} \sum_{n=m+1}^{N} C_n\right| \\ &\le p\sum_{m=0}^{N-1}\sum_{n=m+1}^{N} C_n \\ &\le p\sum_{n=1}^{N} nC_n \\ &\le p\,\overline{\nu} = k_{\text{eff}}\,. \end{aligned} \tag{32}$$

Thus for $k_{\text{eff}} < 1$ we have $|h_0(e^{i\phi})| < |f_0(e^{i\phi})| = 1$, and $B_0(z)$ has no roots within the unit circle. This completes the proof that there is one and only one root for $B(z,\theta)$ within the unit circle for any value of θ in the range $-\pi \le \theta < \pi$.

D. Extension to the multiplicity distribution for spontaneous fission-initiated chains

The generating function $\mathcal{S}(z)$ of the sum of two independent random variables x_1 and x_2 is the product of the generating functions for x_1 and x_2; $\mathcal{S}(z) = \mathcal{X}_1(z)\mathcal{X}_2(z)$. For a compound process, the generating function of a sum of a random number of random variables $x_1, x_2, \cdots, x_n$, where n is itself a random variable with generating function $\mathcal{N}(z)$, is $\mathcal{N}\left[\mathcal{S}(z)\right]$.

For fission chains initiated by spontaneous fission, it becomes necessary to compute the probability distribution $\mathcal{P}_{\text{S}n}$ which is the probability that a fission chain initiated by a spontaneous fission creates n neutrons. Starting with the probability $C_{\text{S}\nu}$ that a spontaneous fission creates ν neutrons, the corresponding generating function is

$$\mathcal{C}_{\text{S}}(x) = \sum_{\nu=0}^{\nu_{\max}} C_{\text{S}\nu}x^{\nu}\,. \tag{33}$$

The generating function for the number of neutrons a spontaneous fission-initiated fission chain creates is then

$$\mathcal{P}_{\text{S}}(y) = \mathcal{C}_{\text{S}}\left[\mathcal{P}_{\text{I}}(y)\right] \tag{34}$$

where, in the generating function $\mathcal{C}_{\text{S}}(x)$, $x \to \mathcal{P}_{\text{I}}(y)$. The values of the probability distribution $\mathcal{P}_{\text{S}n}$ that we want are the coefficients on y^n in $\mathcal{P}_{\text{S}}(y)$, Eq. 34,

$$\mathcal{P}_{\text{S}}(y) = \sum_{n=0}^{\infty} P_{\text{S}n}y^n \tag{35}$$

This relation directly translates for the characteristic functions:

$$g_{\text{S}}(\theta) = \mathcal{C}_{\text{S}}\left[g(\theta)\right]\,. \tag{36}$$

The multiplicity distribution for spontaneous fission-initiated fission chains $\mathcal{P}_{\text{S}n}$ is obtained from the Fourier transform as before:

$$\mathcal{P}_{\text{S}n} = \frac{1}{2\pi}\int_{-\pi}^{\pi} g_{\text{S}}(\theta)e^{-in\theta}\,d\theta\,. \tag{37}$$

E. Extension to number of detected neutrons

Applying the same logic developed for a compound process again, the probabilities $\text{e}_{\text{I}m}$ and $\text{e}_{\text{S}m}$ of detecting m of the n neutrons created by induced fission-initiated and a spontaneous fission-initiated fission chain are calculated as

$$\mathcal{P}_{\text{I}}(y) = \mathcal{P}_{\text{I}}\left[\mathcal{E}(y)\right] \tag{38}$$

$$\begin{aligned} \mathcal{P}_{\text{S}}(y) &= \mathcal{P}_{\text{S}}\left[\mathcal{E}(y)\right] \\ &= \mathcal{C}_{\text{S}}\left\{\mathcal{P}_{\text{I}}\left[\mathcal{E}(y)\right]\right\} \\ &= \mathcal{C}_{\text{S}}\left[\mathcal{P}_{\text{I}}(y)\right] \end{aligned} \tag{39}$$

where in the absence of detector double-pulsing, the generating function $\mathcal{E}(y)$ for a detection efficiency of ϵ is

$$\mathcal{E}(y) = (1-\epsilon) + \epsilon y \tag{40}$$

For induced fission-initiated fission chains, Eq. 11 becomes

$$\begin{aligned} &\underbrace{pC_{\nu_{\max}}}_{\nu_{\max}^{\text{th}}}\left[\mathcal{P}_{\text{I}}(y)\right]^{\nu_{\max}} + \cdots + \underbrace{pC_2}_{2^{\text{nd}}}\left[\mathcal{P}_{\text{I}}(y)\right]^2 \\ &+ \underbrace{(pC_1 - 1)}_{1^{\text{st}}}\mathcal{P}_{\text{I}}(y) + \underbrace{pC_0 + (1-p)\epsilon y + (1-p)(1-\epsilon)}_{0^{\text{th}}} = 0 \end{aligned} \tag{41}$$

These computations can easily be checked by compar-

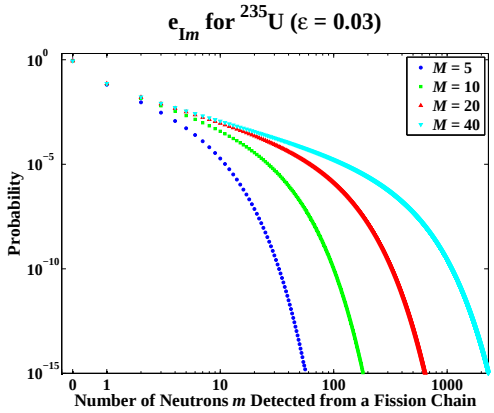

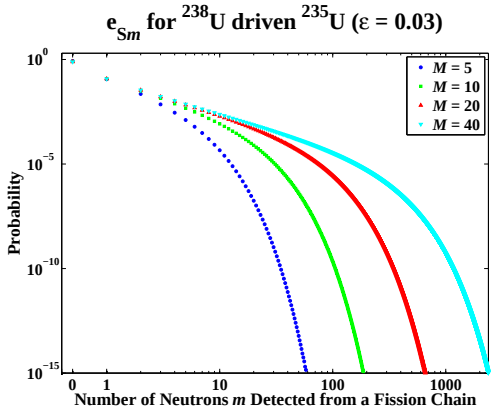

FIG. 18. The probability to detect m neutrons from a fission chain in ^{235}U initiated by a single neutron $\mathrm{e}_{\mathrm{I}m}$ (top plot) and initiated by spontaneous-fissions in^{238}U $\mathrm{e}_{\mathrm{S}m}$ (bottom plot). Detection efficiency $\epsilon = 0.03$.

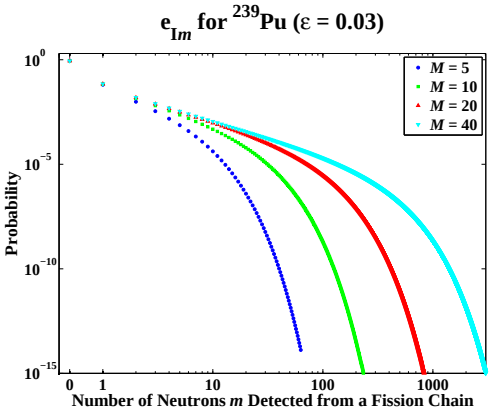

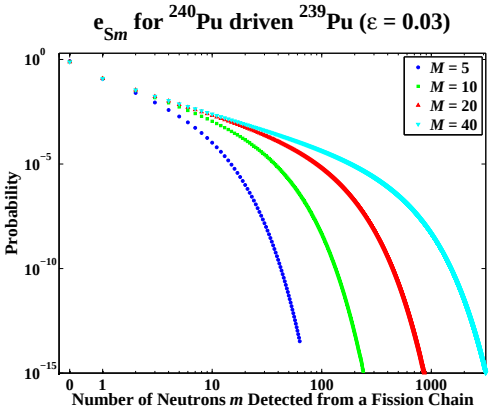

FIG. 19. The probability to detect m neutrons from a fission chain in ^{239}Pu initiated by a single neutron $\mathrm{e}_{\mathrm{I}m}$ (top plot) and initiated by spontaneous-fissions in^{240}Pu $\mathrm{e}_{\mathrm{S}m}$ (bottom plot). Detection efficiency $\epsilon = 0.03$.

ing the combinatorial moments of the $\mathrm{e}_{\mathrm{I}m}$ or $\mathrm{e}_{\mathrm{S}m}$ distributions to first-principles calculations. For fission chains initiated by a single neutron inducing a fission, the quantity

$$R_{\mathrm{I}j} = \sum_{m=j}^{\infty} \binom{m}{j} \mathrm{e}_{\mathrm{I}m} \,. \tag{42}$$

From first-principles, it can be shown that[11]

$$R_{\mathrm{I}j} = \epsilon^j F_{\mathrm{I}} \begin{cases} M_{\mathrm{e}} & j = 1 \\ M_{\mathrm{e}}^2 \dfrac{M_{\mathrm{e}} - 1}{\overline{\nu} - 1} \overline{\nu_2} & j = 2 \\ M_{\mathrm{e}}^3 \dfrac{M_{\mathrm{e}} - 1}{\overline{\nu} - 1} \left[\overline{\nu_3} + 2 \dfrac{M_{\mathrm{e}} - 1}{\overline{\nu} - 1} \overline{\nu_2}^2 \right] & j = 3 \end{cases} \tag{43}$$

where the escape multiplication is defined as

$$M_{\mathrm{e}} = \frac{1 - p}{1 - p\overline{\nu}} \tag{44}$$

and where

$$\overline{\nu_\mu} = \sum_{\nu=\mu}^{\infty} \binom{\nu}{\mu} C_\nu \quad = \quad \frac{\nu_{(\mu)}}{\mu!} \tag{45}$$

are the combinatorial moments of the neutron multiplicity distribution for induced fission.

For fission chains initiated by a spontaneous fission, the quantity

$$R_{\mathrm{S}j} = \sum_{m=j}^{\infty} \binom{m}{j} \mathrm{e}_{\mathrm{S}m} \tag{46}$$

and from first-principles, it can again be shown that[11]

$$R_{\mathrm{S}j} = \epsilon^j F_{\mathrm{S}} \begin{cases} M_{\mathrm{e}} \overline{\nu_{\mathrm{S1}}} & j = 1 \\ M_{\mathrm{e}}^2 \left[\overline{\nu_{\mathrm{S2}}} + \dfrac{M_{\mathrm{e}} - 1}{\overline{\nu} - 1} \overline{\nu_{\mathrm{S1}}}\ \overline{\nu_2} \right] & j = 2 \\ M_{\mathrm{e}}^3 \Bigg[\overline{\nu_{\mathrm{S3}}} + \dfrac{M_{\mathrm{e}} - 1}{\overline{\nu} - 1} \left(\overline{\nu_{\mathrm{S1}}}\ \overline{\nu_3} + 2\overline{\nu_{\mathrm{S2}}}\ \overline{\nu_2} \right) + 2 \left(\dfrac{M_{\mathrm{e}} - 1}{\overline{\nu} - 1} \right)^2 \overline{\nu_{\mathrm{S1}}}\ \overline{\nu_2}^2 \Bigg] & j = 3 \end{cases} \tag{47}$$

where the combinatorial moments of the neutron multiplicity distribution for spontaneous fission are

$$\overline{\nu_{\mathrm{S}\mu}} = \sum_{\nu=\mu}^{\infty} \binom{\nu}{\mu} C_{\mathrm{S}\nu} \ . \tag{48}$$

The neutron multiplicity distributions used for these comparisons are shown in Table II. Results of the comparisons are shown in Table III. For both induced (I) fission- and spontaneous (S) fission-initiated fission chains, the comparisons show the ratio

$$\frac{\Delta R_j}{R_j} = \frac{R_j^{\mathrm{Computed}} - R_j^{\mathrm{First-Principles}}}{R_j^{\mathrm{First-Principles}}} \ . \tag{49}$$

		C_ν		$C_{\mathrm{S}\nu}$	
		^{235}U (1 MeV)	^{239}Pu (1 MeV)	^{238}U	^{240}Pu
n	0	0.0237898	0.0084842	0.0798571	0.0631852
	1	0.1555525	0.0790030	0.2467090	0.2319644
	2	0.3216515	0.2536175	0.3538440	0.3333230
	3	0.3150433	0.3289870	0.2356090	0.2528207
	4	0.1444732	0.2328111	0.0772832	0.0986461
	5	0.0356013	0.0800161	0.0104521	0.0180199
	6	0.0034339	0.0155581	0.0006964	0.0020406
	7	0.0004546	0.0011760		
	8		0.0003469		
$\overline{\nu}$		2.5236703	3.0088797	—	
$\overline{\nu_2}$		2.5506884	3.7053872		
$\overline{\nu_3}$		1.3335380	2.4321410		
$\overline{\nu_{\mathrm{S1}}}$		—		2.0267958	2.1540000
$\overline{\nu_{\mathrm{S2}}}$				1.6320733	1.8944699
$\overline{\nu_{\mathrm{S3}}}$				0.6602522	0.8684162

TABLE II. Measured values of C_ν for ^{235}U[17] and ^{239}Pu,[17] and $C_{\mathrm{S}\nu}$ for ^{238}U[18] and ^{240}Pu.[17]

Isotopes	M	Dist.	$\Delta R_1/R_1$	$\Delta R_2/R_2$	$\Delta R_3/R_3$
^{238}U driving ^{235}U	5	$\mathrm{e}_{\mathrm{I}m}$	-4.6×10^{-8}	-1.6×10^{-7}	-2.7×10^{-7}
		$\mathrm{e}_{\mathrm{S}m}$	-4.6×10^{-8}	-1.5×10^{-7}	-2.6×10^{-7}
	10	$\mathrm{e}_{\mathrm{I}m}$	-5.5×10^{-8}	-1.8×10^{-7}	-3.0×10^{-7}
		$\mathrm{e}_{\mathrm{S}m}$	-5.5×10^{-8}	-1.7×10^{-7}	-2.9×10^{-7}
	20	$\mathrm{e}_{\mathrm{I}m}$	-6.0×10^{-8}	-1.9×10^{-7}	-3.4×10^{-7}
		$\mathrm{e}_{\mathrm{S}m}$	-6.0×10^{-8}	-1.8×10^{-7}	-3.2×10^{-7}
	40	$\mathrm{e}_{\mathrm{I}m}$	-6.3×10^{-8}	-2.1×10^{-7}	-5.4×10^{-7}
		$\mathrm{e}_{\mathrm{S}m}$	-6.3×10^{-8}	-2.0×10^{-7}	-4.5×10^{-7}
^{240}Pu driving ^{239}Pu	5	$\mathrm{e}_{\mathrm{I}m}$	3.6×10^{-8}	1.2×10^{-7}	1.9×10^{-7}
		$\mathrm{e}_{\mathrm{S}m}$	3.6×10^{-8}	1.1×10^{-7}	1.8×10^{-7}
	10	$\mathrm{e}_{\mathrm{I}m}$	4.3×10^{-8}	1.3×10^{-7}	2.2×10^{-7}
		$\mathrm{e}_{\mathrm{S}m}$	4.3×10^{-8}	1.3×10^{-7}	2.2×10^{-7}
	20	$\mathrm{e}_{\mathrm{I}m}$	4.6×10^{-8}	1.4×10^{-7}	1.8×10^{-7}
		$\mathrm{e}_{\mathrm{S}m}$	4.6×10^{-8}	1.4×10^{-7}	2.1×10^{-7}
	40	$\mathrm{e}_{\mathrm{I}m}$	4.7×10^{-8}	1.2×10^{-7}	-6.5×10^{-7}
		$\mathrm{e}_{\mathrm{S}m}$	4.8×10^{-8}	1.3×10^{-7}	9.4×10^{-7}

TABLE III. Comparison of the first three moments of the calculated distributions $\mathrm{e}_{\mathrm{I}m}$ and $\mathrm{e}_{\mathrm{S}m}$ to first-principles computations. The quantity $\Delta R_j = R_j^{\mathrm{Computed}} - R_j^{\mathrm{First-Principles}}$. In all cases, the distributions were carried out to m such that $\mathrm{e}_{\mathrm{I}m} > 10^{-15}$ and $\mathrm{e}_{\mathrm{S}m} > 10^{-15}$. Detection efficiency was taken to be $\epsilon = 0.03$.

F. Conclusions

Using the Fourier transform to calculate the probability that a fission chain will produce n neutrons yields very accurate results when enough terms are carried to take the distributions out to a large n with a sufficiently small probability.

The Fourier transform method is inherently fast because the basic problem is one of calculating the roots of a low order polynomial (typically less than tenth order) as a function of the parameter y from the generating function. The characteristic function is obtained by computing the roots of the generating function of the Böhnel equation after the simple replacement $y \to e^{i\theta}$. The physical roots lie within the unit circle on the complex plain. The fission chain multiplicities can then be calculated by taking the fast Fourier transform of the resulting characteristic function which is periodic on any interval of length 2π.

The need to take multiple terms of the Stirling series to evaluate factorials of large order in the analytic formula is quite significant. Even then, less accurate results tend to be obtained compared to the simple, direct application of the inherently simple and efficient Fourier

approach. It is fairly obvious that the Fourier method will always beat out the direct evaluation approach in any fair speed comparison. The error of the Fourier approach is also easier to control since it comes down to accurate root finding for low order polynomials which is a well-understood numerical problem.

The probability distribution for a fission chain initiated by a spontaneous fission to produce n neutrons is obtained by modifying the generating function of the Böhnel equation to account for a compound process. The same logic applies to calculating probability distributions for the number of detected neutrons as well as the situation when the neutrons from a spontaneous fission don't all make it to the multiplying medium. Distributions for detected neutrons are considerably faster to compute as the detection efficiency makes it necessary to carry far fewer terms.

III. BACKGROUND NEUTRONS

A. Introduction

Background neutrons often show correlations in time — i.e. a single event (usually a remnant from a high-energy cosmic ray air shower) can create many neutrons. A multiplicity distribution specifies the probability of counting a given number of neutrons within a randomly triggered time gate of a given duration T. A statistical model of correlated background neutrons can be constructed from a measured multiplicity distribution.

A multiplicity distribution is made by breaking the observation time up into successive randomly-triggered time gates and counting the number of neutrons detected within each. Suppose in an experiment, N time gates of duration T were examined, and let $B_n(T)$ be the number of those time gates in which n neutrons were detected. So for example, suppose that during the first time gate, four neutrons were counted; B_4 would be incremented by one. During the next time gate, say two neutrons were counted; B_2 would be incremented by one, and so on for all N time gates. In this way, the count distribution $B_n(T)$ is built up. The probability distribution $b_n(T) \approx B_n(T)/N$ for $N \ggg 1$.

The total probability to detect n neutrons is the *generalized Poisson distribution*,[12]

$$b_n = \sum_{\sum k m_k = n} \left[\prod_{k=1}^{n} \left(\frac{\Lambda_k^{m_k}}{m_k!} \right) \right] e^{-\left(\sum_{k=1}^{\infty} \Lambda_k\right)} \tag{50}$$

where $\Lambda_k(T)$ is the average rate of detecting k neutrons from a single event within time T.[10] There is no simple formula for the probabilities b_n in terms of the average number of instances of counting k neutrons from a single event Λ_k, but it is possible instead to give a very concise formula for the sum of a power series whose coefficients are the probabilities b_n that we're interested in.[13] A generating function can be constructed by simply multiplying the probabilities b_n by z^n and summing over n,[10,12]

$$\begin{aligned} \not{b}(z) &= \sum_{n=0}^{\infty} z^n b_n(T) \qquad (51) \\ &= e^{-\left(\sum_{k=1}^{\infty} \Lambda_k\right)} \left[1 + z\Lambda_1 + z^2 \left(\frac{\Lambda_1^2}{2!} + \Lambda_2 \right) + \cdots \right] \\ &= e^{-\left(\sum_{k=1}^{\infty} \Lambda_k\right)} \\ &\quad \times \left[1 + \left(\sum_{j=1}^{\infty} z^j \Lambda_j \right) + \frac{1}{2!} \left(\sum_{j=1}^{\infty} z^j \Lambda_j \right)^2 + \cdots \right] \\ &= e^{-\left(\sum_{k=1}^{\infty} \Lambda_k\right)} e^{\left(\sum_{j=1}^{\infty} z^j \Lambda_j\right)} \\ &= b_0 e^{\not{\Lambda}} \qquad (52) \end{aligned}$$

where, throughout, the Feynman-slash notation denotes the generating function corresponding to a distribution.

B. Background Measurement

A background measurement was made using the Large Epithermal Multiplicity Counter[19–22] (LEMC)— a high-efficiency well counter consisting of a high-density polyethylene (HDPE) annulus 85.8 cm in diameter and 87.8 cm in height. The HDPE houses 126 ^{3}He tubes 2.54 cm in diameter and 76.2 cm in length.

A total of 3,926,094 background neutrons were counted over 497,409.6 seconds (5.75 days). Multiplicity distributions $b_n(T)$ for $T = 1, 2, 3, \cdots, 512$ μs were made using the time-binning structure shown in Fig. 21. The multiplicity distribution $b_n(512\,\mu s)$ is shown in Fig. 25. The second moments, $Y_{2F}(T)$, are shown in Fig. 24. The waiting time distribution for background neutrons is shown in Fig. 28.

C. Determining Background Parameters from Measured Data

The Average Number of Instances of Detecting k Neutrons from a Single Event

If the multiplicity distribution $b_n(T)$ is known, the average number of instances of detecting k neutrons from a single event within time gate T, $\Lambda_k(T)$, can be computed. Starting with the generating function for the multiplicity distribution, Eq. 52, taking the log of both sides,

$$\log[\not{b}(z)] = \log b_0 + \not{\Lambda} \tag{53}$$

and expanding the left-hand side around b_0 gives

$$\frac{(\not{b} - b_0)}{b_0} - \frac{(\not{b} - b_0)^2}{2b_0^2} + \frac{(\not{b} - b_0)^3}{3b_0^3} - \cdots = \not{\Lambda} \tag{54}$$

The generating function for Λ_k can then readily be seen to be

$$\not{\Lambda} = \sum_{k=1}^{\infty} (-1)^{k-1} \frac{\left(\not{b} - b_0\right)^k}{k b_0^k} = \sum_{k=1}^{\infty} \frac{(-1)^{k-1}}{k b_0^k} \left(\sum_{n=1}^{\infty} z^n b_n \right)^k \quad (55)$$

If instead the count distribution with N time gates, $B_n(T) = N b_n(T)$, is known, Eq. 55 requires no modification to compute $\Lambda_k(T)$ other than the simple replacement of $b_n(T)$ with $B_n(T)$,

$$\not{\Lambda} = \sum_{k=1}^{\infty} \frac{(-1)^{k-1}}{k B_0^k} \left(\sum_{n=1}^{\infty} z^n B_n \right)^k \quad (56)$$

The variance on the $\Lambda_k(T)$ is then found by taking the derivative of this generating function (Eq. 56) with respect to $B_n(T)$,

$$\frac{\partial \not{\Lambda}}{\partial B_n} = \sum_{k=1}^{\infty} \frac{(-1)^{k-1}}{B_0^k} \left(\sum_{n=1}^{\infty} z^n B_n \right)^{k-1} \left(\sum_{n=1}^{\infty} z^n \right) - \sum_{k=1}^{\infty} \frac{(-1)^{k-1}}{B_0^{k+1}} \left(\sum_{n=1}^{\infty} z^n B_n \right)^k \quad (57)$$

$$= \sum_{k=1}^{\infty} z^k \mathbf{D}_{\mathbf{\Lambda}_k} \quad (58)$$

where $\mathbf{D}_{\mathbf{\Lambda}_k}$ is a row vector from $k = 1$ to $k_{\max}$. The variance on $\Lambda_k(T)$ can then be written

$$\sigma^2_{\Lambda_k} = \mathbf{D}_{\mathbf{\Lambda}_k} V \mathbf{D}^T_{\mathbf{\Lambda}_k} \quad (59)$$

where the superscript T denotes transpose and where the covariance matrix V is

$$V_{mn} = \begin{cases} -\dfrac{B_m B_n}{N} & m \neq n \\ B_n \left(1 - \dfrac{B_n}{N}\right) & m = n \end{cases} \quad (60)$$

Rates for Detecting Multiple Neutrons From the Same Event

Consider an event which produces n neutrons. The probability of detecting exactly m neutrons out of the possible n neutrons, if the probability of detection is ϵ, is just the binomial distribution,[14]

$$P_\epsilon(m|n) = \binom{n}{m} \epsilon^m (1-\epsilon)^{n-m} \quad (61)$$

If $\mathcal{P}_n$ is the probability that an event creates n neutrons, the probability of detecting m neutrons from such an event is therefore the product of these probabilities summed over all the possible ways of detecting m neutrons,[12]

$$\mathrm{e}_m(\epsilon) = \sum_{n=m}^{\infty} \mathcal{P}_n P_\epsilon(m|n) = \sum_{n=m}^{\infty} \mathcal{P}_n \binom{n}{m} \epsilon^m (1-\epsilon)^{n-m} \quad (62)$$

The rate r_m of detecting m neutrons from a single event is then the rate at which events are initiated F_{Init} times this probability,

$$r_m = F_{\text{Init}} \mathrm{e}_m(\epsilon) \quad (63)$$

If measured background count distributions $B_n(T)$ for multiple values of T are available, then $\Lambda_k(T)$, and the respective variances $\sigma^2_{\Lambda_k}$, can be calculated from Eqs. 56 – 59. An example is shown is Fig. 20. The objective then is to calculate the rates r_m that characterize the measured background.

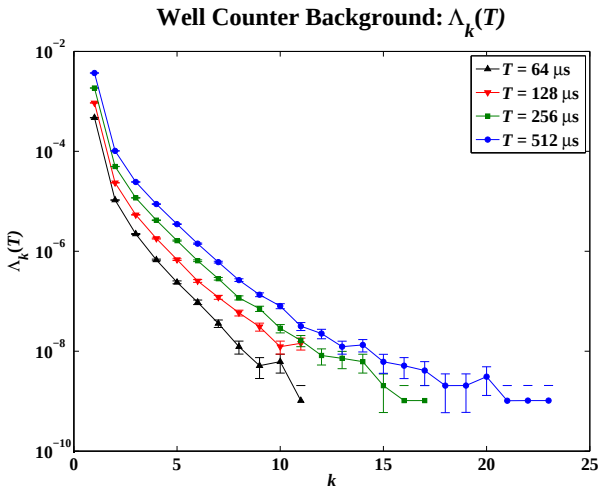

FIG. 20. The average number of instances of detecting k neutrons from a single event within time gate T as computed from multiplicity histograms of background neutrons measured by a high-efficiency well counter over 497,409.6 seconds.

The average number of instances of detecting k neutrons from a single event within time gate T is defined as

$$\Lambda_k(T) = \sum_{n=k}^{\infty} \mathcal{P}_n \sum_{m=k}^{n} P_\epsilon(m|n) \Delta_{mk} \quad (64)$$

The term Δ_{mk} is defined as

$$\Delta_{mk} = \binom{m}{k} \left\{ \int_{-\infty}^{0} \left[\int_0^T e^{-\lambda(t-s)} \lambda \, dt \right]^k \left[1 - \int_0^T e^{-\lambda(t-s)} \lambda \, dt \right]^{m-k} F_{\text{Init}} \, ds \right.$$
$$\left. + \int_0^T \left[\int_s^T e^{-\lambda(t-s)} \lambda \, dt \right]^k \left[1 - \int_s^T e^{-\lambda(t-s)} \lambda \, dt \right]^{m-k} F_{\text{Init}} \, ds \right\} \quad (65)$$
$$= \frac{F_{\text{Init}}}{\lambda} \binom{m}{k} B[(1 - e^{-\lambda T}); \, k, \, m-k] \quad (66)$$

and is the probability of detecting k out of the total m detected neutrons within the time gate T and λ is the inverse of the neutron diffusion time.[10] Δ_{mk} is just a binomial distribution where the first term accounts for neutrons created before the time gate T and the second term accounts for neutrons created during the time gate T. The integrals evaluate to an incomplete Beta function $B(z; a, b)$.[23]

Let us define

$$\psi_{nm} = \mathcal{P}_n P_\epsilon(m|n) \quad (67)$$

Rewriting $\Lambda_k(T)$ in terms of ψ_{nm} and Δ_{mk},

$$\Lambda_k(T) = \sum_{n=k}^{\infty} \sum_{m=k}^{n} \psi_{nm} \Delta_{mk} \quad (68)$$

If we write out the terms in $\Lambda_k(T)$ explicitly, we see a pattern:

$$\begin{aligned} \Lambda_1(T) &= \psi_{11}\Delta_{11} + \\ &\quad \psi_{21}\Delta_{11} + \psi_{22}\Delta_{21} + \\ &\quad \psi_{31}\Delta_{11} + \psi_{32}\Delta_{21} + \psi_{33}\Delta_{31} + \cdots \\ \Lambda_2(T) &= \psi_{22}\Delta_{22} + \\ &\quad \psi_{32}\Delta_{22} + \psi_{33}\Delta_{32} + \cdots \\ \Lambda_3(T) &= \psi_{33}\Delta_{33} + \cdots \\ \vdots \quad &= \cdots \end{aligned} \quad (69)$$

The $\mathrm{e}_m(\epsilon)$, Eq. 62, can also be written in terms of ψ_{nm} as

$$\mathrm{e}_m(\epsilon) = \sum_{n=m}^{\infty} \psi_{nm} \quad (70)$$

Writing out $\mathrm{e}_m(\epsilon)$ explicitly:

$$\begin{aligned} \mathrm{e}_1(\epsilon) &= \psi_{11} + \psi_{21} + \psi_{31} + \cdots \\ \mathrm{e}_2(\epsilon) &= \psi_{22} + \psi_{32} + \cdots \\ \mathrm{e}_3(\epsilon) &= \psi_{33} + \cdots \\ \vdots \quad &= \cdots \end{aligned} \quad (71)$$

We can now see that $\Lambda_k(T)$ can easily be written in terms of e_m

$$\begin{aligned} \Lambda_1(T) &= \mathrm{e}_1\Delta_{11} + \mathrm{e}_2\Delta_{21} + \mathrm{e}_3\Delta_{31} + \cdots \\ \Lambda_2(T) &= \mathrm{e}_2\Delta_{22} + \mathrm{e}_3\Delta_{32} + \cdots \\ \Lambda_3(T) &= \mathrm{e}_3\Delta_{33} + \cdots \\ \vdots \quad &= \cdots \end{aligned} \quad (72)$$

This can be written as a matrix equation with the column vector Λ_k equal to the matrix Δ_{mk} multiplying the column vector e_m,

$$\begin{pmatrix} \Lambda_1 \\ \Lambda_2 \\ \Lambda_3 \\ \vdots \end{pmatrix} = \begin{pmatrix} \Delta_{11} & \Delta_{21} & \Delta_{31} & \cdots \\ 0 & \Delta_{22} & \Delta_{32} & \cdots \\ 0 & 0 & \Delta_{33} & \cdots \\ \vdots & \vdots & \vdots & \ddots \end{pmatrix} \begin{pmatrix} \mathrm{e}_1 \\ \mathrm{e}_2 \\ \mathrm{e}_3 \\ \vdots \end{pmatrix}$$
$$\mathbf{\Lambda} = \Delta \mathbf{e} \quad (73)$$

Now let us define ∇_{mk} such that

$$\Delta_{mk} = F_{\text{Init}} \nabla_{mk} \quad (74)$$

and rewrite Eq. 73 in terms of ∇_{mk},

$$\mathbf{\Lambda} = F_{\text{Init}} \nabla \mathbf{e} \quad (75)$$
$$= \nabla \mathbf{r} \quad (76)$$

where the vector $\mathbf{r} \equiv r_m$ was defined above in Eq. 63. The matrix ∇ is defined as

$$\nabla_{mk} = \frac{1}{\lambda} \binom{m}{k} B[(1 - e^{-\lambda T}); \, k, \, m-k] \quad (77)$$

We can get the needed rates r_m by multiplying both sides of Eq. 76 from the left by ∇^{-1},

$$\mathbf{r} = \nabla^{-1} \mathbf{\Lambda} \quad (78)$$

The matrix ∇ is a function of T and λ; λ^{-1} is the neutron lifetime against detection. This time includes thermalization in or near the medium in which the neutron was created, time of flight to the detector, and diffusion in the detector prior to being counted.

Neutron Lifetime Against Detection λ^{-1}

The quantity λ can be determined from the count distributions $B_n(T)$ by fitting the second moments $Y_{2F}(T)$.[11]

The rate of counting j neutrons all coming from the same fission event can be determined by computing the combinatorial moments of the $\Lambda_k(T)$,

$$Y_j(T) = \sum_{k=j}^{\infty} \binom{k}{j} \Lambda_k(T) \tag{79}$$

It can be shown that an explicit form for $Y_j(T)$ is

$$Y_j(T) = \sum_{n=j}^{\infty} \mathcal{P}_n \binom{n}{j} \epsilon^j F_{\text{Init}} \left\{ \frac{\left(1-e^{-\lambda T}\right)^j}{\lambda j} + T - \frac{1}{\lambda} \sum_{n=0}^{j-1} B[(1-e^{-\lambda T});\, j-n,\, 1] \right\} \tag{80}$$

where, again, $B(z;\, a,\, b)$ is the incomplete beta function.[23] We can define the leading terms to be

$$R_j = \sum_{n=j}^{\infty} \mathcal{P}_n \binom{n}{j} \epsilon^j F_{\text{Init}} \tag{81}$$

resulting in[11]

$$Y_1(T) = R_1 T \tag{82}$$

$$Y_2(T) = R_2 \left(T - \frac{1-e^{-\lambda T}}{\lambda} \right) \tag{83}$$

It is then convenient to define

$$Y_{2\text{F}} = \frac{Y_2}{Y_1} \tag{84}$$

$$R_{2\text{F}} = \frac{R_2}{R_1} \tag{85}$$

Applying Eqs. 82 and 83, the quantity of interest is found to be[8,11,24,25]

$$Y_{2\text{F}}(T) = R_{2F} \left(1 - \frac{1-e^{-\lambda T}}{\lambda T} \right) \tag{86}$$

To extract the rates $Y_j(T)$ experimentally from a measured count distribution $B_n(T) \approx N b_n(T)$ for $N \ggg 1$ randomly-triggered time gates of length T requires the combinatorial moments of the count distribution,

$$\mathcal{M}_j(T) = \frac{1}{N} \sum_{n=j}^{\infty} \binom{n}{j} B_n(T) \tag{87}$$

The $\mathcal{M}_j$ for $j = 1,\, 2$ expressed in terms of the Λ_k are

$$\mathcal{M}_1 = \sum_{k=1}^{\infty} \binom{k}{1} \Lambda_k \tag{88}$$

$$= Y_1 \tag{89}$$

$$\mathcal{M}_2 = \sum_{k=2}^{\infty} \binom{k}{2} \Lambda_k + \frac{1}{2!} \left[\sum_{k=1}^{\infty} \binom{k}{1} \Lambda_k \right]^2 \tag{90}$$

$$= Y_2 + \frac{Y_1^2}{2!} \tag{91}$$

Solving for Y_1 and Y_2 in terms of $\mathcal{M}_1$ and $\mathcal{M}_2$ yields

$$Y_1 = \mathcal{M}_1 \tag{92}$$

$$Y_2 = \mathcal{M}_2 - \frac{\mathcal{M}_1^2}{2!} \tag{93}$$

leading to

$$Y_{2\text{F}}(T) = \frac{\mathcal{M}_2(T)}{\mathcal{M}_1(T)} - \frac{\mathcal{M}_1(T)}{2!} \tag{94}$$

As a practical matter, the combinatorial moments $\mathcal{M}_j$ of the counting distribution $B_n(T)$ are easy to compute from Eq. 87.

The quantities λ and $R_{2\text{F}}$ are determined by minimizing

$$\chi^2 = \mathbf{E_{2F}}^T W^{-1} \mathbf{E_{2F}} \tag{95}$$

where the superscript T denotes transpose and where the error vector $\mathbf{E_{2F}}$ is defined as

$$\mathbf{E_{2F}} = \frac{\mathcal{M}_2(T_i)}{\mathcal{M}_1(T_i)} - \frac{\mathcal{M}_1(T_i)}{2!} - R_{2F} \left(1 - \frac{1-e^{-\lambda T_i}}{\lambda T_i} \right) \tag{96}$$

and is understood to be a column vector corresponding to the values for T_i. The covariance matrix W depends on how the different values of T are chosen.

To compute the statistical errors on $Y_{2\text{F}}$, we define the

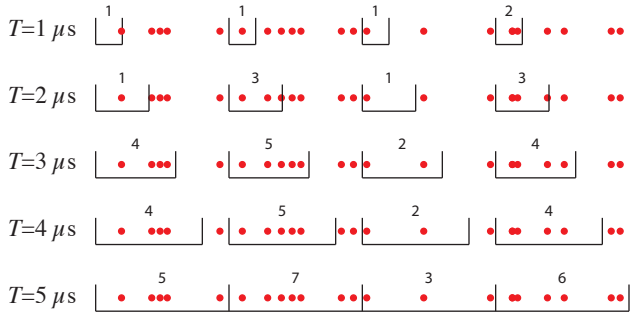

FIG. 21. Time-binning structure used in the background measurement. In this illustration, time runs from left to right and covers a total of 20 μs. The dots represent neutron arrival times. Here, time is divided into cycles of length 5 μs, so there are four cycles shown. The $B_n(T = 1\ \mu\text{s})$ distribution is constructed by counting the number of cycles with $n = 0, 1, 2, 3 \cdots$ neutrons in the first μs. In this example, there were three cycles where one neutron was counted in the first 1 μs and one cycle where two neutrons were counted in the first 1 μs. The $B_n(T = 2\ \mu\text{s})$ distribution is constructed by counting the number of cycles with $n = 0, 1, 2, 3 \cdots$ neutrons in the first 2 μs. In this example, there were two cycles where one neutron was counted in the first 2 μs and two cycles where three neutrons were counted in the first 2 μs. And so on.

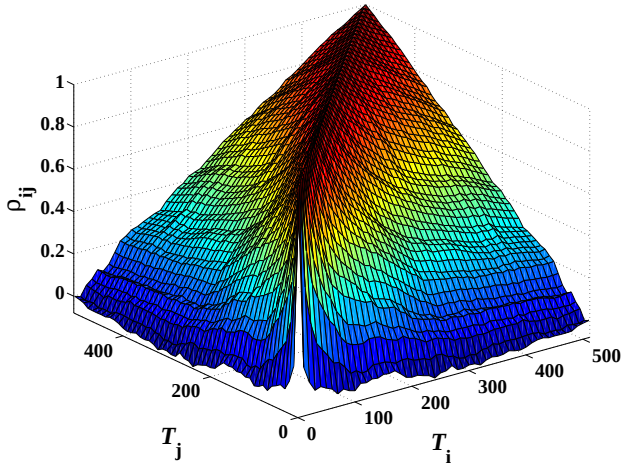

FIG. 22. Estimated correlation matrix ρ_{ij} calculated from 1,000 1-hour Monte Carlo simulations of 10 ng of ^{252}Cf with diffusion time $\lambda^{-1} = 100\ \mu$s and detection efficiency $\epsilon = 0.03$.

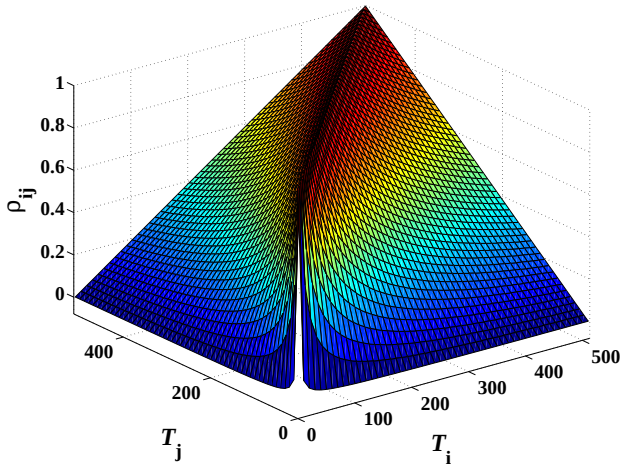

FIG. 23. Correlation matrix $\rho_{ij} = T_</T_>$ with $T_< = \min(T_i, T_j)$ and $T_> = \max(T_i, T_j)$.

row vector

$$\mathbf{D_{2F}} = \frac{\partial Y_{2F}}{\partial B_n} \tag{97}$$

which are of length $n_{\max}$. It is straight forward to show that

$$\frac{\partial Y_{2F}}{\partial B_n} = \binom{n}{2} \frac{1}{\mathcal{M}_1 N} - \frac{n Y_{2F}}{\mathcal{M}_1 N} - \frac{n}{N} \tag{98}$$

The variance on Y_{2F} is then calculated in the usual way as

$$\sigma^2_{Y_{2F}} = \mathbf{D_{2F}}\, V\, \mathbf{D_{2F}}^T \tag{99}$$

where the superscript T denotes transpose and where V is defined in Eq. 60.

The covariance matrix W in Eq. 95 depends on the structure of the time gates. For the measurement of background neutrons here, we divided the observation time up into cycles which contain a single example of each time interval $T = 1, 2, 3, \cdots, 512\ \mu$s. This is illustrated in Fig. 21. Because of this time-binning structure, the data used to generate the $B_n(T_i)$ distribution gets partially reused to generate the $B_n(T_j)$ distribution ($T_i \neq T_j$). The covariance matrix W in Eq. 95 is therefore not diagonal.

A Monte Carlo simulation using the methods discussed below in §III D was used to estimate the correlation between values of $Y_{2F}(T_i)$ and $Y_{2F}(T_j)$. A thousand one-hour simulations of 10 ng of ^{252}Cf configured such that the diffusion time $\lambda^{-1} = 100\ \mu$s and the detection efficiency $\epsilon = 3\%$ were used to calculate a correlation matrix. The resulting correlation matrix ρ_{ij} is shown in Fig. 22. This estimate indicated that the correlation matrix was well approximated by

$$\rho_{ij} = \frac{T_<}{T_>} \tag{100}$$

$$T_< = \min(T_i, T_j) \tag{101}$$

$$T_> = \max(T_i, T_j) \tag{102}$$

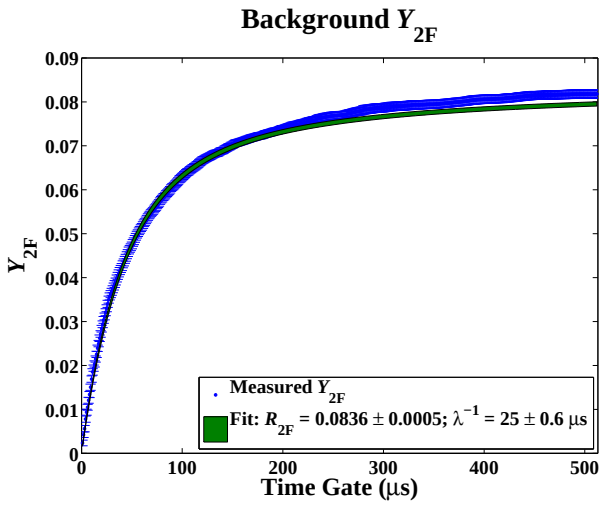

FIG. 24. $Y_{2F}(T)$ as computed from multiplicity histograms of background neutrons measured by a high-efficiency well counter over 497,409.6 seconds.

and is shown for comparison in Fig. 23. Given the correlation matrix ρ_{ij}, the covariance matrix was then easy to calculate:

$$W_{ij} = \rho_{ij}\sigma_{Y_{2F}}(T_i)\sigma_{Y_{2F}}(T_j) \tag{103}$$

Sparse Sampling

A problem with Eq. 56 appears when this procededure is put into practice. The computation of $\Lambda_n(T)$ poses no problems as long as $B_n(T) > 0$. However, for count distributions where sparse sampling causes $B_n(T) = 0$ for certain values of n interspersed with $B_n(T) \neq 0$, some of the resulting values of $\Lambda_n(T)$ can become negative which is unphysical.

For the sparsely-sampled region of $b_n(T)$, we propose taking an average. Suppose the sparsely-sampled region of $b_n(T)$ runs from $n = x$ to $n = y$, i.e. $B_n(T) \geq 0$ for $x \leq n \leq y$ where x is the smallest value of n for which $B_n(T) = 0$ and where y is the largest value of n for which $B_n(T) > 0$. For $N \gg 1$ and $B_n(T) \approx 1$, $\Lambda_n \approx B_n/N$. Therefore the average number of instances of detecting $x \leq n \leq y$ neutrons from a single event within a time gate T can be taken as

$$\Lambda_{x\leq n\leq y} \approx \frac{1}{N}\sum_{n=x}^{y} B_n(T) \tag{104}$$

The value for $\Lambda_{x\leq n\leq y}$ then needs to be placed into the context of the larger vector Λ_n in a sensible way. Let $\bar{n}$ be the average number of neutrons detected in time gate T over the sparsely-sampled region of the count distribution,

$$\bar{n} = \frac{\sum_{n=x}^{y} nB_n(T)}{\sum_{n=x}^{y} B_n(T)} \tag{105}$$

An obvious choice would be to place $\Lambda_{x\leq n\leq y}$ at the index $\bar{n}$. However, $\bar{n}$ is not in general an integer. We propose simply rounding to the nearest integer, $\lfloor\bar{n}\rceil$, thus $\Lambda_{x\leq n\leq y} \rightarrow \Lambda_{\lfloor\bar{n}\rceil}$. The corresponding matrix element needed to compute the rate $r_{\lfloor\bar{n}\rceil}$ is then $\nabla_{\lfloor\bar{n}\rceil\lfloor\bar{n}\rceil}$.

We then propose distributing the rate $r_{\lfloor\bar{n}\rceil}$ evenly across the sparsely-sampled region $x \leq n \leq y$,

$$r_m = \frac{r_{\lfloor\bar{n}\rceil}}{y - x + 1} \qquad x \leq m \leq y \tag{106}$$

This seems to give good results that compare well with the data as can be seen in Figs. 25 and 28 (blue circles). In Fig. 25, note that the high-multiplicity tail of the distribution is well-reproduced.

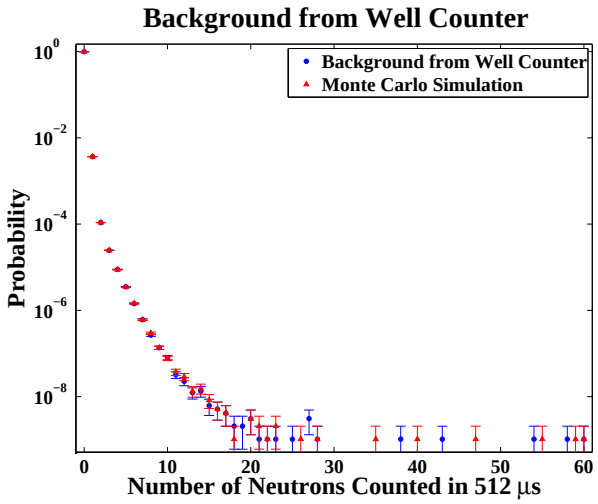

FIG. 25. Data vs. a Monte Carlo simulation for the multiplicity distribution $b_n(512\,\mu s)$. Parameters used in the simulation were computed using the methods detailed in §III C from multiplicity histograms of 3,926,094 background neutrons measured by a high-efficiency well counter over 497,409.6 seconds. The Monte Carlo simulation used the methods discussed in §III D.

D. Monte Carlo Methods for Time-Correlated Neutrons

Creating Poisson-Distributed Random Numbers[26]

In general, a probability density function $f(x)$ on the range $0 < x < \infty$ has a corresponding cumulative distri-

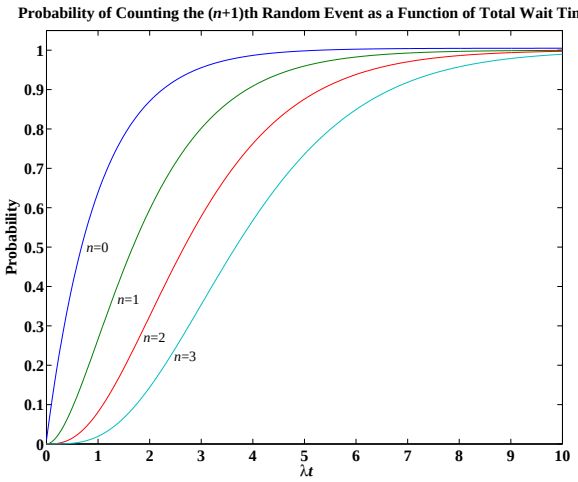

FIG. 26. Probability to count the $(n+1)$th (i.e. next) random event as a function of total waiting time t in units of r^{-1}.

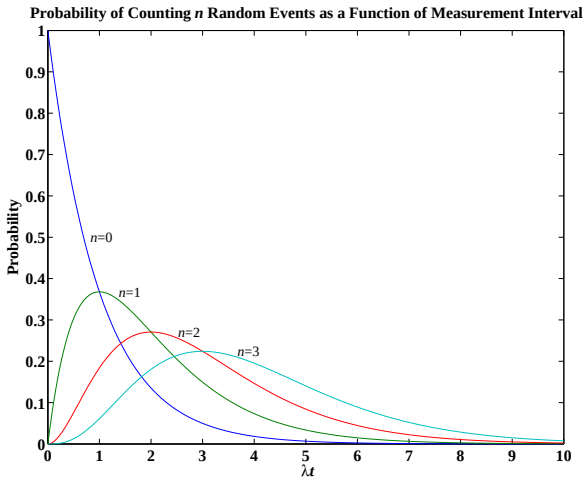

FIG. 27. Probability to count $n = k - 1$ events as a function of measurement interval t in units of r^{-1}.

bution function

$$F(a) = \int_0^a f(x)\,dx \tag{107}$$

which expresses the probability that $x \leq a$. If a is chosen with probability density $f(a)$, then the integrated probability up to point a, $F(a)$, is itself a random variable which will occur with uniform probability density on $[0, 1]$,

$$u = F(a) \tag{108}$$

We can thus find a unique x chosen from the probability density function $f(x)$ for a given u by

$$x = F^{-1}(u) \tag{109}$$

The Poisson distribution gives the probability of counting n random events occurring at a rate of r per unit time during a measurement interval t. The probability of counting the $(n+1)$th random event after waiting an amount of time t is just the cumulative distribution function F of the Poisson distribution,

$$\begin{aligned} F(t) &= r\int_0^t \frac{(rx)^n e^{-rx}}{n!}dx \\ &= 1 - r\int_t^\infty \frac{(rx)^n e^{-rx}}{n!}dx \\ &= 1 - \frac{\Gamma(n+1, rt)}{n!} \end{aligned} \tag{110}$$

This is shown in Fig. 26. For a process that generates events as a function of time according to a Poisson distribution, the probability distribution of waiting times from an arbitrary starting point (which may be some particular event) to the kth event, where we have defined $k = n + 1$, is then obtained by differentiating the cumulative distribution function F (Eq. 110) with respect to t,

$$\begin{aligned} \frac{dF}{dt} &= \frac{d}{dt}\left(1 - \frac{\Gamma(k, rt)}{(k-1)!}\right) \\ &= \frac{r^k t^{k-1} e^{-rt}}{(k-1)!} \\ &= \frac{r^k t^{k-1} e^{-rt}}{\Gamma(k)} \quad = \quad \gamma(t; r, k) \end{aligned} \tag{111}$$

This is the gamma distribution and is shown in Fig. 27. The time-to-next event corresponds to $k = 1$ and is called the *exponential* distribution.

If we want to generate waiting times δ between random events, we simply apply the above technique to the exponential distribution, $\gamma(t; r, 1) = re^{-rt}$ (Eq. 111 above with $k \to 1$). Starting with a random number u which is uniformly distributed on $[0, 1]$,

$$\begin{aligned} u \quad = \quad F(\delta) &= \int_0^\delta \gamma(t; r, 1)\,dt \\ &= \int_0^\delta re^{-rt}\,dt \\ &= 1 - e^{-r\,\delta} \end{aligned} \tag{112}$$

$$\delta \quad = \quad F^{-1}(u) = -\frac{\ln u}{r} \tag{113}$$

Time-Correlated Neutron Arrival Times

Consider an event which produces n neutrons. The neutron multiplicity $\mathcal{P}_n$ is the probability that an event generates n neutrons. The probability of detecting ex-

actly m neutrons out of a possible n neutrons, if the probability of detection is ϵ, is just the binomial distribution, Eq. 61. The probability of detecting m neutrons from such an event is Eq. 62. The rate r_m of detecting m neutrons from a single event is then Eq. 63.

These rates r_m can be used to generate waiting times between events from which m neutrons were detected. From Eq. 113, a list of times is generated as

$$\begin{aligned} t_{m,i} &= \delta_{m,i} + t_{m,i-1} \\ &= -\frac{\ln u_i}{r_m} + t_{m,i-1} \end{aligned} \tag{114}$$

with $t_{m,0} = 0$. Iteration is stopped once $t_{m,i}$ exceeds the observation time.

The neutron does not get detected the instant it is created, however. The neutron lifetime against detection λ^{-1} represents the time scale for the neutron to move from the site of creation out to the detector. Thus, for each $t_{m,i}$, a second list of waiting times τ_j, $j = 1, 2, \cdots, m$ must be generated according to

$$\tau_j = -\frac{\ln u_j}{\lambda} \tag{115}$$

The neutron detection times $t_{m,k}$ are thus

$$t_{m,k} = t_{m,i} + \tau_j \tag{116}$$

$$k = m(i-1) + j \tag{117}$$

To produce the final list of detection times, all the $t_{m,k}$ must simply be combined and sorted. In this way, time-tagged neutron data can be produced quickly.

E. Time Interval Distributions

For multiplying nuclear material sources, the waiting time between successive neutrons is[27]

$$I_0 \Delta T = \underbrace{\frac{1}{R_1} \sum_{m=1}^{\infty} F_{\mathrm{S}} \mathrm{e}_{\mathrm{S}m} \left(\sum_{k=0}^{m-1} e^{-k\lambda T} \right) \mathrm{n}_0(T) R_1 \Delta T}_{\text{Next neutron from different fission chain}} + \underbrace{\frac{1}{R_1} \sum_{m=2}^{\infty} F_{\mathrm{S}} \mathrm{e}_{\mathrm{S}m} \left(\sum_{k=1}^{m-1} k e^{-k\lambda T} \right) b_0(T) \lambda \Delta T}_{\text{Next neutron from same fission chain}} \tag{118}$$

The term F_{S} is the rate of spontaneous fissions,

$$F_{\mathrm{S}} = \frac{N_{\mathrm{A}}}{A} \frac{\ln 2}{t_{1/2}} \frac{t_{1/2}}{t_{1/2}^{\mathrm{SF}}} m_{\mathrm{S}} \tag{119}$$

where N_{A} is Avogadro's number, A is the atomic mass, m_{S} is the mass of the spontaneously fissioning isotope, $t_{1/2}$ is the half-life, and $t_{1/2}^{\mathrm{SF}}$ is the half-life against spontaneous fission. The distribution $\mathrm{e}_{\mathrm{S}m}$ is the probability of detecting m neutrons from a spontaneous fission-initiated fission chain, b_0 is the probability of counting zero neutrons in a randomly-triggered time gate of duration T, and n_0 is the probability of counting zero neutrons in a time gate of duration T triggered by a neutron count.

Eq. 118 works just as well for background neutrons from cosmic ray air showers with the trivial replacement $F_{\mathrm{S}} \mathrm{e}_{\mathrm{S}m} \rightarrow r_m^{\mathrm{Bkg}}$ for $m \geq 1$ from Eq. 78,

$$I_0^{\mathrm{Bkg}} \Delta T = \underbrace{\frac{1}{R_1^{\mathrm{Bkg}}} \sum_{m=1}^{\infty} r_m^{\mathrm{Bkg}} \left(\sum_{k=0}^{m-1} e^{-k\lambda_{\mathrm{Bkg}} T} \right) \mathrm{n}_0^{\mathrm{Bkg}}(T) R_1^{\mathrm{Bkg}} \Delta T}_{\text{Next neutron from different air shower}} + \underbrace{\frac{1}{R_1^{\mathrm{Bkg}}} \sum_{m=2}^{\infty} r_m^{\mathrm{Bkg}} \left(\sum_{k=1}^{m-1} k e^{-k\lambda_{\mathrm{Bkg}} T} \right) b_0^{\mathrm{Bkg}}(T) \lambda_{\mathrm{Bkg}} \Delta T}_{\text{Next neutron from same air shower}} \tag{120}$$

In Eqs. 118 and 120, for both terms, the first count occurs at $t = 0$ and a second count occurs at $t = T$ where T is the time interval between neutrons. The logic of the first term is:

1. Probability that the first count is from a fission chain but no count from the same chain happens within time T: $1/R_1 \sum_{m=1}^{\infty} F_{\mathrm{S}} \mathrm{e}_m \left(\sum_{k=0}^{m-1} e^{-k\lambda T} \right)$
2. Probability of no counts from a fission chain in time T following a trigger count at $T = 0$: $n_0(T)$
3. Probability that a neutron from a fission chain is counted within ΔT: $R_1 \, \Delta T$

The logic of the second term is:

1. Probability that the first count is from a fission chain and another count from the same chain escapes detection until time T: $1/R_1 \sum_{m=2}^{\infty} F_{\mathrm{S}} \mathrm{e}_m \left(\sum_{k=1}^{m-1} k e^{-k\lambda T} \right)$

2. Probability of no counts from a fission chain in time T: $b_0(T)$

3. Probability that a diffusing neutron from a fission chain is counted within ΔT: $\lambda\,\Delta T$

For Eq. 120, r_m^{Bkg} can be determined from a measured background count distribution as described above in §III C. The terms[27]

$$b_0^{\mathrm{Bkg}}(T) = e^{-\left(\sum_{k=1}^{\infty}\Lambda_k^{\mathrm{Bkg}}\right)} \tag{121}$$

$$\mathrm{n}_0^{\mathrm{Bkg}}(T) = b_0^{\mathrm{Bkg}}(T)\frac{1}{R_1^{\mathrm{Bkg}}}\sum_{m=1}^{\infty} r_m^{\mathrm{Bkg}}\left(\sum_{k=0}^{m-1} e^{-k\lambda_{\mathrm{Bkg}}T}\right) \tag{122}$$

F. Fission Chains Combined With Correlated Backgrounds

A complication arrises if a correlated background is combined with fission chains from a multiplying source. Instead of the time interval distribution having only two terms, there will be six terms that take into account the following possibilities:

1. The first neutron is from a fission chain and the second neutron is from a different fission chain;
2. The first neutron is from a fission chain and the second neutron is from the same fission chain;
3. The first neutron is from an air shower and the second neutron is from a different air shower;
4. The first neutron is from an air shower and the second neutron is from the same air shower;
5. The first neutron is from an air shower and the second neutron is from a fission chain;
6. The first neutron is from a fission chain and the second neutron is from an air shower.

$$\begin{aligned} I_0\Delta T = &\underbrace{\frac{1}{R_1^{\mathrm{Total}}}\sum_{m=1}^{\infty} F_{\mathrm{S}}\mathrm{e}_m\left(\sum_{k=0}^{m-1} e^{-k\lambda T}\right)\mathrm{n}_0 b_0^{\mathrm{Bkg}} R_1\Delta T}_{\text{First from fission chain; next from different fission chain}} + \underbrace{\frac{1}{R_1^{\mathrm{Total}}}\sum_{m=2}^{\infty} F_{\mathrm{S}}\mathrm{e}_m\left(\sum_{k=1}^{m-1} k e^{-k\lambda T}\right) b_0 b_0^{\mathrm{Bkg}}\lambda\Delta T}_{\text{First from fission chain; next from same fission chain}} \\ &+ \underbrace{\frac{1}{R_1^{\mathrm{Total}}}\sum_{m=1}^{\infty} r_m^{\mathrm{Bkg}}\left(\sum_{k=0}^{m-1} e^{-k\lambda_{\mathrm{Bkg}}T}\right)\mathrm{n}_0^{\mathrm{Bkg}} b_0 R_1^{\mathrm{Bkg}}\Delta T}_{\text{First from air shower; next from different air shower}} + \underbrace{\frac{1}{R_1^{\mathrm{Total}}}\sum_{m=2}^{\infty} r_m^{\mathrm{Bkg}}\left(\sum_{k=1}^{m-1} k e^{-k\lambda_{\mathrm{Bkg}}T}\right) b_0^{\mathrm{Bkg}} b_0\lambda_{\mathrm{Bkg}}\Delta T}_{\text{First from air shower; next from same air shower}} \\ &+ \underbrace{\frac{1}{R_1^{\mathrm{Total}}}\sum_{m=1}^{\infty} r_m^{\mathrm{Bkg}}\left(\sum_{k=0}^{m-1} e^{-k\lambda_{\mathrm{Bkg}}T}\right)\mathrm{n}_0^{\mathrm{Bkg}} b_0 R_1\Delta T}_{\text{First from air shower; next from fission chain}} + \underbrace{\frac{1}{R_1^{\mathrm{Total}}}\sum_{m=1}^{\infty} F_{\mathrm{S}}\mathrm{e}_m\left(\sum_{k=0}^{m-1} e^{-k\lambda T}\right)\mathrm{n}_0 b_0^{\mathrm{Bkg}} R_1^{\mathrm{Bkg}}\Delta T}_{\text{First from fission chain; next from air shower}} \end{aligned} \tag{123}$$

where $R_1^{\mathrm{Total}} = R_1 + R_1^{\mathrm{Bkg}}$.

The logic of the first term is:

1. Probability that the first count is from a fission chain but no count from the same chain happens within time T: ${}^1/_{R_1^{\mathrm{Total}}}\sum_{m=1}^{\infty} F_{\mathrm{S}}\mathrm{e}_m\left(\sum_{k=0}^{m-1} e^{-k\lambda T}\right)$
2. Probability of no counts from a fission chain within time T following a trigger count at $T = 0$: $n_0(T)$
3. Probability of no counts from an air shower within time T: $b_0^{\mathrm{Bkg}}(T)$
4. Probability that a neutron from a fission chain is counted within ΔT: $R_1\,\Delta T$

The logic of the second term is:

1. Probability that the first count is from a fission chain and another count from the same chain escapes detection until time T: ${}^1/_{R_1^{\mathrm{Total}}}\sum_{m=2}^{\infty} F_{\mathrm{S}}\mathrm{e}_m\left(\sum_{k=1}^{m-1} k e^{-k\lambda T}\right)$
2. Probability of no counts from a fission chain within time T: $b_0(T)$
3. Probability of no counts from an air shower within time T: $b_0^{\mathrm{Bkg}}(T)$

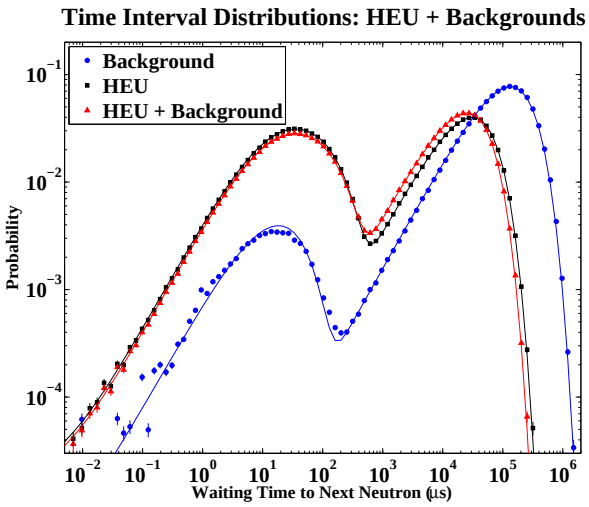

FIG. 28. Time interval distribution for 3,926,094 background neutrons (blue circles) as measured by a high-efficiency well counter over 497,409.6 seconds. Time interval distribution for fission chains from a notional multiplying highly-enriched uranium source with $k_{\text{eff}} = 0.9$ and neutron diffusion time $\lambda^{-1} = 100$ μs driven by the spontaneous fissions from 25 kg of ^{238}U and observed by a neutron multiplicity counter with detection efficiency $\epsilon = 0.03$ (black squares). Time interval distribution for both fission chains from the multiplying HEU and the correlated background (red triangles). The corresponding solid lines are the theoretical distributions, Eq. 120, Eq. 118, and Eq. 123 respectively.

4. Probability that a diffusing neutron from a fission chain is counted within ΔT: $\lambda\,\Delta T$

The logic of the third term is:

1. Probability that the first count is from an air shower but no count from the same air shower happens within time T: ${}^{1}/_{R_1^{\text{Total}}} \sum_{m=1}^{\infty} r_m^{\text{Bkg}} \left(\sum_{k=0}^{m-1} e^{-k\lambda_{\text{Bkg}} T} \right)$
2. Probability of no counts from an air shower within time T following a trigger count at $T = 0$: $n_0^{\text{Bkg}}(T)$
3. Probability of no counts from a fission chain within time T: $b_0(T)$
4. Probability that a neutron from an air shower is counted within ΔT: $R_1^{\text{Bkg}}\,\Delta T$

The logic of the fourth term is:

1. Probability that the first count is from an air shower and another count from the same air shower escapes detection until time T: ${}^{1}/_{R_1^{\text{Total}}} \sum_{m=2}^{\infty} r_m^{\text{Bkg}} \left(\sum_{k=1}^{m-1} k e^{-k\lambda_{\text{Bkg}} T} \right)$
2. Probability of no counts from an air shower within time T: $b_0^{\text{Bkg}}(T)$
3. Probability of no counts from a fission chain within time T: $b_0(T)$
4. Probability that a diffusing neutron from an air shower is counted within ΔT: $\lambda_{\text{Bkg}}\,\Delta T$

The logic of the fifth term is:

1. Probability that the first count is from an air shower but no count from the same air shower happens within time T: ${}^{1}/_{R_1^{\text{Total}}} \sum_{m=1}^{\infty} r_m^{\text{Bkg}} \left(\sum_{k=0}^{m-1} e^{-k\lambda T} \right)$
2. Probability of no counts from an air shower within time T following a trigger count at $T = 0$: $n_0^{\text{Bkg}}(T)$
3. Probability of no counts from a fission chain within time T: $b_0(T)$
4. Probability that a neutron from a fission chain is counted within ΔT: $R_1\,\Delta T$

The logic of the sixth term is:

1. Probability that the first count is from a fission chain but no count from the same chain happens within time T: ${}^{1}/_{R_1^{\text{Total}}} \sum_{m=1}^{\infty} F_{\text{S}} e_m \left(\sum_{k=0}^{m-1} e^{-k\lambda T} \right)$
2. Probability of no counts from a fission chain within time T following a trigger count at $T = 0$: $n_0(T)$
3. Probability of no counts from an air shower within time T: $b_0^{\text{Bkg}}(T)$
4. Probability that a neutron from an air shower is counted within ΔT: $R_1^{\text{Bkg}}\,\Delta T$

Equation 123 can be simplified by combining some of the terms. If the first neutron is from a fission chain, the two possibilities that the next neutron is from a different fission chain or the next neutron is from an air shower can be combined. Similarly, if the first neutron is from an air shower, the two possibilities that the next neutron is from a different air shower or the next neutron is from a fission chain can be combined. Letting $R_1^{\text{Total}} = R_1 + R_1^{\text{Bkg}}$ gives

$$I_0\Delta T = \underbrace{\frac{1}{R_1^{\text{Total}}}\sum_{m=1}^{\infty} F_{\text{S}}\text{e}_m\left(\sum_{k=0}^{m-1} e^{-k\lambda T}\right)\text{n}_0 b_0^{\text{Bkg}} R_1^{\text{Total}}\Delta T}_{\text{First from fission chain; next from different chain or air shower}} + \underbrace{\frac{1}{R_1^{\text{Total}}}\sum_{m=2}^{\infty} F_{\text{S}}\text{e}_m\left(\sum_{k=1}^{m-1} ke^{-k\lambda T}\right) b_0 b_0^{\text{Bkg}}\lambda\Delta T}_{\text{First from fission chain; next from same fission chain}}$$
$$+ \underbrace{\frac{1}{R_1^{\text{Total}}}\sum_{m=1}^{\infty} r_m^{\text{Bkg}}\left(\sum_{k=0}^{m-1} e^{-k\lambda_{\text{Bkg}} T}\right)\text{n}_0^{\text{Bkg}} b_0 R_1^{\text{Total}}\Delta T}_{\text{First from air shower; next from different shower or fission chain}} + \underbrace{\frac{1}{R_1^{\text{Total}}}\sum_{m=2}^{\infty} r_m^{\text{Bkg}}\left(\sum_{k=1}^{m-1} ke^{-k\lambda_{\text{Bkg}} T}\right) b_0^{\text{Bkg}} b_0\lambda_{\text{Bkg}}\Delta T}_{\text{First from air shower; next from same air shower}} \tag{124}$$

Time-correlated neutrons from a notional multiplying highly-enriched uranium source with $k_{\text{eff}} = 0.9$ and neutron diffusion time $\lambda^{-1} = 100$ μs driven by the spontaneous fissions from 25 kg of ^{238}U and observed by a neutron multiplicity counter with detection efficiency $\epsilon = 0.03$ were simulated using the methods described in §III D. The distribution of waiting times between neutron arrivals is shown in Fig. 28 (black squares).

The simulated neutrons were combined with the measured background neutrons by combining the two lists of neutron arrival times and sorting. The distribution of waiting times between neutron arrivals for the combination of HEU + background is shown in Fig. 28 (red triangles).

G. Fission Chains Combined With an External Random Source

If the external source is not a correlated background but rather a random source, Eq. 123 simplifies. Letting $R_1^{\text{Total}} = R_1 + R_1^{\text{Rnd}}$ gives

$$I_0\Delta T = \underbrace{\frac{1}{R_1^{\text{Total}}}\sum_{m=1}^{\infty} F_{\text{S}}\text{e}_m\left(\sum_{k=0}^{m-1} e^{-k\lambda T}\right)\text{n}_0 e^{-R_1^{\text{Rnd}}} R_1\Delta T}_{\text{First from fission chain; next from different fission chain}} + \underbrace{\frac{1}{R_1^{\text{Total}}}\sum_{m=2}^{\infty} F_{\text{S}}\text{e}_m\left(\sum_{k=1}^{m-1} ke^{-k\lambda T}\right) b_0 e^{-R_1^{\text{Rnd}}}\lambda\Delta T}_{\text{First from fission chain; next from same fission chain}}$$
$$+ \underbrace{\frac{1}{R_1^{\text{Total}}} R_1^{\text{Rnd}} e^{-R_1^{\text{Rnd}}} b_0 R_1^{\text{Rnd}}\Delta T}_{\text{First from random source; next from random source}} + \underbrace{\frac{1}{R_1^{\text{Total}}} R_1^{\text{Rnd}} e^{-R_1^{\text{Rnd}}} b_0 R_1\Delta T}_{\text{First from random source; next from fission chain}}$$
$$+ \underbrace{\frac{1}{R_1^{\text{Total}}}\sum_{m=1}^{\infty} F_{\text{S}}\text{e}_m\left(\sum_{k=0}^{m-1} e^{-k\lambda T}\right)\text{n}_0 e^{-R_1^{\text{Rnd}}} R_1^{\text{Rnd}}\Delta T}_{\text{First from fission chain; next from random source}} \tag{125}$$

Equation 125 can be simplified by combining some of the terms. If the first neutron is from a fission chain, the two possibilities that the next neutron is from a different fission chain or the random source can be combined. Similarly, if the first neutron is from the random source, the two possibilities that the next neutron is from the random source or a fission chain can also be combined.

$$I_0\Delta T = \underbrace{\frac{1}{R_1^{\text{Total}}}\sum_{m=1}^{\infty} F_{\text{S}}\text{e}_m\left(\sum_{k=0}^{m-1} e^{-k\lambda T}\right)\text{n}_0 e^{-R_1^{\text{Rnd}}} R_1^{\text{Total}}\Delta T}_{\text{First from fission chain; next from different chain or random source}} + \underbrace{\frac{1}{R_1^{\text{Total}}}\sum_{m=2}^{\infty} F_{\text{S}}\text{e}_m\left(\sum_{k=1}^{m-1} ke^{-k\lambda T}\right) b_0 e^{-R_1^{\text{Rnd}}}\lambda\Delta T}_{\text{First from fission chain; next from same fission chain}}$$
$$+ \underbrace{\frac{1}{R_1^{\text{Total}}} R_1^{\text{Rnd}} e^{-R_1^{\text{Rnd}}} b_0 R_1^{\text{Total}}\Delta T}_{\text{First from random source; next from fission chain or random source}} \tag{126}$$

H. Conslusions

We have extended the theory for the probability distributions of the spacing between neutron counts from fissioning systems[27] to correlated background neutron bursts from cosmic ray air showers as well as background neutrons combined with neutrons from fissioning sys-

tems. We have also detailed methods to parameterize background neutrons.

I. Acknowledgements

We would like to thank L. Nakae, D. Pugh, and P. Kerr for supplying us with the experimental data.

IV. SEQUENTIAL BAYESIAN ALGORITHM

A. Sequential Detection of Fission Chains

In order to develop a sequential processor[28,29], we must test the binary hypothesis that the measured inter-arrival times have evolved from a fissioning SNM threat. The basic decision problem is simply stated as:

GIVEN a set of uncertain neutron multiplicity detector inter-arrival measurements $\{\tau_m\}; m = 0, 1, \cdots, M$ from an unknown source, DECIDE whether or not the source is a threat (SNM). If so, "extract" its characteristic parameters, Θ to "classify" its type.

We are to test the hypothesis that the set of measured neutron inter-arrivals T_M have evolved from a threat or non-threat source. Therefore, we specify the hypothesis test by

$$\begin{aligned} \mathcal{H}_0 :\ T_M &= \mathcal{T}_B\Big(\underline{\mathrm{m}}; \Theta_b\Big) + \mathcal{T}_V\Big(\underline{\mathrm{m}}\Big) \qquad \text{[NON-THREAT]} \\ \mathcal{H}_1 : T_M &= \mathcal{T}_S\Big(\underline{\mathrm{m}}; \Theta_s\Big) + \mathcal{T}_B\Big(\underline{\mathrm{m}}; \Theta_b\Big) + \mathcal{T}_V\Big(\underline{\mathrm{m}}\Big) \text{[THREAT]} \end{aligned} \tag{127}$$

where $\mathcal{T}_S$ is the unknown source inter-arrivals with parameters Θ_s, $\mathcal{T}_B$ is the background inter-arrivals (cosmic rays, etc.) with parameters Θ_b, $\mathcal{T}_V$ is the zero-mean, Gaussian measurement (instrumentation) inter-arrival noise, $T_M := \{\tau_0, \tau_1, \cdots, \tau_M\}$ and $\underline{\mathrm{m}} := 0, 1, \cdots, M$.

The fundamental approach of classical detection theory to solving this binary decision problem is to apply the Neyman-Pearson criterion of maximizing the detection probability for a specified false alarm rate[28] with the parameters Θ *known*. The result leads to a *likelihood ratio* decision function defined by[28,29]

$$\mathcal{L}(T_M; \Theta) := \frac{\Pr[T_M|\Theta; \mathcal{H}_1]}{\Pr[T_M|\Theta; \mathcal{H}_0]} \begin{array}{c} \mathcal{H}_1 \\ > \\ < \\ \mathcal{H}_0 \end{array} \mathcal{T} \tag{128}$$

with threshold $\mathcal{T}$. This expression implies a "batch" decision, that is, we gather the M inter-arrivals T_M, calculate the likelihood (Eq. 128) over the entire batch of data and compare it to the threshold $\mathcal{T}$ to make the decision.

Sequential Processor

An alternative to the batch approach is the sequential method which can be developed by expanding the likelihood ratio for each inter-arrival to obtain

$$\mathcal{L}(T_M; \Theta) = \frac{\Pr[T_M|\Theta; \mathcal{H}_1]}{\Pr[T_M|\Theta; \mathcal{H}_0]} = \frac{\Pr[\tau_0, \tau_1, \cdots, \tau_M|\Theta; \mathcal{H}_1]}{\Pr[\tau_0, \tau_1, \cdots, \tau_M|\Theta; \mathcal{H}_0]} \tag{129}$$

From the chain rule of probability and Bayes' rule[30] for $\ell = 0, 1$, we have that

$$\begin{aligned} \Pr[T_M|\Theta; \mathcal{H}_\ell] &= \Pr[\tau_M, T_{M-1}|\Theta; \mathcal{H}_\ell] \\ &= \Pr[\tau_M|T_{M-1}, \Theta; \mathcal{H}_\ell] \times \Pr[T_{M-1}|\Theta; \mathcal{H}_\ell] \end{aligned} \tag{130}$$

Substituting these expressions into the likelihood ratio above, replacing $m \to M$ and grouping, we obtain

$$\mathcal{L}(T_m; \Theta) = \left[\frac{\Pr[T_{m-1}|\Theta; \mathcal{H}_1]}{\Pr[T_{m-1}|\Theta; \mathcal{H}_0]}\right] \times \frac{\Pr[\tau_m|T_{m-1}, \Theta; \mathcal{H}_1]}{\Pr[\tau_m|T_{m-1}, \Theta; \mathcal{H}_0]} \tag{131}$$

and the recursion or equivalently *sequential likelihood ratio* for the m-th inter-arrival follows as

$$\mathcal{L}(T_m; \Theta) = \mathcal{L}(T_{m-1}; \Theta) \times \frac{\Pr[\tau_m|T_{m-1}, \Theta; \mathcal{H}_1]}{\Pr[\tau_m|T_{m-1}, \Theta; \mathcal{H}_0]}; m = 0, \cdots, M \tag{132}$$

with $\Pr[\tau_0|T_{-1}, \Theta; \mathcal{H}_\ell] = \Pr[\tau_0|\Theta; \mathcal{H}_\ell]$, the *prior* under each hypothesis.

Therefore, the Wald *sequential probability-ratio test* is[31,32]

$$\begin{array}{rlll} \mathcal{L}(T_m; \Theta) & > \mathcal{T}_1(m) & \text{Accept} & \mathcal{H}_1 \\ \mathcal{T}_0(m) \leq \mathcal{L}(T_m; \Theta) & \leq \mathcal{T}_1(m) & \text{Continue} & \\ \mathcal{L}(T_m; \Theta) & < \mathcal{T}_0(m) & \text{Accept} & \mathcal{H}_0 \end{array} \tag{133}$$

where the thresholds are specified in terms of the false alarm (P_{FA}) and miss (P_M) probabilities as

$$\mathcal{T}_0(m) = \frac{\mathrm{P}_M(m)}{1 - \mathrm{P}_{FA}(m)} \qquad \mathcal{T}_1(m) = \frac{1 - \mathrm{P}_M(m)}{\mathrm{P}_{FA}(m)} \tag{134}$$

These thresholds are determined from a receiver operating characteristic (ROC) curve (detection versus false alarm probabilities) obtained by simulation or a controlled experiment to calculate the decision function. That is, an operating point is selected from the ROC corresponding to specific detection (or equivalently miss) and false-alarm probabilities specifying the required thresholds which are calculated according to Eq. 134 for each parameter update.

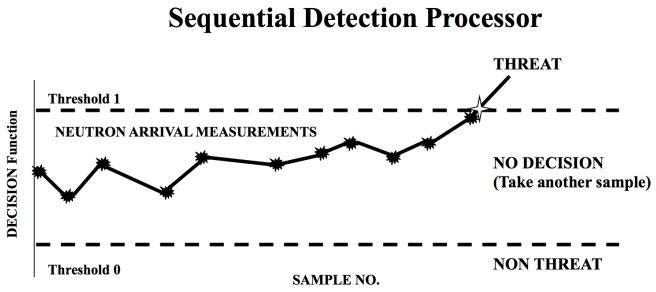

FIG. 29. As each individual inter-arrival is extracted, it is discriminated, estimated, the decision function calculated and compared to thresholds to DECIDE if the targeted threat is detected. Quantitative performance and sequential thresholds are determined from estimated ROC curve and the selected operating point (detection/false alarm probability).

It should be noted that the non-sequential Bayesian detection technique is optimum in the sense that no other hypothesis test can achieve a smaller average risk (smallest error probabilities[31,32]). This approach was developed under the assumption that the number of measurements required to achieve this optimum is known (fixed) in advance. In relaxing this constraint, sequential detection techniques are superior to fixed non-sequential Bayesian detection in the sense that "on the average" a substantially smaller number of measurements are required to achieve the same error probabilities. The disadvantage though is that this number of measurements required is random.

With this in mind, it is possible to show that the *average number of measurements* required to reach a decision is given by[32]:

A reasonable approach to this problem of making a reliable decision with high confidence in a timely manner is to develop a sequential detection processor as illustrated in Fig. 29. At each neutron arrival (at τ_m), we *sequentially update* the decision function and compare it to the thresholds to perform the detection—"neutron-by-neutron". Here as each neutron is monitored producing the inter-arrival sequence, the processor takes each inter-arrival measurement and attempts to "decide" whether or not it evolves from a threat or non-threat. For each inter-arrival, the decision function is "sequentially" updated and compared to the detection thresholds obtained from the ROC curve operating point enabling a rapid decision. Once the threshold is crossed, the decision (threat or non-threat) is made and the arrival is processed; however, if not enough data is available to make the decision, then another measurement is obtained.

Generalized Likelihood-Ratio Test

For our problem, we typically have information about the background, disturbance and noise parameters, but we rarely have the source information. Therefore, we still can make a decision, but require estimates of the unknown parameters, that is, $\hat{\Theta} \rightarrow \Theta$. In this case, we must construct a *composite* or *generalized* likelihood-ratio test (GLRT).

Therefore from the batch likelihood decision function of Eq. 129, we can consider the two cases of the GLRT: (i) parameters are *random* or (ii) parameters are *deterministic* but *unknown*.

When the conditional distributions of our problem contain a set of parameters that are *random*, then the distributions of interest are joint, that is, $\Pr[T_M, \Theta|\mathcal{H}_\ell]$ must be incorporated in the likelihood ratio such that

$$\mathcal{L}(T_M;\Theta) = \frac{\Pr[T_M|\mathcal{H}_1]}{\Pr[T_M|\mathcal{H}_0]} = \frac{\int \Pr[T_M,\Theta|\mathcal{H}_1]d\Theta}{\int \Pr[T_M,\Theta|\mathcal{H}_0]d\Theta} \tag{135}$$

Applying Bayes' rule to expand the distributions, we have the general solution for the random case as

$$\mathcal{L}(T_M;\Theta) = \frac{\Pr[T_M|\mathcal{H}_1]}{\Pr[T_M|\mathcal{H}_0]} = \frac{\int \Pr[T_M|\Theta;\mathcal{H}_1]\Pr[\Theta|\mathcal{H}_1]d\Theta}{\int \Pr[T_M|\Theta;\mathcal{H}_0]\Pr[\Theta|\mathcal{H}_0]d\Theta} \tag{136}$$

Assuming *known* parametric distributions, $\Pr[\Theta|\mathcal{H}_\ell]$, then by integrating over Θ, the likelihood ratio can be determined reducing the composite problem to a simple hypothesis testing problem.

In the second case, Θ is considered to be deterministic but unknown. Here the approach is to estimate the unknown parameter vector $\hat{\Theta} \rightarrow \Theta$ under each hypothesis and proceed with the simple testing. A *maximum likelihood estimate* $\hat{\Theta}_{ML}$, can be used to create the GLRT such that

$$\mathcal{L}(T_M;\Theta) = \frac{\max\limits_{\Theta_1} \Pr[T_M|\Theta_1;\mathcal{H}_1]}{\max\limits_{\Theta_0} \Pr[T_M|\Theta_0;\mathcal{H}_0]} \tag{137}$$

This is the approach we employ *initially*. The batch solution for the GLRT can also be extended to the sequential case as before giving the solution by simply replacing $\hat{\Theta}_{ML} \rightarrow \Theta$, that is,

$$\mathcal{L}(T_m;\hat{\Theta}) = \mathcal{L}(T_{m-1};\hat{\Theta}) \times \frac{\Pr[\tau_m|T_{m-1},\hat{\Theta}_1;\mathcal{H}_1]}{\Pr[\tau_m|T_{m-1},\hat{\Theta}_0;\mathcal{H}_0]}; \quad m = 0,1,\cdots,M \tag{138}$$

Anticipating Gaussian models (exponential family[30]) for our unknown parameters, we develop the logarithmic form of the sequential likelihood decision function. Simply taking the natural logarithm of Eq. 138, that is, $\Lambda(T_M;\Theta) := \ln \mathcal{L}(T_M;\Theta)$ we obtain the *log-likelihood* sequential decision function as

$$\Lambda(T_m;\hat{\Theta}) = \Lambda(T_{m-1};\hat{\Theta}) + \ln \Pr[\tau_m|T_{m-1},\hat{\Theta}_1;\mathcal{H}_1] - \ln \Pr[\tau_m|T_{m-1},\hat{\Theta}_0;\mathcal{H}_0] \quad (139)$$

Using these formulations, we develop the detection algorithm for our problem next. We should note that we only consider the "threat detection problem" in this paper.

B. Physics-Based Models for Detection

In this section we discuss the development of a physics-based fission model capturing the joint distribution of the overall fission processes and their underlying statistics. As mentioned above, this development is based on the fundamental theory and modeling.[12] We start with the basic neutron physics and progress to the full propagation leading to the desired probability distribution.

Fission-Based Processing Model

A neutron arriving at a detector at energy level α and arrival time t_m can be characterized as a single impulse $\epsilon_m\delta(t-t_m)$. A train of neutrons is defined as a set of arrivals that do *not* overlap in time and can be written simply as

$$\eta(t) := \sum_{m=0}^{M} \epsilon_m \delta(t-t_m) \quad (140)$$

Inter-arrival times are defined as $\tau_m := t_m - t_{m-1}$ for $m = 0, 1, \cdots, M$ with $t_{-1} := 0$ and the complete set of inter-arrivals by $T_M := \{\tau_0, \tau_1, \cdots, \tau_M\}$. These arrivals are measured by a neutron multiplicity counter[33] that is basically a neutron detector that evaluates the inter-arrival time probability distribution of neutrons emitted spontaneously by fissionable materials. Recall that the radioactive decay of each unstable nucleus produces multiple neutrons that can interact with other nuclei exciting them to energy levels enabling them to split into smaller unequal fission fragments which are also unstable and decay even further (emitting neutrons) toward stable nuclei. The detection of these neutrons, which can pass through heavy shielding, provides a methodology to detect special nuclear material. The key issue with threat materials is that the number of neutrons released are produced by a single decay defining its *multiplication*. These "correlated" neutrons offer a unique SNM signature that indicates both its multiplication and the mass of spontaneous fission isotopes. Thus, the *neutron multiplicity counter* or *neutron detector* is a stochastic measurement system creating an estimated time-interval probability distribution that is used in the neutron detection process to alarm on SNM. Thus, the essential ingredient of these measurements is its underlying time-interval probability distribution.

A simplistic model of the multiplication process consists of a fission chain generated by a spontaneous fission under the assumption that the source is characterized by an inhomogeneous Poisson process with a varying fission rate.[6,10] During a single fission chain ν-neutrons are emitted with probability P_ν. These emissions are slowed in a moderator and diffuse exponentially in time as thermal neutrons. Then the probability that n of the ν neutrons are absorbed in the detector and converted to electrical pulses is

$$\Pr[\nu;T_M] = P_\nu(\,{}^{\nu}_{n}\,)\epsilon^n(1-\epsilon)^{\nu-n} \quad (141)$$

where ϵ is the probability of neutron detection (detection efficiency). Mathematically, we can represent the N_ν-neutron burst sequence emitted by

$$\eta(\tau_m;\Theta_S) = \sum_{i=1}^{N_\nu} \alpha_i \delta(\tau - \tau_m(\Theta_S)); m = 0, \cdots, M; \tau_m < T_M \quad (142)$$

for α the i-th energy of the neutron at the m-th inter-arrival in the M-th time interval. Typically, we ignore the neutron energy and concentrate on the inter-arrival, since the source information is contained in $\tau_m(\Theta_S)$.

For spontaneous fissions, the quantity, k_{eff}, is the average number of neutrons from one fission that initiates another fission[34]. Any remaining neutrons are absorbed or escape. The value of k_{eff} specifies how a chain will proceed. For instance, the $k_{\text{eff}} = 1$ (critical mass) leads to a fission level that is constant and is typical to power plant operation, while $k_{\text{eff}} > 1$ (super-critical mass) for an event implies that there may be k_{eff}-events to follow which is typical in weapons applications. For the latter, the number of fission reactions *increase* exponentially. We will use Eq. 142 in developing the subsequent fission detection schemes to follow.

Inter-arrival Distribution

Theoretically, the conditional distribution of inter-arrival times τ conditioned on a set of source parameters Θ is given by[12,27]

$$\Pr[\tau|\Theta] = \underbrace{R_1 r_0 \mathrm{n}_0}_{\textit{Time between chain initiations}} + \underbrace{\frac{F_S}{R_1}\sum_{n=2}^{\infty} \mathrm{e}_n(\epsilon)\left(\sum_{k=1}^{n-1} k e^{-k\lambda\tau}\right)\lambda b_0(\tau)}_{\textit{Time between neutrons in same chain}} \quad (143)$$

where

R_1 is the count rate;

r_0 is the probability that NO neutrons are detected within the time-interval τ;

n_0 is the probability of zero counts in time interval τ;

τ is the time interval or inter-arrival time;

F_S is the fission rate;

$\mathrm{e}_n(\epsilon)$ is the probability of detecting n neutrons from the same fission chain;

λ is the inverse of the diffusion time scale; and

$b_0(\tau)$ is the probability of NO counts in time interval τ.

Embedded in Eq. 143 is a set of various relations that capture the time-interval probability:

$$Fs = \frac{N_A}{A}\frac{\ln 2\ t_{1/2}}{t_{1/2}\ t_{1/2}^{SF}} m_{\mathrm{S}}$$

$$R_1 = \epsilon\ q\ M\ \overline{\nu}_S\ F_S$$

for

m_{S} mass of the source;

ϵ is the detection efficiency;

p is the probability that a neutron induces a fission;

q is the escape probability ($q = 1 - p$);

M is the system multiplication;

$\overline{\nu}_S$ is the average neutron count from a spontaneous fission;

$\overline{\nu}_I$ is the average neutron count from an induced fission;

N_A is Avogadro's number;

A is the atomic weight; and

$t_{1/2}$ is the half-life.

with *multiplication* given by

$$M = \frac{1}{1 - p\overline{\nu}_I} = \frac{1}{1 - k_{\mathrm{eff}}}$$

For $k_{\mathrm{eff}} < 1$ the *escape multiplication* $M_e = q \times M$ and *detection efficiency* ϵ are related by $\epsilon = {}^{a}/_{(bM_e^2 + cM_e)}$; $0 \leq \epsilon \leq 1$; a, b, c are fit parameters. The *probability* of detecting n-neutrons of the ν emitted with probability P_ν is given by

$$\mathrm{e}_n(\epsilon) = \sum_{\nu=n}^{\infty} P_\nu \begin{pmatrix} \nu \\ n \end{pmatrix} \epsilon^n (1-\epsilon)^{\nu-n} \tag{144}$$

The following probabilities complete the distribution

$$r_0 = \frac{F_S}{R_1} \sum_{n=1}^{\infty} \mathrm{e}_n(\epsilon) \Big(\sum_{k=0}^{n-1} e^{-k\lambda\tau} \Big) \tag{145}$$

and

$$b_0(\tau) = \exp\left[- F_S \int_0^\tau \frac{1}{1 - e^{-\lambda t}} \left(1 - \sum_{\nu=0}^{\infty} P_\nu (1 - \epsilon(1 - e^{-\lambda t}))^\nu \right) dt \right] \tag{146}$$

$$\mathrm{n}_0(\tau) = r_0(\tau) \times b_0(\tau)$$

Since the objective is to "decide" whether or not a fissioning source is present, we require a-priori knowledge of the source parameters: mass, multiplication, detection efficiency and diffusion time scale parameters. Notationally, we define the source parameters as $m_{\mathrm{S}}, k_{\mathrm{eff}}, \epsilon$ and λ respectively and note their intimate relations in the overall probability distribution function.

In order to investigate the subsequent processors and evaluate their performance, a simulation of neutron arrival times was developed using the following well-founded[12,35] approach: (1) a set of Poisson *rates* dependent on k_{eff}, source mass m_{S}, and efficiency ϵ for the detection of a given number of neutrons from the same fission chain is calculated; (2) *occurrence times* are sampled from a Poisson process for fission chains where a specified number of neutrons are detected; (3) sampling is repeated for *each* rate corresponding to the number of neutrons that can be detected out to a minimum probability of 10^{-15}; (4) *n diffusion time increments* are sampled from an exponential distribution with parameter λ (inverse diffusion time scale) for a chain where n neutrons were detected; (5) these diffusion time increments are then added to the occurrence time of the parent fission chain to obtain a *detection time*; and (6) all of the resulting detection times are merged to produce the synthesized time-tagged data for processor performance analysis. For more details and the underlying mathematics see[12,35].

A calculation of this underlying theoretical distribution for a set of source parameters is shown in Fig. 28

where we observe the characteristic bimodal time interval probability (solid line)[12]. A simulation was performed and its distribution estimated from the synthesized data samples. These estimated probabilities are the points lying on the curve of Fig. 28, that is, they lie on the calculated theoretical waiting time distribution curve[12] indicating a reasonable realization.

It should be noted that developing a simulator that is not scenario dependent is the usual approach in model-based (physics-based) processor design[36] in order to decouple extraneous and unpredictable events that detract from a focused processor performance analysis. We apply the processor to data synthesized from the MCNP Monte Carlo simulator[37] for a scenario illustrating a high multiplication events in §IV E.

Sequential Detection for Fission Processes

Here we start with the results of the previous section and incorporate the physics of the fission process. For fission detection, we start with the simple neutron model of Eq. 142 at inter-arrival time τ_m leading to the subsequent (sequential) hypothesis test:

$$\mathcal{H}_0 : \ \tau_m = \mathcal{T}_B\Big(m;\Theta_b\Big) + \mathcal{T}_V\Big(m\Big) \quad \text{[NON-THREAT]}$$

$$\mathcal{H}_1 : \tau_m = \mathcal{T}_S\Big(m;\Theta_s\Big) + \mathcal{T}_B\Big(m;\Theta_b\Big) + \mathcal{T}_V\Big(m\Big) \text{[THREAT]} \tag{147}$$

The sequential detection solution (as before) for this problem with unknown source parameters follows directly from the GLRT results of Eq. 138 to yield

$$\mathcal{L}(T_m;\hat{\Theta}) = \mathcal{L}(T_{m-1};\hat{\Theta}) \times \frac{\Pr[\tau_m|T_{m-1},\hat{\Theta};\mathcal{H}_1]}{\Pr[\tau_m|T_{m-1},\Theta;\mathcal{H}_0]} \tag{148}$$

To implement the processor, we must first determine the required conditional probabilities in order to specify the decision function, that is,

$$\begin{aligned}\Pr[\tau_m|T_{m-1},\hat{\Theta};\mathcal{H}_1] = \Pr[\mathcal{T}_S(m;\Theta_S)|T_{m-1},\hat{\Theta}_S;\mathcal{H}_1] + \\ \Pr[\mathcal{T}_B(m;\Theta_b)|T_{m-1},\Theta_b;\mathcal{H}_1] + \\ \Pr[\mathcal{T}_V(m)]\end{aligned} \tag{149}$$

and under the null hypothesis

$$\begin{aligned}\Pr[\tau_m|T_{m-1},\Theta;\mathcal{H}_0] = \Pr[\mathcal{T}_B(m;\Theta_b)|T_{m-1},\Theta_b;\mathcal{H}_0] \\ +\Pr[\mathcal{T}_V(m)]\end{aligned} \tag{150}$$

where the Gaussian inter-arrival noise is distributed as $\mathcal{T}_V \sim \mathcal{N}(0,\sigma^2_{vv})$ and the known background disturbances[38] are ignored (at this point) while the inter-arrival distribution is specified (instantaneously at τ_m) by Eq. 143 with $\tau_m \to \tau$ to give:

$$\begin{aligned}\Pr[\mathcal{T}_S(m;\Theta_S)|T_{m-1},\hat{\Theta}_S;\mathcal{H}_1] = R_1 r_0 \mathrm{n}_0 + \\ \frac{F_S}{R_1}\sum_{n=2}^{\infty}\mathrm{e}_n(\epsilon)\left(\sum_{k=1}^{n-1} k e^{-k\lambda\tau_m}\right)\lambda b_0(\tau_m)\end{aligned} \tag{151}$$

$$\Pr[\mathcal{T}_V(m)] = \frac{1}{\sqrt{2\pi\sigma^2_{vv}}}\exp\Big\{-\frac{1}{2}\frac{\mathcal{T}^2_V(m)}{\sigma^2_{vv}}\Big\} \tag{152}$$

Therefore, the likelihood ratio becomes (simply)

$$\begin{aligned}&\mathcal{L}(T_m;\Theta) = \mathcal{L}(T_{m-1};\Theta) \times \\ &\Big[R_1 r_0 \mathrm{n}_0 + \frac{F_S}{R_1}\sum_{n=2}^{\infty}\mathrm{e}_n(\epsilon)\left(\sum_{k=1}^{n-1} k e^{-k\lambda\tau_m}\right)\lambda b_0(\tau_m) \\ &+\frac{1}{\sqrt{2\pi\sigma^2_{vv}}}\exp\Big\{-\frac{1}{2}\frac{\mathcal{T}^2_V(m)}{\sigma^2_{vv}}\Big\}\Big]\Big/ \\ &\frac{1}{\sqrt{2\pi\sigma^2_{vv}}}\exp\Big\{-\frac{1}{2}\frac{\mathcal{T}^2_V(m)}{\sigma^2_{vv}}\Big\}\end{aligned} \tag{153}$$

which completes the case with Θ_S, an unknown constant to be estimated independently.

The equivalent *log-likelihood ratio* is given by

$$\begin{aligned}&\Lambda(T_m;\Theta) = \Lambda(T_{m-1};\Theta) + \\ &\ln\Big[R_1 r_0 \mathrm{n}_0 + \frac{F_S}{R_1}\sum_{n=2}^{\infty}\mathrm{e}_n(\epsilon)\left(\sum_{k=1}^{n-1} k e^{-k\lambda\tau_m}\right)\lambda b_0(\tau_m) \\ &+\frac{1}{\sqrt{2\pi\sigma^2_{vv}}}\exp\Big\{-\frac{1}{2}\frac{\mathcal{T}^2_V(m)}{\sigma^2_{vv}}\Big\}\Big] \\ &-\ln\Big(\frac{1}{\sqrt{2\pi\sigma^2_{vv}}}\Big) + \frac{1}{2}\frac{\mathcal{T}^2_V(m)}{\sigma^2_{vv}}\end{aligned} \tag{154}$$

We can also extend the problem to the *random* parameter case. Suppose we assume that each of the independent source parameters are governed by a *random walk/random constant* model. The parameters are assumed piecewise constant and subjected to zero-mean, Gaussian, random uncertainties, $w_\Theta(\tau_m)$ driving the process with covariance $R_{w_\Theta w_\Theta}(\tau_m)$[39], then in this case we have that the initial parameters, $\Theta(\tau_0) \sim \mathcal{N}\big(m_\Theta(\tau_0), R_{\Theta\Theta}(\tau_0)\big)$, where $m_\Theta(\tau_o)$ is the initial mean with $R_{\Theta\Theta}(\tau_0)$ its corresponding covariance. A more detailed discussion follows subsequently when we discuss the underlying parameter estimation problem in §IV C (see Eq. 168). Thus, the corresponding multivariate source parameter distribution is given by

$$\begin{aligned}&\Pr[\Theta(\tau_m)] = (2\pi)^{-N_\Theta/2}|R_{\Theta\Theta}(\tau_m)|^{-1/2} \times \\ &\exp\Big\{-1/2\ (\Theta(\tau_m) - m_\Theta(\tau_m))' R^{-1}_{\Theta\Theta}(\tau_m)(\Theta(\tau_m) - \Theta(\tau_m))\Big\}\end{aligned} \tag{155}$$

and the log-likelihood ratio becomes

$$\Lambda(T_m;\Theta) = \Lambda(T_{m-1};\Theta) + \ln \Pr[\tau_m, \Theta(\tau_m)|T_{m-1};\mathcal{H}_1] - \ln \Pr[\tau_m|T_{m-1},\Theta;\mathcal{H}_0] \tag{156}$$

where the second term can be expanded further by applying Bayes' rule to give

$$\Pr[\tau_m, \Theta(\tau_m)|T_{m-1};\mathcal{H}_1] = \Pr[\tau_m|T_{m-1},\Theta(\tau_m);\mathcal{H}_1] \times \Pr[\Theta(\tau_m)|T_{m-1};\mathcal{H}_1] \tag{157}$$

Substituting this expression for the source distribution of Eq. 149 gives

$$\Pr[\mathcal{T}_S(m;\Theta_S)|T_{m-1},\hat{\Theta}_S;\mathcal{H}_1] \longrightarrow \Pr[\tau_m|T_{m-1},\Theta(\tau_m);\mathcal{H}_1] \times \Pr[\Theta(\tau_m)|T_{m-1};\mathcal{H}_1] \tag{158}$$

With this in mind, the sequential log-likelihood can be calculated directly by substituting the prescribed distributions into Eq. 156 to give

$$\begin{aligned}\Lambda(T_m;\Theta) = \Lambda(T_{m-1};\Theta) + \ln\Bigg(R_1 r_0 \mathrm{n}_0 + \frac{F_S}{R_1}\sum_{n=2}^{\infty}\mathrm{e}_n(\epsilon)\left(\sum_{k=1}^{n-1} k e^{-k\lambda\tau_m}\right)\lambda b_0(\tau_m) \\ \times(2\pi)^{-N_\Theta/2}|R_{\Theta\Theta}(\tau_m)|^{-1/2}\times\exp\Big\{-1/2\ (\Theta(\tau_m)-m_\Theta(\tau_m))' R^{-1}_{\Theta\Theta}(\tau_m)(\Theta(\tau_m)-\Theta(\tau_m))\Big\} \\ + \frac{1}{\sqrt{2\pi\sigma^2_{vv}}}\exp\Big\{-\frac{1}{2}\frac{\mathcal{T}^2_V(m)}{\sigma^2_{vv}}\Big\}\Bigg) + \frac{1}{2}\ln\left(2\pi\sigma^2_{vv}\right) - \frac{1}{2}\frac{\mathcal{T}^2_V(m)}{\sigma^2_{vv}}\end{aligned} \tag{159}$$

This completes the development of the sequential Bayesian detection approach for fission processes. Next we must consider the parameter estimation problem in more detail.

C. Bayesian Parameter Estimation

In order to implement the GLRT of the previous section, we must estimate the unknown parameters Θ at each arrival. We first develop the batch scheme and then its sequential version similar to the sequential Bayesian detector of the previous section. Here we develop the Bayesian parameter estimator that can be applied to the following problem:

GIVEN a set of uncertain multiplicity counter (inter-arrival time) measurements, T_M; FIND the "best" estimate $\hat{\Theta}$ of the unknown fission source parameters, Θ.

From a statistical perspective, we would like to estimate the posterior distribution of source parameters Θ given the entire inter-arrival data set T_M or $\Pr[\Theta|T_M]$. Applying Bayes' theorem we have that

$$\Pr[\Theta|T_M] = \frac{\Pr[T_M|\Theta]\times\Pr[\Theta]}{\Pr[T_M]} \tag{160}$$

Due to the sequential nature of our problem, that is, the neutron multiplicity counter measures each neutron arrival time individually—neutron-by-neutron; we require a *sequential version.*

Sequential Bayesian Processor

It can be shown[39] that a sequential Bayesian solution can be developed for the posterior. Starting with the first term of Eq. 160 and applying Bayes' rule we have

$$\Pr[T_M|\Theta] = \Pr[\tau_M, T_{M-1}|\Theta] = \Pr[\tau_M|T_{M-1},\Theta]\times\Pr[T_{M-1}|\Theta] \tag{161}$$

and for the denominator term we have

$$\Pr[T_M] = \Pr[\tau_M, T_{M-1}] = \Pr[\tau_M|T_{M-1}]\times\Pr[T_{M-1}] \tag{162}$$

Substituting Eqs. 161 and 162 into Eq. 160 and grouping terms, we obtain

$$\Pr[\Theta|T_M] = \underbrace{\left(\frac{\Pr[\tau_M|T_{M-1},\Theta]}{\Pr[\tau_M|T_{M-1}]}\right)}_{W(\tau_m)} \times \underbrace{\left(\frac{\Pr[T_{M-1}|\Theta]\times\Pr[\Theta]}{\Pr[T_{M-1}]}\right)}_{\Pr[\Theta|T_{M-1}]} \tag{163}$$

or

$$\Pr[\Theta|T_M] = W(\tau_m)\times\Pr\left[\Theta|T_{M-1}\right] \tag{164}$$

which is the sequential form of the *posterior distribution*. If we further assume that the inter-arrivals are Markovian with the current arrival depending only on the previous, that is, $(\tau_m, T_{M-1}) \longrightarrow (\tau_m, \tau_{m-1})$, then we have the desired expression for sequentially propagating the posterior as

$$\Pr[\Theta|\tau_m] = W(\tau_m) \times \Pr[\Theta|\tau_{m-1}] \tag{165}$$

where

$$W(\tau_m) = \frac{\Pr[\tau_m|\tau_{m-1}, \Theta]}{\Pr[\tau_m|\tau_{m-1}]} \tag{166}$$

Here we assumed that the parameter vector is a random constant Θ with no associated dynamics to construct a sequential Bayesian processor. However, in the real-world case, it is clear that when measuring neutron inter-arrivals from an unknown source, then there can easily be variations or uncertainties associated with each parameter. Perhaps a more reasonable model for these parametric variations is the *random-walk/constant* introduced in the previous section[39]. That is, we know in continuous-time that the walk is given by $\frac{d}{dt}\Theta(\tau) = w_\Theta(\tau)$ and by taking first differences to approximate the derivative we can obtain a sampled-data representation[39] as

$$\Theta(\tau_m) = \Theta(\tau_{m-1}) + \triangle\tau_m \; w_\Theta(\tau_{m-1}) \tag{167}$$

where $\triangle\tau_m := \tau_m - \tau_{m-1}$ for the parametric uncertainty included in $\Theta(\tau_m) \sim \mathcal{N}(m_\Theta(\tau_m), R_{\Theta\Theta}(\tau_m))$, since $w_\Theta \sim \mathcal{N}(0, R_{w_\theta w_\theta}(\tau_m))$. The variations of each Θ-parameter can be controlled by its initial guess $\Theta(\tau_0)$ and variance, $R_{\Theta\Theta}(\tau_0)$.

The statistics of the *random walk/constant* model are given by the sequential *Gauss-Markov structure*

$$\begin{aligned}
\Theta(\tau_m) &= \Theta(\tau_{m-1}) + \triangle\tau_m \; w_\Theta(\tau_{m-1}) && \text{[STATE]} \\
m_\Theta(\tau_m) &= m_\Theta(\tau_{m-1}) && \text{[MEAN]} \\
R_{\Theta\Theta}(\tau_m) &= R_{\Theta\Theta}(\tau_{m-1}) + (\triangle\tau_m)^2 R_{w_\theta w_\theta}(\tau_{m-1}) && \text{[VARIANCE]}
\end{aligned} \tag{168}$$

Physically we have that $R_{w_\theta w_\theta} = \text{diag}[\sigma^2_{MM} \;\; \sigma^2_{k_{\text{eff}}k_{\text{eff}}} \;\; \sigma^2_{\epsilon\epsilon} \;\; \sigma^2_{\lambda^{-1}\lambda^{-1}}]$ and the subsequent search can include a bounded uniform variate for each initial value, $\Theta_0 = \mathcal{U}[a, b]$ enabling a more pragmatic approach to modeling the parameter set with their individual accompanying uncertainties. With this model in mind, we re-derive the sequential Bayesian processor as before starting with the *batch* approach. We would like to estimate $\Theta(\tau_m)$ with the complete parameter set defined by $\Theta_M := \{\Theta(\tau_0), \Theta(\tau_1) \cdots, \Theta(\tau_M)\}$. The batch posterior is given by Bayes' theorem as before

$$\Pr[\Theta_M|T_M] = \frac{\Pr[T_M|\Theta_M] \times \Pr[\Theta_M]}{\Pr[T_M]} \tag{169}$$

The first term can be decomposed by applying Bayes' rule as

$$\begin{aligned}
\Pr[T_M|\Theta_M] &= \Pr[\tau_m, T_{M-1}|\Theta(\tau_m), \Theta_{M-1}] \\
&= \Pr[\tau_m|T_{M-1}, \Theta(\tau_m), \Theta_{M-1}] \\
&\times \Pr[T_{M-1}|\Theta(\tau_m), \Theta_{M-1}]
\end{aligned} \tag{170}$$

The inter-arrival time τ_m is independent Θ_{M-1} and T_{M-1}, so that the first term in Eq. 170 becomes $\Pr[\tau_m|\Theta(\tau_m)]$, while the second term simplifies to $\Pr[\tau_{M-1}|\Theta_{M-1}]$, since the parameter vector $\Theta(\tau_m)$ is assumed independent of the past measurement data. Therefore, we have

$$\Pr[T_M|\Theta_M] = \Pr[\tau_m|\Theta(\tau_m)] \times \Pr[T_{M-1}|\Theta_{M-1}] \tag{171}$$

The second term of Eq. 169 can be decomposed similarly as

$$\Pr[\Theta_M] = \Pr[\Theta(\tau_m), \Theta_{M-1}] = \Pr[\Theta(\tau_m)|\Theta_{M-1}] \times \Pr[\Theta_{M-1}] \tag{172}$$

and the decomposition of $\Pr[T_M]$ in the denominator is given in Eq. 161 above.

Substituting these relations (Eqs. 161, 171, 172) into Eq. 169, and assuming a Markovian process as before, we obtain

$$\begin{aligned}
\Pr[\Theta_M|T_M] &= \Big(\Pr[\tau_m|\Theta(\tau_m)] \times \Pr[T_{M-1}|\Theta_{M-1}]\Big) \\
&\times \Big(\Pr[\Theta(\tau_m)|\Theta(\tau_{m-1})] \times \Pr[\Theta_{M-1}]\Big) \\
&/ \; \Pr[\tau_m|\tau_{m-1}] \times \Pr[T_{M-1}]
\end{aligned} \tag{173}$$

Now grouping the terms the desired posterior distribution becomes

$$\begin{aligned}
\Pr[\Theta_M|T_M] &= \Big(\frac{\Pr[\tau_m|\Theta(\tau_m)] \times \Pr[\Theta(\tau_m)|\Theta(\tau_{m-1})]}{\Pr[\tau_m|\tau_{m-1}]}\Big) \\
&\times \Big(\frac{\Pr[T_{M-1}|\Theta_{M-1}] \times \Pr[\Theta_{M-1}]}{\Pr[T_{M-1}]}\Big)
\end{aligned} \tag{174}$$

or simply (replacing $\tau_m \longrightarrow T_M$)

$$\Pr[\Theta_m|T_m] = W(\tau_m) \times \Pr[\Theta_{m-1}|T_{m-1}] \tag{175}$$

where

$$W(\tau_m) := \frac{\Pr[\tau_m|\Theta(\tau_m)] \times \Pr[\Theta(\tau_m)|\Theta(\tau_{m-1})]}{\Pr[\tau_m|\tau_{m-1}]} \tag{176}$$

which is the sequential Bayesian solution for the dynamic parametric model (random walk/constant). A particle filter is an implementation of this recursion[39,40]. We develop the particle filter generically in Appendix A.

Particle Filter for Fission Processes

Particle filtering is a technique that evolves from the "importance sampling" approach to statistical sampling of data. The key idea is to select particles (or parameters in our problem) from the regions of highest probabilities or equivalently regions of *highest importance*. Once the resulting importance weight is determined, the desired posterior distribution is approximated by a non-parametric probability mass function (PMF) as

$$\hat{\Pr}[\Theta_M|T_M] = \sum_i \mathcal{W}_i(\tau_m)\ \delta\Big(\Theta(\tau_m) - \Theta_i(\tau_m)\Big) \quad (177)$$

where $\mathcal{W}_i$ is the *normalized* weighting function given as the ratio of the posterior at inter-arrival time τ_m and the designed importance distribution q as

$$W_i(\tau_m) := \frac{\Pr[\Theta(\tau_m)|T_m]}{q[\Theta(\tau_m)|T_m]} = \frac{\Pr[\tau_m|\Theta(\tau_m)]}{q[\tau_m|\Theta(\tau_m)]} \times \frac{\Pr[\Theta(\tau_m)]}{q[\Theta(\tau_m)|\Theta_{m-1},\tau_m]} \quad (178)$$

The normalized weight is simply

$$\mathcal{W}_i(\tau_m) := \frac{W_i(\tau_m)}{\sum_i W_i(\tau_m)} \quad (179)$$

The "bootstrap" processor is the most popular technique[39]. Here the proposal is selected as the *transition* prior and the weighting function becomes simply the likelihood

$$W(\tau_m) = W(\tau_{m-1}) \times \Pr[\tau_m|\Theta(\tau_m)] \quad (180)$$

With these relations in mind, the sequential Bayesian processor can be developed for our problem. We start with the basic bootstrap technique (see Fig. 30) to estimate the unknown source parameters that will eventually become part of the log-likelihood decision function. Initially, we assume the prior distributions are uniformly distributed with bounds selected over some pragmatic intervals $\mathcal{U}(a,b)$. The dynamic parameter updates are given by the random-walk/constant model of Eq. 168 driven by zero-mean, Gaussian noise with covariance $R_{w_\Theta w_\Theta}$ with initial mean (constant) $\Theta(\tau_0)$ and corresponding parametric covariance $R_{\Theta\Theta}(\tau_0)$. The likelihood distribution embeds the "fission physics" of Eq. 143.

The bootstrap algorithm performs the following steps shown in the flow chart BOOTSTRAP PF FOR FISSION PROCESSING.

BOOTSTRAP PF FOR FISSION PROCESSING

PRIOR

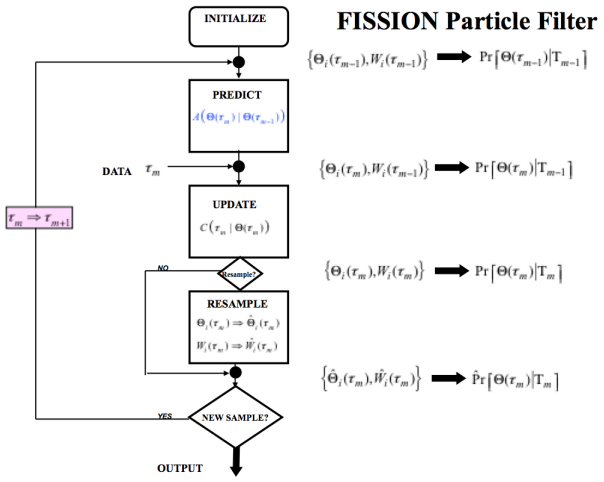

FIG. 30. Bootstrap Particle Filter Technique: Priors, Prediction, Update, Resampling and Posterior PMF estimate.

$$\Theta_i(\tau_0) \sim \Pr(\Theta(\tau_0)) \rightarrow \mathcal{U}(\theta_a,\theta_b);\ W_i(\tau_0) = \frac{1}{N_p}$$

$i = 1, \cdots, N_p$ [sample]

PREDICTION

$\Theta_i(\tau_m) = \Theta_i(\tau_{m-1}) + w_i(\tau_{m-1}); w_i \sim \mathcal{N}(0, R_{w_i w_i})$ [transition]

$\hat{\tau}_m = \max_{\tau \in T} \mathcal{L}[\tau_m]$ [Measurement Pred.]

Weight (Likelihood) Update:

$W_i(\tau_m) = \mathcal{L}\left[\tau_m|\Theta_i(\tau_m)\right]$ [weight/likelihood]

Weight normalization:

$$\mathcal{W}_i(\tau_m) = \frac{W_i(\tau_m)}{\sum_{i=1}^{N_p} W_i(\tau_m)}$$

RESAMPLING DECISION

$$\hat{N}_{eff} = \frac{1}{\sum_{i=1}^{N_p} W_i^2(\tau_m)} \quad \text{[effective samples]}$$

$$\hat{N}_{eff} = \begin{cases} \text{Resample} & \leq N_{thresh} \\ \text{Accept} & > N_{thresh} \end{cases}$$

RESAMPLING

$\hat{\Theta}_i(\tau_m) \Rightarrow \Theta_i(\tau_m)$

POSTERIOR DISTRIBUTION

$$\hat{\Pr}(\Theta(\tau_m)|T_m) \approx \sum_{i=1}^{N_p} \mathcal{W}_i(\tau_m)\delta(\Theta(\tau_m) - \hat{\Theta}_i(\tau_m))$$

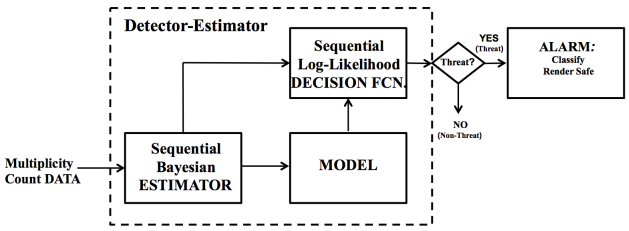

FIG. 31. Fission detection/estimation processing: Count data, fission parameter estimation, sequential detection and alarm.

D. SNM Detection and Estimation: Feasibility Data

In this section we investigate the performance of the sequential Bayesian detector/estimator on simulated feasibility data with *no* background. We assume a set of parameters to statistically synthesize a set of arrivals used to calculated the inter-arrivals $\{\tau_m\}$; $m = 0, 1, \cdots, M$. We start with the results from the sequential Bayesian detection algorithm that incorporates the Bayesian parameter estimator as part of its inherent structure as illustrated in Fig. 31. Note that the unknown source parameter vector to be estimated has the following physical parameters (from the inter-arrival PDF): $\Theta := [m_{\rm S}\ k_{\rm eff}\ \epsilon\ \lambda^{-1}]^T$—the mass of the source, effective multiplication ($k_{\rm eff}$), detector efficiency and inverse diffusion time, respectively.

The bootstrap PF was applied to a synthesized neutron arrival sequence shown in Fig. 31. We note from the figure that the inter-arrival data is processed by the sequential Bayesian estimator to provide predicted estimates of the source parameters, $\hat{\Theta}(\tau_m|\tau_{m-1})$. These estimates are then input to the physics-based likelihood to predict the corresponding PDF which is a part of the log-likelihood decision function. These predicted parameters are also provided directly as individual inputs to the log-likelihood decision function. Once the decision function is calculated at τ_m, it is compared to the thresholds to "decide" whether or not a threat is present. If so, the alarm is initiated. If not, another measurement is processed on arrival (take more data).

There exists a variety of metrics that can be applied to evaluate detection performance ranging from confusion matrices to statistical hypothesis tests[41], but perhaps the most basic and most robust method is the calculation of the receiver operating characteristic curve. The ROC curve is simply a graph of detection (P_{DET}) versus false alarm (P_{FA}) probabilities parameterized by threshold, $\mathcal{T}$ with *perfect* performance occurring when $P_{DET} = 1$ and $P_{FA} = 0$. The ROC curve provides all of the fundamental information from which most other metrics are derived. Thus, there are many individual metrics that can be extracted directly from a ROC curve including sensitivity, specificity, cost/benefit analysis along with a set of specific features like area-under-ROC-curve (AUC$\approx$ 1) and minimum probability of error (MinE)[41].

As mentioned above, it is necessary to calculate a ROC curve to select an operating point (detection and false-alarm probabilities) to calculate the sequential thresholds. In order to generate the ROC, we synthesize an ensemble of 30-members each consisting of 100-arrivals selected directly from a feasibility simulation data set using the following source (uranium) parameters: $m_{\rm S} = 25$ kg, $k_{\rm eff} = 0.9$; $\epsilon = 0.03$; $\lambda^{-1} = 0.01$. This ensemble of overlayed realizations is depicted in Fig. 32 with the arrows annotating a typical arrival realization. We chose to use a signal-to-noise ratio (SNR) of 6.9 dB defined by the 10 log-ratio of the signal energy to noise energy (variance). The local ROC for each member realization was estimated and then the *average* ROC was used for the calculation as shown in Fig. 33. Performance metrics such as AUC are also calculated to assess detection performance (AUC=0.95). For "perfect" performance, the detection probability is unity and false-alarm probability zero corresponding to an AUC of unity. The optimum operating point (P_{FA}, P_{DET}) is calculated by minimizing the Bayes' risk (see[41] for details) yielding a detection probability of 92% for a false alarm probability of 0.1% at this SNR. Substituting these values into the threshold calculation of Eq. 134 and taking the natural logarithm give the thresholds $(\ln\tau_0, \ln\tau_1)$ as $(-2.48, 7.23)$. A typical realization of sequential Bayesian detection results for a member of the ensemble is shown in Fig. 34 showing the decision function exceeding the upper threshold thereby indicating a threat and subsequent alarm.

Only 100 inter-arrivals were investigated to observe the feasibility of this approach. We observe the uncertainty of the inter-arrivals caused by the randomness of the fission process. The physical parameters were estimated with the results shown in Fig. 35. We selected a 10% error in the initial starting parameter values and drew them from a uniform distribution. The parameter estimates are quite reasonable for this realization at 6.9 dB. For parameter estimation performance metrics, we use the average RMS-error (absolute/relative errors) of each estimator to give: mass (RMS-error = 0.03/0.28% kg); effective multiplication (RMS-error = 0.0025/0.12%); efficiency (RMS-error = 0.00006/0.20%); and inverse diffusion time (λ) (RMS-error = 0.00004/0.4% μs^{-1}).

Note that the true parameter value is shown as the line (dashed) and both the maximum a-posterior (MAP) and conditional mean (CM) estimates are shown (arrows) on the plots. They appear to track the physical parameters quite well (small RMS errors) for this realization based

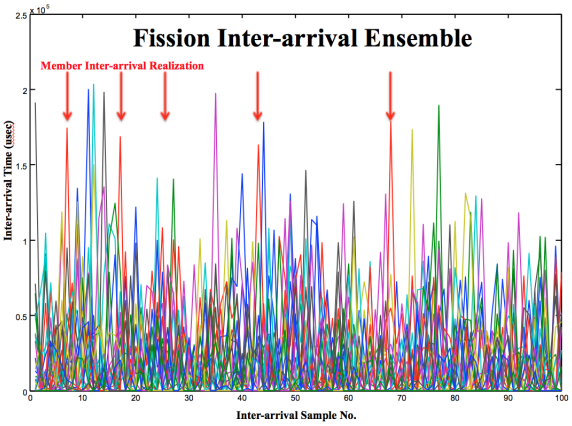

FIG. 32. Synthesized ensemble of inter-arrival data for ROC curve analysis: 30 realizations of 100 samples each with typical member realization shown with arrows locating largest times.

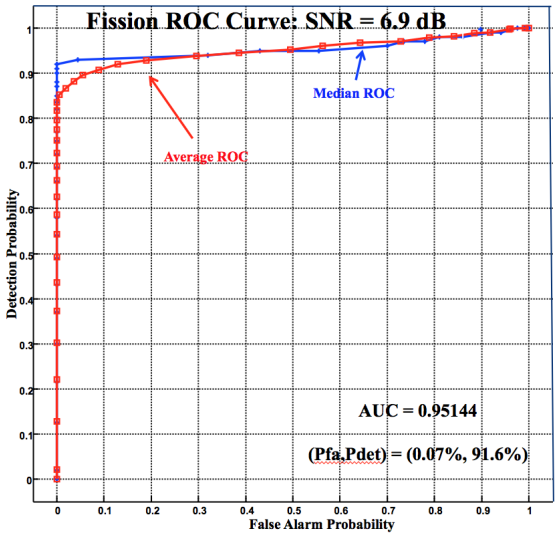

FIG. 33. Ensemble average and median receiver operating characteristic (ROC) curves for SNR=6.9 dB simulation with AUC = 0.95, (P_{FA}, P_{DET})=(0.0007, 0.916).

on the initializing the parameter estimators with a 10% error.

In order to evaluate the processor performance, we perform a sequence of 100 realizations and calculate ensemble statistics. Finally we observe the estimated parameter posterior PMF s in Figs. 36 and 37. We see the estimated parameter posterior PMF of the mass and effective multiplication (k_{eff}) parameters in Fig. 36 and the efficiency and inverse diffusion time (λ^{-1}) parameters in Fig. 37. Note that the distributions are multimodal (multiple peaks) and are centered somewhere about the mean value (true values) of each parameter. Finally we show a set of for snapshots (or slices) at various inter-arrival samples $(75, 100)$ throughout the simulation. Note that each is a slice of the $3D$ PMF s shown for all of the physical

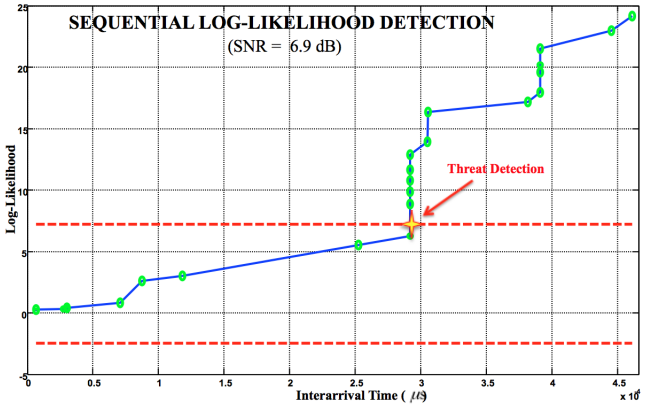

FIG. 34. Sequential Bayesian (log-likelihood) threat detection for (P_{FA}, P_{DET})=(0.0007, 0.916) and thresholds at $(\ln \tau_0, \ln \tau_1)$=$(-2.48, 7.23)$.

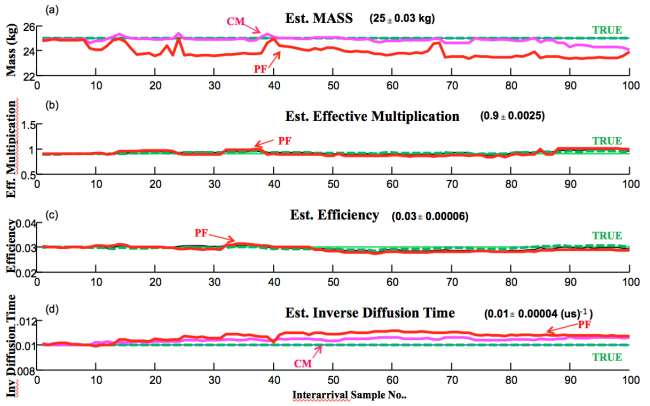

FIG. 35. Sequential Bayesian parameter estimates (arrows) and absolute RMS error for a SNR=6.9dB: (a) Mass (25±0.03 kg). (b) Effective multiplication ($k_{\text{eft}} = 0.90 \pm 0.0025$). (c) Efficiency ($0.03 \pm 0.00006$). (d) Inverse diffusion time ($\lambda = 0.01 \pm 0.00004\ \mu\text{s}^{-1}$).

parameters. Also note how the estimated particles coalesce (as expected) about the highest probability regions which are annotated by the arrows in Fig. 38.

E. Case Study

The critical part of this technique is the estimation of the source and associated fission parameters: mass of the source, effective multiplication, detector efficiency and the inverse diffusion time. From these parameters various sources can be detected directly and classified. Here we investigate the performance of the sequential Bayesian processor employing the time interval distribution of Prasad and Snyderman[12,27]. We use the Monte Carlo N-Particle Transport Code (MCNP) to synthesize the fission processes, since it has the capability to simulate particle interactions involving neutrons, photons, and electrons. We develop a high multiplication scenario

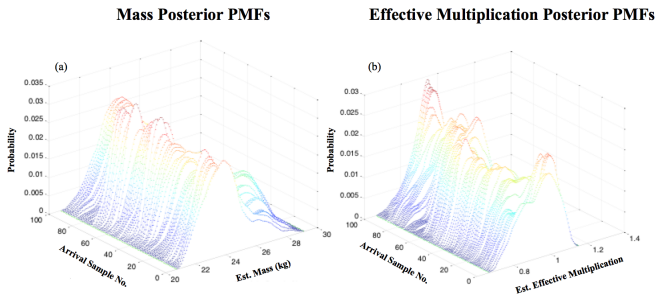

FIG. 36. Ensemble of posterior PMF parameter estimates for physics (source parameters): (a) Mass ($m_S = 25$ kg). (b) Effective multiplication ($k_{\text{eff}} = 0.90$).

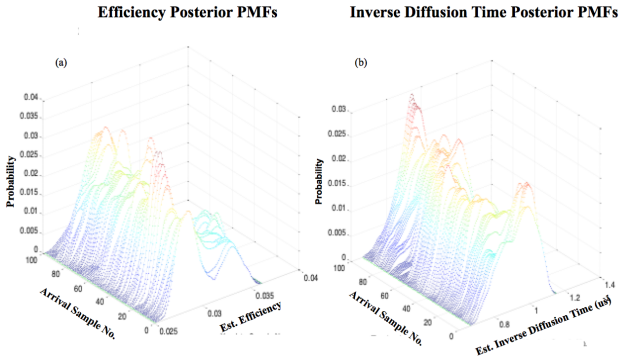

FIG. 37. Ensemble of posterior PMF parameter estimates for physics (source parameters): (a) Efficiency ($\epsilon_0 = 0.03$). (b) Inverse diffusion time ($\lambda = 0.01\ \mu s^{-1}$).

for highly enriched uranium (HEU) in steel.

Using MCNP we simulated the scenario incorporating a model of the recently developed MC-15 multiplicity counter which consists of 15 1-inch diameter by 15-inch long tubes each containing 10 atm of helium-3 and embedded in high-density polyethylene. The front panel has a single row of seven tubes and the main detector has eight tubes consisting of a forward row of six tubes and a back row of two tubes. We also incorporated background into the simulations detailed in[42]. Here Poisson uncertainties are incorporated directly into the physics-based likelihood distribution to capture the background interactions.

HEU in Steel: MCNP Test

The synthesized scenario is a highly-enriched uranium (HEU) ball in a steel shell that has a high multiplication with $k_{\text{eff}} = 0.951 \equiv M = 20.5$. Because the system has no hydrogenous material to moderate the neutrons, the diffusion time $\lambda^{-1} \approx 40\ \mu s$ which coincides with the diffusion time in the MC-15 joint multiplicity counter. Detection efficiency using a single MC-15 joint multiplicity counter with the front and back panels separated was

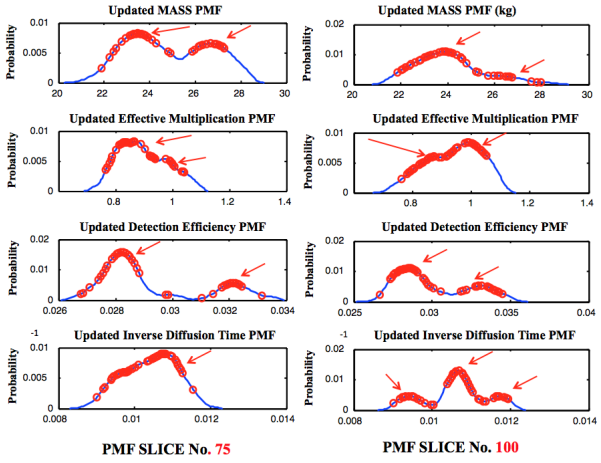

FIG. 38. Posterior PMF of various slices (75, 100 interarrivals) illustrating the multimodal (arrows) nature of the distributions as well as the coalescing of particles (circles) in highest probability regions.

$\epsilon = 1.511 \pm 0.007\%$. The MCNP simulation parameters and geometry are:

1. HEU (93% enriched): $r = 7.5$ cm, $m = 33$ kg, $\rho = 18.67$ g/cm^3, mass of ^{238}U $m_S = 1.837$ kg
2. 72:18:10 (Fe:Cr:Ni) Steel: $r = 10.0$ cm, thickness $= 2.5$ cm, $m = 19.13$ kg, $\rho = 7.9$ g/cm^3
3. Inside air-filled, 1 mm thick 72:18:10 (Fe:Cr:Ni) Steel drum: $r = 30.0$ cm, $l = 88.0$ cm, $m = 17.57$ kg, $\rho = 7.9$ g/cm^3
4. One MC-15 joint multiplicity counter, front and back panels separated on either side of the drum 31 cm from the center of the source (shown in red in Fig. 39).
5. Source and detector center 1 m above a 30 cm thick concrete floor. Source center 2.7 m from 30 cm thick concrete walls and ceiling.

The results of applying the PF parameter estimator are shown in Fig. 40 for the case of HEU in steel—the high multiplication case. An ensemble of 100 runs with background was created using the MCNP simulation software with the parameter estimates shown along with their ensemble averages for both the conditional mean and maximum a-posterior (MAP) estimators. Both estimators track one another well. The converged parameter estimates as shown in the figure are listed in Table IV where we see reasonable estimates for the effective multiplication with a relative error of 2% and inverse diffusion time. The mass and detection efficiency estimates are poor with large relative errors.

The detection performance over the ensemble can be bounded using the true parameter values. That is, we used the "true" source parameters to calculate the sequential log-likelihood decision function providing an estimate of the *best* (no parameter error) detection performance possible as indicated by the ROC curve with the

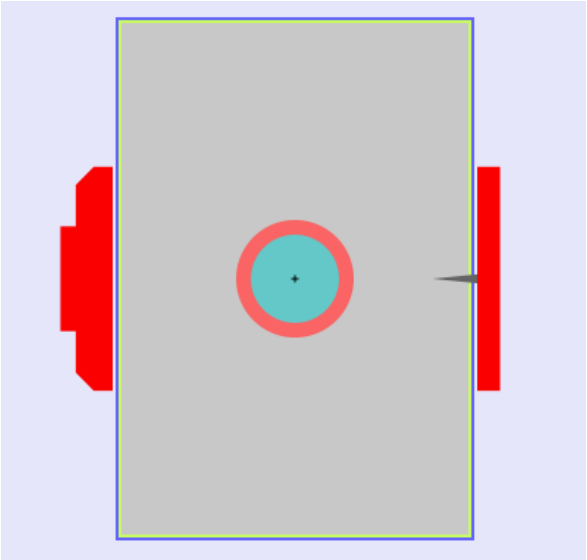

FIG. 39. Schematic of the setup of the HEU in steel configuration used in the MCNP simulation.

Case Study		
Parameters/Metrics	Feasibility	HEU Steel
Mass(kg)	25.00 ± 0.03	3.0 ± 6.0
Eff.Mult.	0.900 ± 0.003	0.932 ± 0.016
Det.Effic.	0.030 ± 0.0006	0.030 ± 0.010
Inv.Diff.$(\mu s)^{-1}$	0.010 ± 0.00004	0.027 ± 0.007
P_{DET}	0.916	0.820
P_{FA}	0.007	0.017
AUC	0.951	0.89

TABLE IV. Parameter estimation/detection results from the Monte Carlo simulation of HEU in steel.

detailed inset of Fig. 41. This approach was selected in order to bound the estimated ROC curve enabling us to determine the required thresholds for the sequential detector. The detection and false alarm probabilities are quite reasonable for this case, that is, for HEU in steel the optimum operating point of $P_{FA} = 0.017$ and $P_{DET} = 0.820$ was calculated indicating a detection performance bound along with the area-under-ROC-curve (AUC=0.89) for this case[41].

The inverse of the neutron diffusion time, λ, indicates that no neutron-moderating hydrogenous material was present: $\lambda^{-1} = 37.0$ μs is the neutron diffusion time of the polyethylene in the MC-15 neutron multiplicity counter itself.

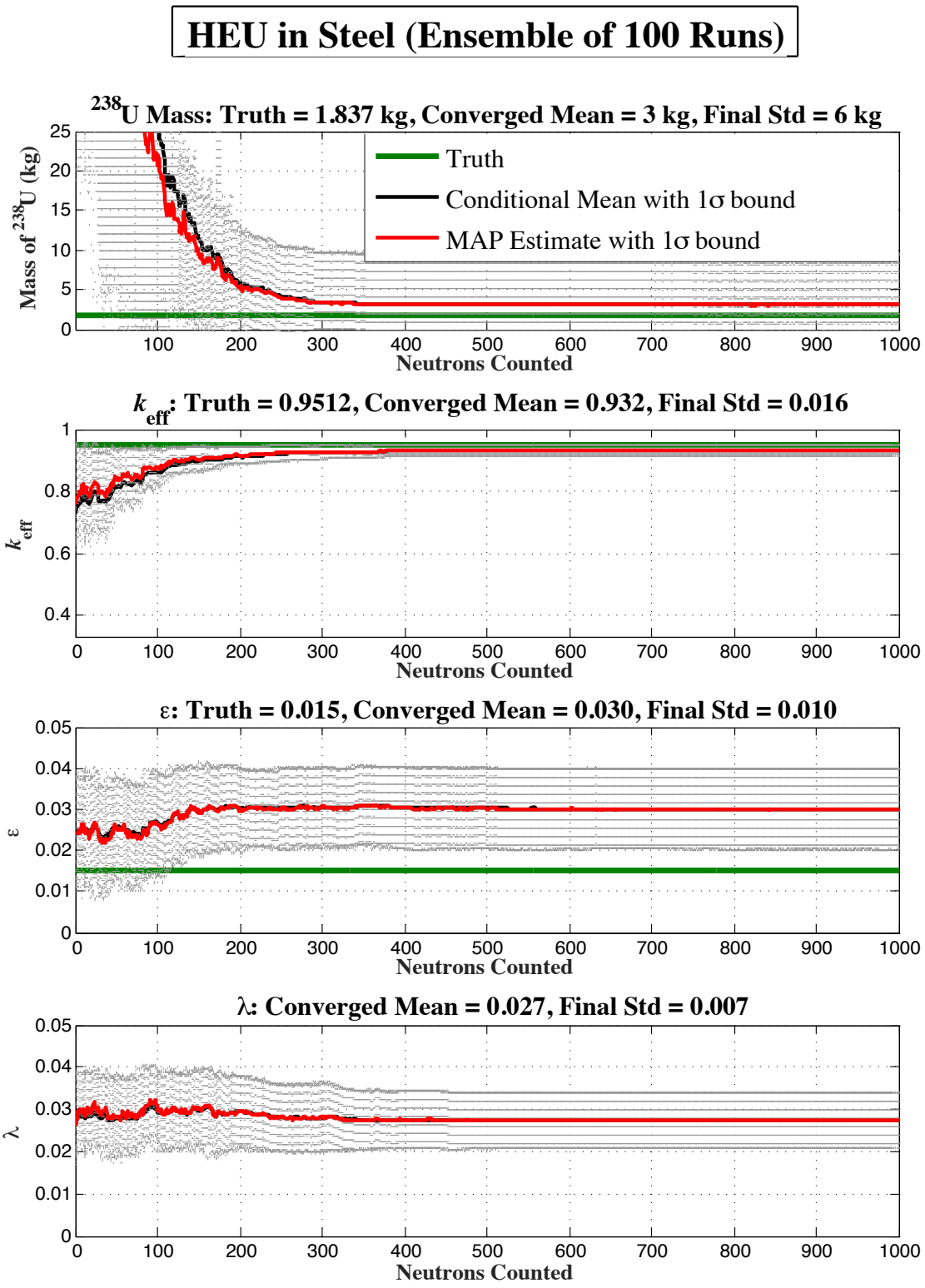

FIG. 40. Parameter estimates of HEU in steel MCNP simulation: (a) Mass of ^{238}U. (b) k_{eff}. (c) Detection efficiency ϵ. (d) Inverse diffusion time.

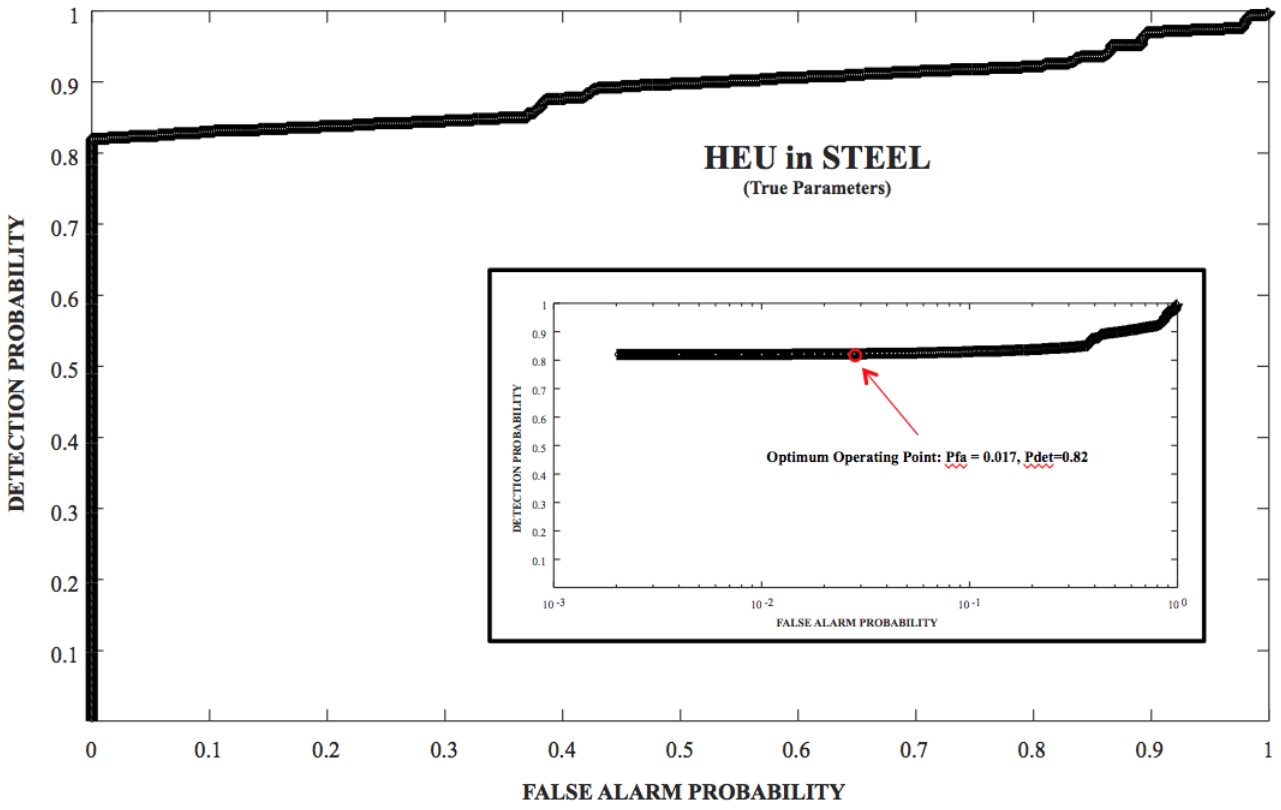

FIG. 41. Receiver operating characteristic (ROC) curve *bound* for HEU in steel obtained using "true" parameters with optimum operating point of $P_{FA} = 0.017$, $P_{DET} = 0.820$, and the $AUC = 0.89$.

V. REFERENCES

[1]E. D. Courant and P. Wallace, "Fluctuations of the number of neutrons in a pile," Phys. Rev. **72**, 1038–1048 (1947).
[2]G. I. Bell, "Probability distribution of neutrons and precursors in a multiplying assembly," Annals of Physics , 243–283 (1963).
[3]M. Smith-Nelson *et al.*, "Neutron specialist handbook and informational text," LA-CP-07-1080 (LANL, 2007).
[4]B. Rooney, J. Mattingly, and D. Dietrich, "Next generation neutron multiplicity detector requirements," Tech. Rep. (LANL, LLNL, SNL, 2011).
[5]M. O. Deighton, "Theoretical comparison of the enhanced variance and twin-gate methods for monitoring plutonium waste," Nucl. Instr. and Meth. **165**, 589–605 (1979).
[6]R. Dierckx and W. Hage, "Neutron signal multiplet analysis for the mass determination of spontaneous fission isotopes," Nucl. Sci. Eng. **85**, 325 (1983).
[7]A. A. Robba, E. J. Dowdy, and H. F. Atwater, "Neutron multiplication measurements using moments of the neutrons counting distribution," Nucl. Instr. and Meth. **215**, 473–479 (1983).
[8]F. de Hoffman, *The Science and Engineering of Nuclear Power*, Vol. II (Addison Wesley Press, Cambridge, MA, 1949).
[9]K. Böhnel, "The effect of multiplication on the quantitative determination of spontaneously fissioning isotopes by neutron correlation analysis," Nucl. Sci. Eng. **90**, 75 (1985).
[10]W. Hage and D. M. Cifarelli, "Correlation analysis with neutron count distributions in randomly or signal triggered time intervals for assay of special fissile materials," Nucl. Sci. Eng. **89**, 159 (1985).
[11]W. Hage and D. M. Cifarelli, "Models for a three-parameter analysis of neutron signal correlation measurements for fissile material assay," Nucl. Instr. and Meth. **A251**, 550–563 (1986).
[12]M. K. Prasad and N. J. Snyderman, "Statistical theory of fission chains and generalized poisson neutron counting distributions," Nucl. Sci. Eng. **172**, 300 (2012).
[13]H. S. Wilf, *generatingfunctionology* (Academic Press, Inc., 1994).
[14]J. Matthews and R. L. Walker, *Mathematical Methods of Physics, Second Edition* (Addison-Wesley Publishing Company, Inc., Menlo Park, 1970).
[15]M. J. Lighthill, *An introduction to Fourier analysis and generalised functions* (Cambridge University Press, Cambridge, UK, 1958).
[16]E. Saff and A. Snider, *Fundamentals of Complex Analysis with Applications to Engineering and Science* (Pearson Education Inc., 2003).
[17]J. M. Verbeke, C. Hagmann, and D. Wright, "Simulation of neutron and gamma ray emission from fission and photofission," Tech. Rep. UCRL-AR-228518 (2010).
[18]M. K. Prasad, "Notes on fission chain theory and its implementation in Bigfit & NMAC," (2011).
[19]L. Clark and C. Wilson, AWE, Private Communication.
[20]Canberra, *Epithermal Multiplicity Counter System Hardware Reference Manual*, Canberra.
[21]N. R. McMillan, "Comparison of methods for data analysis of fissile material using a high efficiency neutron counter," Tech. Rep. AWE Report 867/12 (Aldermaston Weapons Establishment, 2012).
[22]R. Venkataraman, *Neutron Multiplicity Counter Characterization Report*, Aldermason/Canberra Harwell Ltd.
[23]M. Abramowitz and I. Stegun, *Handbook of Mathematical Functions with Formulas, Graphs, and Mathematical Tables* (Dover Publications, New York, 1972).
[24]R. P. Feynman, "Statistical behavior of neutron chains," (1946), los Alamos Report LA-591 (Classified).
[25]R. P. Feynman, F. de Hoffman, and R. Serber, "Dispersion of the neutron emission in U-235 fission," Journal of Nuclear Energy **3**, 64–69 (1956).
[26]K. Nakamura et al. (Particle Data Group), "Review of particle physics," J. Phys. **G 37**, 075021 (2010).
[27]M. K. Prasad, N. J. Snyderman, J. M. Verbeke, and R. E. Wurtz, "Time interval distributions and the Rossi correlation function," Nucl. Sci. Eng. **174**, 1–29 (2013).
[28]D. Middleton, *An Introduction to Statistical Communication Theory* (McGraw-Hill, New York, New York, 1960).
[29]H. V. Trees, *Detection, Estimation and Modulation Theory, Part 1* (John Wiley, New York, New York, 1968).
[30]A. Papoulis and S. Pillai, *Probability, Random Variables and Stochastic Processes, 4th Ed.* (McGraw-Hill, New York, New York, 2002).
[31]A. Wald, "Sequential tests of statistical hypothesis," Ann. Math. Stat. , 117–186 (1945).
[32]A. Wald, *Sequential Analysis* (John Wiley (Reprint Dover Publications, 1973), New York, New York, 1947).
[33]ORTEC, "Fission multiplicity counter," ORTEC Report ORT-154 (2012).
[34]R. D. Evans, *The Atomic Nucleus* (McGraw-Hill, New York, New York, 1985).
[35]S. Walston, "The idiot's guide to the statistical theory of fission chains, 2nd ed." Tech. Rep. LLNL-TR-584832 (Lawrence Livermore National Laboratory, 2012).
[36]J. V. Candy, *Model-Based Signal Processing* (John Wiley/IEEE Press, Hoboken, New Jersey, 2006).
[37]E. D. Cashwell and C. J. Everett, *A Practical Manual on the Monte Carlo Method for Random Walk Problems* (Pergamon Press, London: U.K., 1959).
[38]D. B. J. I. V. Mazet, C. Carteret and B. Humbert, "Background removal from spectra by designing and minimizing a non-quadratic cost function," Chemonmetrics and Itelligent Lab. Sys. (2004).
[39]J. V. Candy, *Bayesian Signal Processing, Classical, Modern and Particle Filtering* (John Wiley/IEEE Press, Hoboken New Jersey, 2009).
[40]S. A. B. Ristic B. and N. Gordon, *Beyond the Kalman Filter, Particle Filters for Tracking Applications* (Artech House, Boston, Massachusetts, 2004).
[41]J. V. Candy and E. F. Breitfeller, "Receiver operating characteristic (roc) curves: An analysis tool for detection performance," Tech. Rep. LLNL-TR-642693 (Lawrence Livermore National Laboratory, 2013).
[42]S. Walston and N. Snyderman, "Time interval distributions for background neutrons," Tech. Rep. LLNL-IM-798987 (Lawrence Livermore National Laboratory, 2015).